EPS-HEP 95 Ref. eps0571
Submitted to Pa 1, 8, 14
Pl 4, 11, 18, 19

DELPHI 95-87 PHYS 522
30 June, 1995

# Measurement of the Forward-Backward Asymmetries of $e^+e^- \to Z \to b\bar{b}$ and $e^+e^- \to Z \to c\bar{c}$

DELPHI Collaboration

Paper submitted to the "EPS-HEP 95" Conference
Brussels, 27th July-2nd August 1995

EPS-HEP 95 Ref. eps0571
Submitted to Pa 1, 8, 14
Pl 4, 11, 18, 19

DELPHI 95-87 PHYS 522
30 June, 1995

# Measurement of the Forward-Backward Asymmetries of $e^+e^- \to Z \to b\bar{b}$ and $e^+e^- \to Z \to c\bar{c}$

- Preliminary -

DELPHI Collaboration

P.Antilogus, T.Baroncelli, K.Brand, M.Calvi, J.Dahm,
M.Elsing, U.Flagmeyer, K.Hamacher, K.Mönig, K.Münich,
W.Neumann, A.Passeri, M.Reale, I.Roncagliolo, B.Überschär

**Abstract**

The forward-backward asymmetries of the processes $e^+e^- \to Z \to b\bar{b}$ and $e^+e^- \to Z \to c\bar{c}$ are measured using 3 $10^6$ hadronic Z decays collected by the DELPHI experiment between 1991 and 1994. The tagging of b and c quarks is performed using three approaches. The first is based on the semileptonic decay channels $b/c \to X + \mu$ and $b/c \to X + e$; a precise determination of the parameters $A_{\rm FB}^{\rm b\bar{b}}$ and $A_{\rm FB}^{\rm c\bar{c}}$ is realized by a $\chi^2$ fit to the 3-dimensional $p$ , $p_t$ , $\cos(\theta_{thrust})$ distribution. The second approach uses a lifetime tag and a jet charge reconstruction to extract $A_{\rm FB}^{\rm b\bar{b}}$ ; the purity of the enriched B-sample and the $b\bar{b}$ charge separating power are both evaluated from the data. The third approach uses the polar angle distribution of reconstructed $D$ mesons to extract the parameters $A_{\rm FB}^{\rm c\bar{c}}$ and $A_{\rm FB}^{\rm b\bar{b}}$ . The energy of the $D$ meson and the lifetime tag information were used to separate $c\bar{c}$ and $b\bar{b}$ events.
Combining the different mesurements gives :

$$A_{\rm FB}^{0,b} = 0.1066 \pm 0.0064 \to \sin^2\theta_{eff}^{lep} = 0.2309 \pm 0.0011$$

$$A_{\rm FB}^{0,c} = 0.0814 \pm 0.0104 \to \sin^2\theta_{eff}^{lep} = 0.2297 \pm 0.0024$$

which yields to the effective electroweak mixing angle :

$$\sin^2\theta_{eff}^{lep} = 0.2306 \pm 0.0010$$

# 1 Introduction

The angular distribution for the reaction $e^+e^- \rightarrow q\overline{q}$ can be expressed as :

$$\frac{d\sigma}{d\cos(\theta_q)} \propto (1 + \cos^2\theta_q + \frac{8}{3}A_{\rm FB}^{\rm q\overline{q}}\ \cos\theta_q) \tag{1}$$

Where the asymmetry $A_{\rm FB}^{\rm q\overline{q}}$ is related to the forward and backward cross sections of the quark:

$$A_{\rm FB}^{\rm q\overline{q}} = \frac{(\sigma_F - \sigma_B)}{(\sigma_F + \sigma_B)}$$

To lowest order, the asymmetries $A_{\rm FB}^{\rm b\overline{b}}$ and $A_{\rm FB}^{\rm c\overline{c}}$ at $\sqrt{s} = M_Z$ are directly related to the vector and axial vector couplings of the $b$ and $c$ quarks.

$$A_{\rm FB}^{\rm b\overline{b}} = \frac{3}{4}A_eA_b$$

$$A_{\rm FB}^{\rm c\overline{c}} = \frac{3}{4}A_eA_c$$

with

$$A_i = \frac{2a_iv_i}{a_i^2 + v_i^2}$$

The higher order corrections are large, so that the precise knowledge of these asymmetries allows an accurate test of the Standard Model.

In this paper measurements of $A_{\rm FB}^{\rm b\overline{b}}$ and $A_{\rm FB}^{\rm c\overline{c}}$ at LEP with the DELPHI detector are presented. Three independent techniques are used to perform these measurements:

- The first one uses the semileptonic decays of the $b$ and $c$ quark into muons and electrons. The direction of the thrust axis, oriented by the jet containing the lepton, is used as a measurement of the primary quark direction.

- The second approach uses a lifetime tag and charge flow measurement to extract $A_{\rm FB}^{\rm b\overline{b}}$ ; the purity of the enriched B-sample and the $b\bar{b}$ charge separating power are both evaluated from the data.

- The third approach uses the polar angle distribution of reconstructed $D$ mesons to extract the parameters $A_{\rm FB}^{\rm c\overline{c}}$ and $A_{\rm FB}^{\rm b\overline{b}}$ . The energy of the $D$ meson and the lifetime tag information were used to separate $c\bar{c}$ and $b\bar{b}$ events.

For the analysis presented in this note, the two main capabilities of DELPHI have been used :

- the identification of leptons and hadrons

- the charged tracks and secondary vertecies reconstruction

The DELPHI detector and its perfomances are describe in detail in ref. [1]. Some of the proprieties of the DELPHI sub-detectors used by the analysis presented in this note will be quoted in the text. For an accurate description of the DELPHI detector the reader should refer to ref. [1].

# 2 $A_{\rm FB}^{\rm b\overline{b}}$ and $A_{\rm FB}^{\rm c\overline{c}}$ measurement using leptons

In this section measurements of $A_{\rm FB}^{\rm b\overline{b}}$ and $A_{\rm FB}^{\rm c\overline{c}}$ at LEP with the DELPHI detector using semileptonic events collected in 1994 are presented. The results obtained with the 1994 data sample are combined with the results from 1991-1992 [2] and 1993 [3] DELPHI analysis. The reader will have to refer to these previous analysis for a complete description of the method.

To perform the 1994 measurements the semileptonic decays of $b$ and $c$ quarks into muons and electrons are used. The thrust axis of the event , oriented by the jet containing the lepton, is used as a measurement of the primary quark direction.

The data collected at the $Z$ peak between 1991 and 1993 used in the quoted analysis [2, 3], corresponds to 1 356 000 hadronic events ( 472 000 from 1993 ). In 1993 at 'peak - 2 GeV ' the number of hadronics collected was 90 000 and at 'peak + 2 GeV ', it was 130 000. In 1994, the data sample taken at the $Z$ peak selected for the present analysis contains 1 362 000 hadronic events.

The JETSET 7.3 model [4] was used to generate simulated events. The Lund symmetric fragmentation function [4] described the hadronisation of the $u$,$d$,$s$ quarks while the fragmentation of heavy quarks, $c$ and $b$, was parametrised by the Peterson function [5]. In this analysis, the simulated events were reweighted to the same values used in the preceeding analysis. The corresponding $< X_E >_B$ , $< X_E >_{D^*}$ and the semileptonic branching ratios used are given in table 3. The response of the DELPHI detector to the generated events was simulated using DELSIM [6]. For most of the studies presented here samples of 2340000 simulated hadronic events for 1994 were used.

The main kinematical variable used to measure the flavour composition of the hadronic events containing a lepton is the transverse momentum of the lepton with respect to the closest jet. The value of this variable depends on the jet reconstruction algorithm. Jets were reconstructed using the JADE algorithm [7] with scaled invariant mass cut $y_{cut} = \frac{m_{ij}^2}{E_{vis.}} = 0.01$. The transverse momentum, $p_t$, of the lepton is defined as the momentum transverse to the jet axis when the lepton is excluded from the jet definition. This algorithm was chosen so as to optimise the sample purity and showed good agreement between data and predictions from simulation.

To ensure a good determination of the jet and thrust ($\theta_T$) directions, the analysis is limited to events with $|\cos\theta_T| < 0.9$ for the $\mu$ sample. As electrons used for this analysis are only identified in the barrel region, a cut at $|\cos\theta_T| < 0.7$ is applied in this case to avoid enriching the sample with events with high sphericity.

## 2.1 1994 muon sample

Muon candidates were identified by the muon chambers. The tracks found in the central detectors define a road along which hits in the muon chambers were searched for. The identification algorithm have been described extensively in ref. [1]. Muon candidates above 3 GeV/$c$ and in the region of good geometrical acceptance were selected. It was required that $0.03 < |\cos\theta_\mu| < 0.6$ or $0.68 < |\cos\theta_\mu| < 0.93$ where $\theta_\mu$ is the muon azimuthal angle.

The identification efficiency for muons was checked in $Z \to \mu^+\mu^-$, $Z \to \tau^+\tau^-$ , $\tau^- \to \mu^-\bar{\nu_\mu}\nu_\tau$ and $\gamma\gamma \to \mu^+\mu^-$events. The ratio of the data to the simulation efficiencies

was found to be (96.4±1.2)% in the barrel and (100.5±1.8)% in the forward region. These efficiency discrepancies between data and simulation were corrected for.

As the difference between the number of positive and negative charged particles was computed in small $\theta$ intervals, the sensitivity to the efficiency is small, but to extract $A_{\rm FB}^{\rm b\bar{b},exp}$ from the observed asymmetry a correct description of the fraction of background in the sample is needed. The contamination from misidentified hadrons arises partly from the decay of pions and kaons, but mostly from energetic hadrons which interact at the end of the calorimeter and generate 'punch-through'. $K^0$ particles decaying into two pions were used to measure the rate of pion misidentification. In the 94 data sample, the fraction of misidentified pions obtained was (0.62±0.03)%, while it was (0.49±0.02)% in the simulation.

To monitor the description of the background, the number of muon candidates normalized to the number of hadronic $Z$ decays has been compared between data and simulation in different kinematical regions. The high $p$, high $p_t$ region was used to define an overall efficiency, while the low $p$, low $p_t$ region, highly sensitive to the background level, allowed a fine control of the background description. The results found were compatible with the efficiency difference previously mentioned between data and simulation. The shape of the data/simulation distributions were seen to be compatible with an excess of backround in the data in comparison with the simulation. This excess of background has been estimated to 1.22±0.07 in the barrel and to 1.36±0.10 in the forward region. These last numbers are in agreement with the numbers obtained with the $K^0 \to \pi^+\pi^-$ sample which gives respectively 1.31±0.10 for the barrel and 1.24±0.11 for the forward region. The simulated data have been corrected to agree with the data sample. A systematic error of ±15% has been attributed to the estimated hadronic background and ±3% to the value of the efficiency.

The comparison between the 1994 data and the shape predicted by the simulation for the $p$ and $p_t$ spectra is presented in figures 1 and 2, and the $\cos\theta_\mu$ distribution in figure 5.

## 2.2 1994 electron sample

The electron candidates are identified by combining the electromagnetic shower informations from the HPC and the track ionization measured by the TPC. As well as improving the identification, the redundancy of these to independent methods allows a monitoring of the track selection and the bakground rate in real data and simulation.

In the electron selection it was required that the shower parameters of the candidates be compatible with those expected for electrons. In particular, demands were made on the ratio of electromagnetic energy seen in the HPC to the track momentum , and on the match between the shower position and track extrapolation. In addition a selection criteria is based on the longitudinal shower shape reconstructed by the 9 HPC layers. The energy lost by ionization inside the TPC is required to be compatible with the electron hypothesis. A detailed description of this method is given in [1, 8].

To ensure a good detector acceptance and a reasonable background level, candidates are selected with $P > 3$ GeV/c and

$$0.03 < |\cos\theta_e| < 0.70$$

A sizeable fraction of the selected electrons come from photon conversion. The contamination was reduced by the rejection of all track pairs fitting a secondary vertex with an invariant mass compatible with zero. The converted photons are rejected with an efficiency of 75% and, as measured in the Monte-Carlo, 2.7% of electrons from prompt b are also removed by this cut.

The efficiency of the electron identification was estimated to be 54.7 $\pm$ 0.3 % in the simulation. A study of electrons from a Compton sample shows that the efficiency is lower in the data than in the Monte-Carlo by a factor of 0.95 $\pm$ 0.022, this has been corrected for.

The comparison between the data and the Monte-Carlo for the $p$ and $p_t$ spectra is presented in figures 3 and 4, the $\cos(\theta_e)$ distribution is in figure 6.

From the presented studies we will assign an error of 3% on the electron efficiency and 20% for the contamination from converted gammas and from hadrons.

## 2.3 Sample composition

| Type of process | Value of their asymmetry | Composition of the samples in % for $l = \mu$ | | | for $l = e$ | | |
|---|---|---|---|---|---|---|---|
| | | No cut | $p_t > 1.6$ | $p_{tIN} > 1$ | No cut | $p_t > 1.6$ | $p_{tIN} > 1$ |
| $f_b$ : $b \to l^-$, $b \to \tau \to l^-$, $b \to \bar{c} \to l^-$, $b \to \bar{c} \to \tau^- \to l^-$ | $A_{FB}^{b\bar{b},exp}$ | 33.5 | 74.6 | 72.2 | 26.2 | 71.7 | 70.5 |
| $f_{bc}$ : $\bar{b} \to \bar{c} \to l^-$, $\bar{b} \to \bar{c} \to \tau^- \to l^-$ | $-A_{FB}^{b\bar{b},exp}$ | 11.6 | 4.3 | 6.0 | 7.8 | 3.4 | 5.0 |
| $f_c$ : $\bar{c} \to l^-$, $\bar{c} \to \tau^- \to l^-$ | $-A_{FB}^{c\bar{c}}$ | 16.1 | 7.7 | 5.6 | 11.4 | 6.8 | 4.9 |
| $f_{bg}$ : Total Background | $A_{FB}^{Bkg}$ | 38.8 | 13.4 | 16.2 | 54.6 | 17.8 | 19.6 |
| Number of data candidates | | 88937 | 20614 | 20058 | 54879 | 9592 | 9439 |

Table 1: *Composition of the lepton samples in different kinematical domains. (The $p_{tIN}$ corresponds to the transverse momentum where the lepton is included in the jet.)*

Several channels lead to leptons in the final state, as shown in table 1. The first processes in table 1 are the signal. They give leptons with the same sign in the final states as the initial $b$ quarks and are denoted by the weight $f_b$.

The total asymmetry observed is given by

$$A_{\rm FB}^{\rm obs} = \sum_{x=b,bc,c,bg} f_x . A_{\rm FB}^x$$

where the fractions $f_x$ associated to each channel depend on the kinematical domain selected. The experimental measured $b$ quark asymmetry is then

$$A_{\rm FB}^{\rm b\bar{b},exp} = \frac{A_{\rm FB}^{\rm obs} - \sum_{x=bc,c,bg} f_x . A_{\rm FB}^x}{f_b} \qquad (2)$$

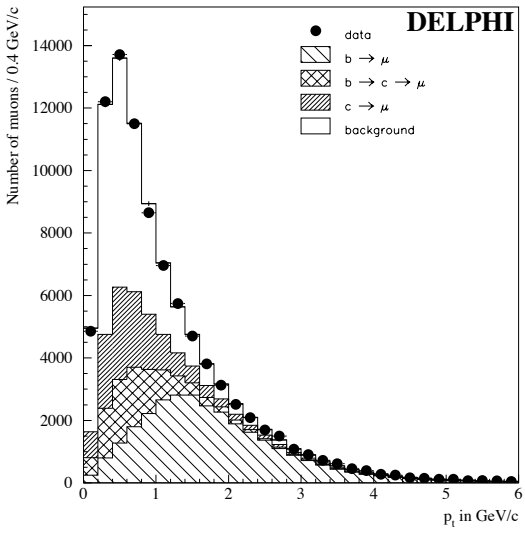


Figure 1: *Transverse momentum distribution for muon candidates*

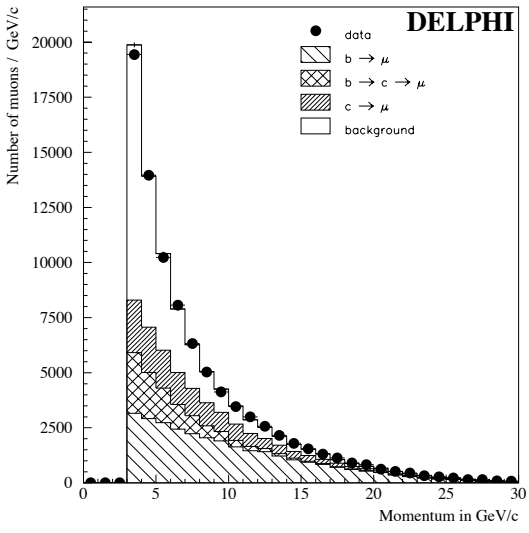


Figure 2: *Momentum distribution for muon candidates*

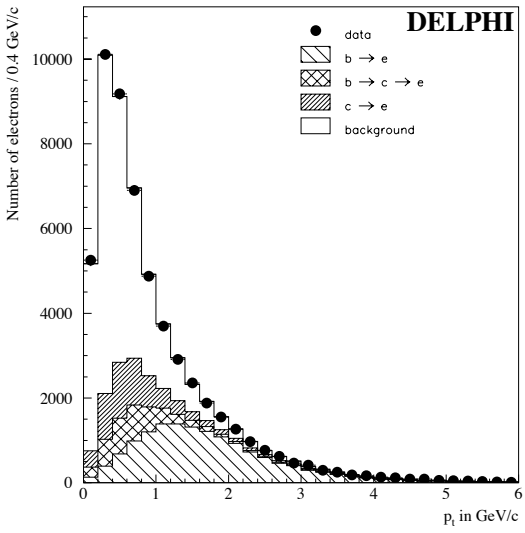


Figure 3: *Transverse momentum distribution for electron candidates*

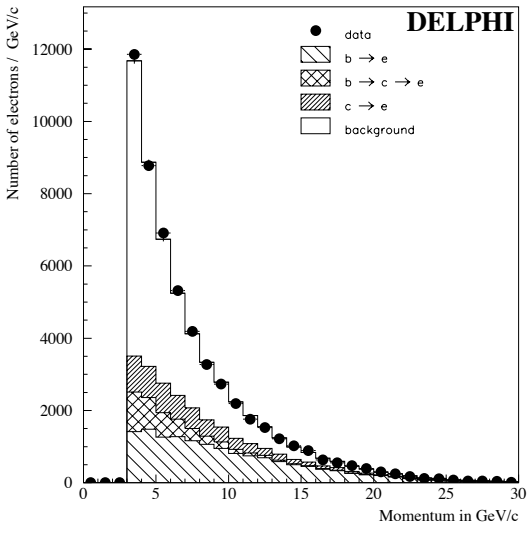


Figure 4: *Momentum distribution for electron candidates*

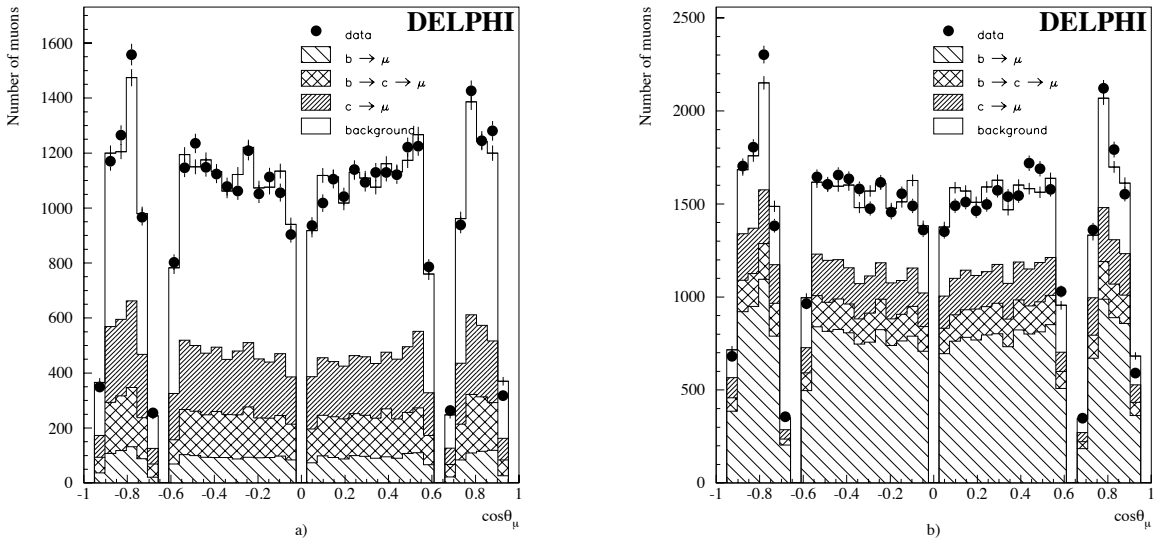


Figure 5: $\cos(\theta_\mu)$ *distribution for muon candidates. The selected muons have* $p_t < 0.7$ GeV/$c$ *in a) and* $p_t > 0.7$ GeV/$c$ *in b).*

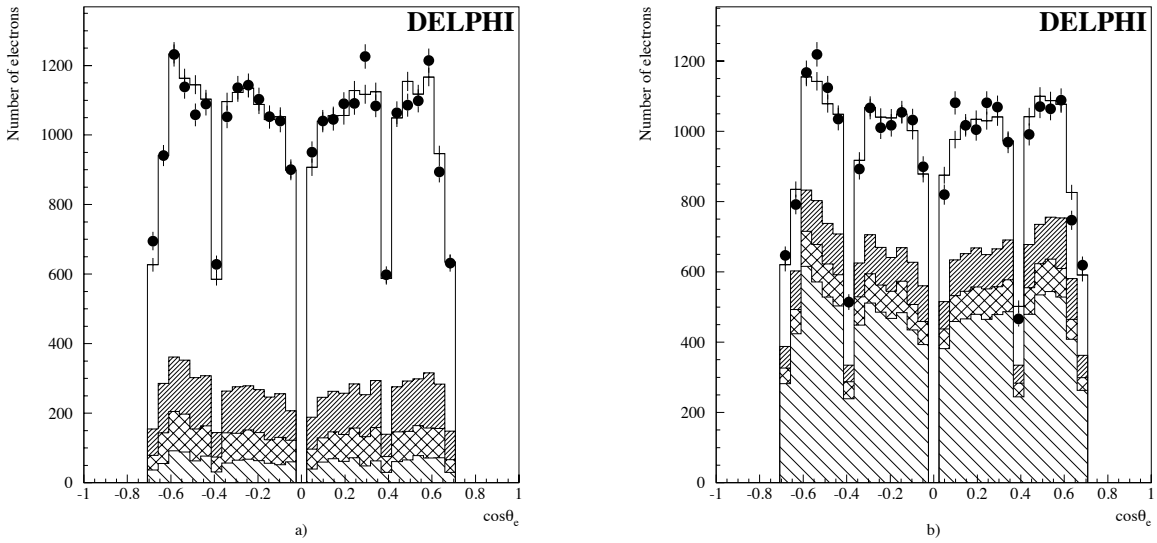


Figure 6: $\cos(\theta_e)$ *distribution for electron candidates. The selected electrons have* $p_t < 0.7$ *GeV/c in a) and* $p_t > 0.7$ *GeV/c in b).*

where $f_b$ is the weighted sum over the first 4 processes of table 1 and $\sum_{x=bc,c,bg} f_x A^x_{\rm FB}$ is the contribution of the other processes to the observed asymmetry.

The coefficients $f_b$, $f_{bc}$, $f_c$, and $f_{bg}$, are functions of the kinematical domain considered, their estimation depends on the details of the simulation. They are function of many parameters involved in the decays and fragmentation of the heavy flavor quarks. A detail description of these parameters can be found in ref [2]. The values considered in this analysis and their variations, are summarised in table 3.

## 2.4 The $\chi^2$ fit of $A_{\rm FB}^{\rm b\bar{b},exp}$

A binned $\chi^2$ fit of the observed charge asymmetry as a function of $\cos\theta_T$ has been performed.
In each bin $i$ of the space ($\cos\theta_T$, $p_l$, $p_t$) an asymmetry was measured :

$$A_{FB}^{obs,i} = \frac{N^-(i) - N^+(i)}{N^-(i) + N^+(i)}$$

where $N^{\pm}(i)$ is the number of events of sign $\pm$ in the bin $i$. A $\chi^2$ fit was then performed over the different bins to obtain the asymmetry $A_{\rm FB}^{\rm b\bar{b},exp}$ and $A_{\rm FB}^{\rm c\bar{c}}$ . The $\chi^2$ had the form:

$$\chi^2 = \sum_i \frac{\left(\left((f_b^i - f_{bc}^i)\, A_{\rm FB}^{\rm b\bar{b},exp} + f_c^i A_{\rm FB}^{\rm c\bar{c}}\right) W_{\theta_T}^i + f_{bg}^i A_{FB}^{bg,i} - A_{FB}^{obs,i}\right)^2}{\sigma^2} \qquad (3)$$

where :

- $W_{\theta_T}^i = \frac{8}{3}\frac{1}{n_{data}^i}\sum_{j=1}^{n_{data}^i} \frac{\cos(\theta_T^j)}{1+\cos(\theta_T^j)^2}$ takes into account the $\theta$ dependence of the asymmetry
- $\sigma$ is the error including effects from both data and simulation statistics
- the other parameters have the same definition as in equation 2. The different $f_x^i$ and $A_{FB}^{bg,i}$ [2] were determined from the simulation

The binning has been adjusted to obtain $\sim 200$ events per bin. A negligible dependence of the result with the number of bins in $\cos\theta_T, p_l, p_t$ has been observed. When the bin size is too wide in $p_t$ the precision of the result deteriorates, as the leptons from $b$ quark decay are not so well separated from the other leptonic classes. The measured asymmetries using the 1994 leptons sample at $\sqrt{\rm s}$ = 91.205 GeV are:

$$A_{\rm FB}^{\rm b\bar{b},exp} = 0.078 \pm 0.008(stat) \pm 0.003(sys)$$

$$A_{\rm FB}^{\rm c\bar{c}} = 0.085 \pm 0.018(stat) \pm 0.013(sys)$$

After $B\bar{B}$ mixing correction, using the LEP average $\chi = 0.116 \pm 0.006$ [9], the $b$ asymmetry is :

$$A_{\rm FB}^{\rm b\bar{b}} = 0.102 \pm 0.010(stat) \pm 0.004(sys) \pm 0.002(mix)$$

The results for the different samples can be found table 2. The systematics from the different sources can be found table 3, for detailed comments see ref. [2].

| Sample | $A_{FB}^{b\bar{b}}$ | | | $A_{FB}^{c\bar{c}}$ | | | $\frac{\chi^2}{ndf}$ |
|---|---|---|---|---|---|---|---|
| $\mu$ 1994 only | 0.0954 | $\pm$ | 0.0120 | 0.0706 | $\pm$ | .0196 | 460 / (431-2) |
| $e$ 1994 only | 0.1272 | $\pm$ | 0.0212 | 0.1540 | $\pm$ | .0428 | 272 / (270-2) |
| $\mu$ and $e$ 1994 | 0.102 | $\pm$ | 0.010 | .085 | $\pm$ | .018 | 736 /(701-2) |

Table 2: *Results and statistical errors of the fit to* $A_{FB}^{b\bar{b}}$ *and* $A_{FB}^{c\bar{c}}$ *for the different samples*

### 2.5 Combined 91-94 results

For $\sqrt{s} = M_Z$, taking into account the correlation between the systematics, the result obtained with the 1994 lepton sample has been combined with the 1991, 1992 and 1993 DELPHI measurements of $A_{FB}^{b\bar{b}}$ and $A_{FB}^{c\bar{c}}$ using leptons [2, 3]. The combined results are at $\sqrt{s} = 91.228$GeV :

$$A_{FB}^{b\bar{b}} = 0.1049 \pm 0.0076(stat) \pm 0.0035(syst) \pm 0.0016(mixing)$$

$$A_{FB}^{c\bar{c}} = 0.084 \pm 0.014(stat) \pm 0.013(syst)$$

The total correlation between $A_{FB}^{b\bar{b}}$ and $A_{FB}^{c\bar{c}}$ at the peak (considering the statistical and systematical errors ) is +20%.
In 1993 the folowing outpeak measurements were also obtained :

$$A_{FB}^{b\bar{b}} = 0.062 \pm 0.038(stat) \pm 0.002(syst) \pm 0.001(mixing) \text{ at } \sqrt{s} = 89.433 \text{ GeV}$$

$$A_{FB}^{b\bar{b}} = 0.147 \pm 0.035(stat) \pm 0.006(syst) \pm 0.002(mixing) \text{ at } \sqrt{s} = 93.017 \text{ GeV}$$

## 3 $A_{FB}^{b\bar{b}}$ measurement using a lifetime tag

In this section a measurement of $A_{FB}^{b\bar{b}}$ using an inclusive lifetime tag of B-hadrons is presented. Two different approaches were followed to extract an asymmetry signal from the tagged sample: the first approach [2, 10], or *counting* method, performed a fit to a kind of $b$-quark angular distribution which was built up on an event by event basis by identifying the $b$ charge using an hemisphere charge algorithm and by approximating its direction via the event thrust axis $\vec{T}$. The second approach measured the *charge flow* $\langle Q_{FB} \rangle$, *i.e.* the average difference between the forward and the backward hemisphere charges, which was connected to the quark forward-backward asymmetries via the so called charge separations $\delta_f$. In the following both approaches will be discussed in detail.

### 3.1 $B$ Enrichment

The generic events and tracks selection criteria are give in table 5. The cut on the single hemisphere energy allows a better hemisphere charge evaluation.

To select an enriched sample of $b\bar{b}$ events a well established $B$-hadrons lifetime tagging technique was used, which was originally proposed by ALEPH [11] and then adopted in DELPHI [12, 13]. Such technique required the measurement of the particles impact parameter $\delta$, defined for every charged track as its distance of closest approach to the $Z$

| Changed parameters | Central value | Variations applied | $\Delta A_{FB}^{bb}$ Peak | $\Delta\ A_{\rm FB}^{c\bar{c}}$ Peak |
|---|---|---|---|---|
| $b$ decay model | $ACCMM$ | $\pm IGSW^{**}$ | $\pm$ 0.0001 | $\pm$ 0.0047 |
| $c$ decay model | $m_s = 1$ MeV | $m_s =^{1}_{153}$ MeV | $\pm$ 0.0018 | $\mp$ 0.0014 |
| | $p_f = 467$ MeV | $p_f =^{353}_{467}$ MeV | | |
| $Br(b \to l)$ | 0.11 | $\pm$ 0.0034 | $\mp$ 0.0011 | $\pm$ 0.0015 |
| $Br(b \to c \to l)$ | 0.079 | $\pm$ 0.005 | $\pm$ 0.00035 | $\mp$ 0.0024 |
| $Br(b \to \bar{c} \to l)$ | 0.013 | $\pm$ 0.005 | $\pm$ 0.0004 | $\pm$ 0.0038 |
| $Br(c \to l)$ | 0.098 | $\pm$ 0.005 | $\pm$ 0.0005 | $\mp$ 0.0034 |
| $\Gamma_{b\bar{b}}/\Gamma_{had}$ | 0.217 | $\pm$ 0.003 | $\mp$ 0.00036 | $\pm$ 0.0005 |
| $\Gamma_{c\bar{c}}/\Gamma_{had}$ | 0.171 | $\pm$ 0.014 | $\pm$ 0.0011 | $\mp$ 0.0051 |
| $\langle X_E \rangle_B$ | 0.700 | $\pm$ 0.004 | $\mp$ 0.0002 | $\mp$ 0.0005 |
| $\langle X_E \rangle_{D^*}$ | 0.495 | $\pm$ 0.010 | $\pm$ 0.0013 | $\mp$ 0.0005 |
| background and | | $\pm$ 15 % | | |
| efficiency for muons | | $\mp$ 3 % | $\pm$ 0.0015 | $\pm$ 0.0035 |
| background and | | $\pm$ 20 % | | |
| efficiency for electrons | | $\mp$ 3 % | $\pm$ 0.0005 | $\pm$ 0.0003 |
| background asymmetry | | $\pm$ 50 % | $\mp$ 0.0006 | $\pm$ 0.0068 |
| $p_t$ and thrust | | | $\pm$ 0.0013 | $\pm$ 0.0009 |
| reconstruction | | | | |
| Sample binning, | | | $\pm$ 0.0013 | $\pm$ 0.0045 |
| fit method | | | | |
| total | | | 0.0038 | 0.0128 |
| $BB$ mixing ($\chi^2$) | 0.116 | $\pm$ 0.006 | $\pm$ 0.0016 | - |

Table 3: Different contributions to the systematic error in the $\chi^2$ fit of the 1994 leptons sample

| Changed parameters | Central value | Variations applied | $\Delta A_{FB}^{b\bar{b}}$ Peak-2 | $\Delta A_{FB}^{b\bar{b}}$ Peak | $\Delta A_{FB}^{b\bar{b}}$ Peak+2 | $\Delta\ A_{\rm FB}^{c\bar{c}}$ Peak |
|---|---|---|---|---|---|---|
| $b$ decay model | $ACCMM$ | $\pm IGSW^{**}$ | $\pm$ 0.0010 | $\pm$ 0.0002 | $\pm$ 0.0026 | $\pm$ 0.0052 |
| $c$ decay model | $m_s = 1$ MeV | $m_s =^{1}_{153}$ MeV | $\pm$ 0.0004 | $\pm$ 0.0018 | $\pm$ 0.0022 | $\mp$ 0.0014 |
| | $p_f = 467$ MeV | $p_f =^{353}_{467}$ MeV | | | | |
| $Br(b \to l)$ | 0.11 | $\pm$ 0.0034 | $\mp$ 0.0003 | $\mp$ 0.0011 | $\mp$ 0.0010 | $\pm$ 0.0015 |
| $Br(b \to c \to l)$ | 0.079 | $\pm$ 0.005 | $\pm$ 0.0001 | $\pm$ 0.0005 | $\pm$ 0.0003 | $\mp$ 0.0024 |
| $Br(b \to \bar{c} \to l)$ | 0.013 | $\pm$ 0.005 | $\pm$ 0.0001 | $\pm$ 0.0005 | $\pm$ 0.0017 | $\pm$ 0.0038 |
| $Br(c \to l)$ | 0.098 | $\pm$ 0.005 | $\pm$ 0.0003 | $\pm$ 0.0004 | $\mp$ 0.0007 | $\mp$ 0.0035 |
| $\Gamma_{b\bar{b}}/\Gamma_{had}$ | 0.217 | $\pm$ 0.003 | $\mp$ 0.0001 | $\mp$ 0.0004 | $\mp$ 0.0004 | $\pm$ 0.0005 |
| $\Gamma_{c\bar{c}}/\Gamma_{had}$ | 0.171 | $\pm$ 0.014 | $\pm$ 0.0001 | $\pm$ 0.0010 | $\mp$ 0.0008 | $\mp$ 0.0052 |
| $\langle X_E \rangle_B$ | 0.700 | $\pm$ 0.004 | $\pm$ 0.0002 | $\mp$ 0.0001 | $\mp$ 0.0001 | $\mp$ 0.0005 |
| $\langle X_E \rangle_{D^*}$ | 0.495 | $\pm$ 0.010 | $\mp$ 0.0001 | $\pm$ 0.0012 | $\pm$ 0.0014 | $\mp$ 0.0004 |
| background and efficiency for muons | | | $\pm$ 0.0013 | $\pm$ 0.0013 | $\pm$ 0.0040 | $\pm$ 0.0029 |
| background and efficiency for electrons | | | - | $\pm$ 0.0007 | - | $\pm$ 0.0010 |
| background asymmetry | | $\pm$ 50 % | $\mp$ 0.0001 | $\mp$ 0.0008 | $\pm$ 0.0001 | $\pm$ 0.0079 |
| $p_t$ and thrust reconstruction | | | $\pm$ 0.0006 | $\pm$ 0.0009 | $\pm$ 0.0020 | $\pm$ 0.0006 |
| Sample binning, fit method | | | $\pm$ 0.0006 | $\pm$ 0.0009 | $\pm$ 0.0020 | $\pm$ 0.0033 |
| total | | | 0.0020 | 0.0035 | 0.0065 | 0.0132 |
| $B\bar{B}$ mixing ($\chi^2$) | 0.116 | $\pm$ 0.006 | $\pm$ 0.0010 | $\pm$ 0.0016 | $\pm$ 0.0023 | - |

Table 4: Different contributions to the systematic error for the 1991-1994 leptons sample.

| Collection of applied cuts | |
|---|---|
| Trackcuts | Eventcuts |
| $0.4\,\mathrm{GeV}/c < \|p\|$ | $N(charged) \geq 5$ |
| $tracklength > 30\,cm$ | $(\sum_{i=1}^{N(charged)} E_i) > 0.12\sqrt{s}$ |
| $\theta > 20°$ | $(\sum_{i=1}^{N(hemisphere)} E_i) > 0.03\sqrt{s}$ |
| $\frac{\Delta p_i}{p_i} < 1.$ | $\|\sum_{i=1}^{N(charged)} \vec{p_i}\| < 0.25\sqrt{s}$ |
| $impact(R\phi) < 4\,cm$ | $\Theta(thrust) > 30°$ |
| $impact(z) < 10\,cm$ | |

Table 5: Cuts to select hadronic events

production point. Particles originating from the decay of long lived hadrons had large and positive impact parameters (a sign was conventionally given to $\delta$ according to the position of the intersection point between the charged track and the jet direction), while particles produced in the primary interaction had $\delta$ values spread around zero according to the detector spatial resolution.

The DELPHI Vertex Detector [14, 15], which starting from 1994 data taking provided also a measurement of the $z$ coordinate, allowed a very precise measurement of spatial points along the charged particles path. To avoid any dependence of the measurement on the polar angle, the $z$ coordinate information was used only in the vertex determination, which was fitted on an event by event basis [12], while the individual impact parameters were evaluated in the plane perpendicular to the colliding beams with an average resolution below $30\,\mu m$.

From the study of the distribution of the ratio between $\delta$ and its estimated error, it was possible to define a probability for each charged track of having been produced in the primary vertex. Probabilities of any group of particles could be combined together as well. Event and hemisphere probabilities obtained from positive impact parameter tracks, namely $F_E^+$ and $F_H^+$, were considered. In figure 7 the simulated distributions of $F_E^+$ for $b\bar{b}$ events and for non-$b$ events were shown: for $b\bar{b}$ events the probability had a sharp peak at low values, while there was a much lower peak in the non-$b$ events (which is mainly given by charm events). By choosing a cut in probability it was then possible to select samples of events with different $B$ purities and efficiencies. The B purity, $P_B$, was defined as the fraction of $b\bar{b}$ events in the selected sample and the B efficiency, $E_B$, was the probability of selecting a $b\bar{b}$ event. Accurate tuning of the Monte Carlo to the data was performed [12] in order to correctly estimate the $B$ purities of the selected samples.

## 3.2 The counting method

This approach was already used for the analysis of the data collected during 1992 and 1993 [2, 10]. Here the extension of the measurement to the 1994 data is described, along with some important improvements in the charge finding efficiency determination. A

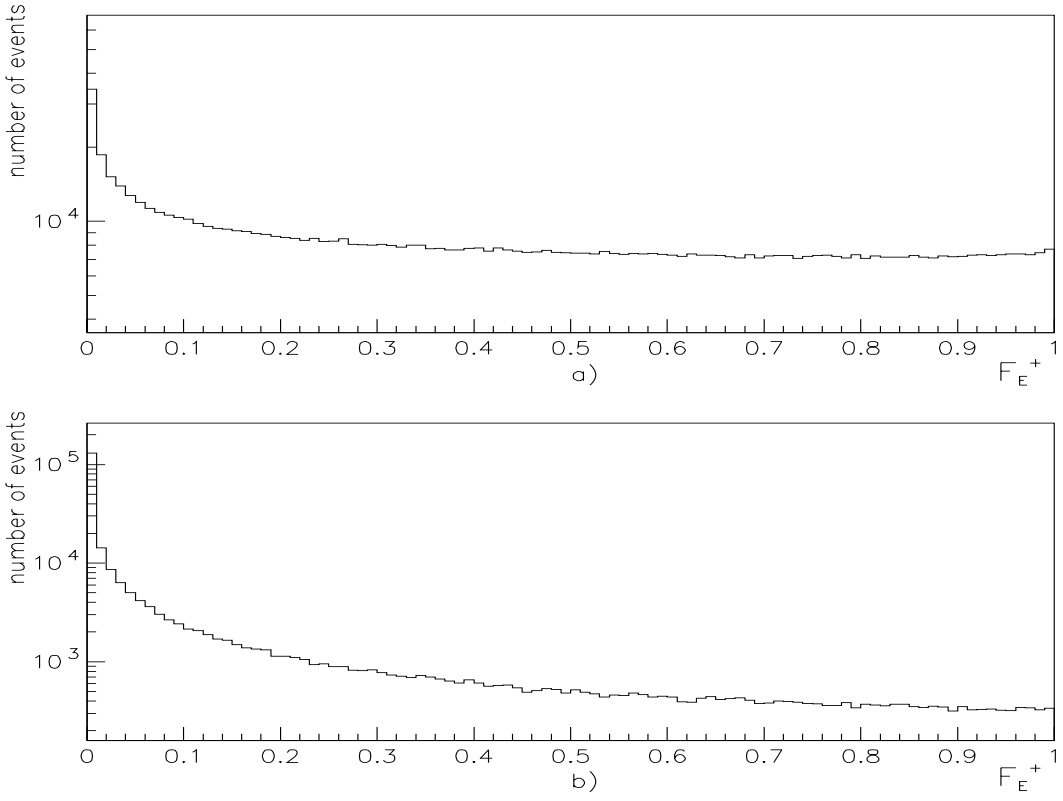


Figure 7: Event probability in simulated events $F_E^{\pm}$ for tracks with positive impact parameter for (a) light quark and charm quark events, and (b) $b$-quark events.

combination of the results from 1992 to 1994 is then performed.

### 3.2.1 Selection and $B$-purity of the sample

The angular acceptance of this analysis was restricted to $|cos\theta_T| \leq 0.7$ (where $\theta_T$ is the thrust axis polar angle) to insure constant $B$ purity and charge finding efficiency over the selected angular range.

Two probabilities $F_H$ were obtained for each event using separately the particles in the two hemispheres, defined by a plane perpendicular to the thrust axis at the interaction point. The event was selected if at least in one hemisphere $F_H$ was lower than a given cut. This allows the use of a double tagging technique to derive from the data itself the B purity and the B efficiency of such an enrichment procedure. The double tagging technique consist of comparing the fractions of tagged hemispheres and events with the Monte Carlo predictions, that can be expressed in terms of $P_B$ and $E_B$ by assuming the experimental value of $\Gamma_{b\bar{b}}/\Gamma_{had}$ measured by DELPHI [16] and an hemisphere-hemisphere correlation factor both for $b\bar{b}$ and non-$b\bar{b}$ events. The related equations were already given and discussed in previous papers [2, 10].

The values obtained for $P_B$ and $E_B$ at some cut choices are listed in table 6. An estimation of the systematic error on $P_B$ is also reported, which was obtained by comparing the two possible solutions of the tag equations when taking from simulation the $b\bar{b}$ hemisphere-hemisphere correlation factor or the light flavours tag efficiency.

| $-log_{10}F_H^+$ cut | $E_B$ (%) | $P_B$ (%) | $P_B$ syst |
|---|---|---|---|
| 1.0 | $94.6 \pm 0.5$ | $46.0 \pm 0.2$ | 3.6 |
| 1.5 | $83.2 \pm 0.5$ | $60.2 \pm 0.3$ | 3.3 |
| 2.0 | $71.4 \pm 0.5$ | $72.7 \pm 0.3$ | 2.1 |
| 2.5 | $59.3 \pm 0.5$ | $81.8 \pm 0.5$ | 1.0 |
| 3.0 | $45.2 \pm 0.5$ | $88.8 \pm 0.7$ | 0.5 |

Table 6: $B$ Efficiency and $B$ purity of the tag (with statistical errors) for different values of the $F_H^+$ cut. The estimated systematics on $P_B$ is also reported.

For the $A_{\rm FB}^{\rm b\bar{b}}$ measurement the tag cut was fixed at $-log_{10}F_H^+ > 2.0$. The non $b$ flavours were assumed to be in the proportion predicted by Monte Carlo.

### 3.2.2 Charge finding technique

The quark charge was identified by means of the jet charge variable [17], which partly retains the quark charge information in hadronic events. The two hemisphere jet charges were defined as:

$$Q_{F(B)} = \frac{\sum_i q_i |\vec{p}_i \cdot \vec{T}|^k}{\sum_i |\vec{p}_i \cdot \vec{T}|^k} \quad , \quad \vec{p}_i \cdot \vec{T} > 0 \, (\vec{p}_i \cdot \vec{T} < 0) \tag{4}$$

where $\vec{T}$ was the thrust unit vector, $q_i$ the particle charge, $\vec{p}_i$ the particle momentum and the exponent $k$ is a positive number. $Q_{F(B)}$ referred to the forward (backward) hemisphere. As the charge information is most accurate when all (or almost all) tracks are included, the track selection cuts showed in table 5 were removed when evaluating $Q_{F(B)}$, apart from

the momentum cut, which was however lowered at $0.2\,\mathrm{GeV}/c$ . Moreover any event which contained a charged particle with reconstructed momentum $> 50\,\mathrm{GeV}/c$ was discarded.

As the charge of b-quark is negative the hemisphere with lower jet charge was assigned to it. Simulated events were used to study the probability $C_b$ that this orientation of the $b$-quark was correct. The value of the exponent $k = 0.5$ was found to give the best $C_b$.

Table 7 summarizes the $C_f$ for the different quark types ($f = u, d, s, c, b$) obtained with simulated events.

| Event type | $C_f$ |
|---|---|
| $u\bar{u}$ | $0.769 \pm 0.001$ |
| $d\bar{d}$ | $0.678 \pm 0.001$ |
| $c\bar{c}$ | $0.671 \pm 0.001$ |
| $s\bar{s}$ | $0.716 \pm 0.001$ |
| $b\bar{b}$ | $0.696 \pm 0.001$ |
| $b\bar{b}$ from data | $0.687 \pm 0.007$ |

Table 7: The probabilities $C_f$ ($f = u, d, s, c, b$) obtained from simulated events. For $b\bar{b}$ events the value obtained from the data, as described in the text, is also reported.

The probabilities $C_f$ depend on several physical parameters of the simulation which are known with large uncertainties. This made a measurement of $C_b$ in real data necessary, while the Monte Carlo values of $C_{f\neq b}$ could be used, their effect on $A_{\mathrm{FB}}^{\mathrm{b\bar{b}}}$ being limited by the $B$-enrichment procedure. In previous measurements [2, 10] the determination of $C_b$ was based on the study of the high $p_t$ lepton sample, where the distributions of hemisphere charges opposite to positive and negative leptons were compared. Such procedure was strongly limited by the leptonic sample statistics, and also suffered from unwanted systematics like the mixing parameter uncertainty, the efficiency of the lepton identification and the modelling of the $b$ and $c$ semileptonic decay. To avoid such disadvantages a new method for the $C_b$ measurement has been developed, which allows to unfold the $Q_b$ and $Q_{\bar{b}}$ hemisphere charge distributions via a fit to the distributions of $Q_F + Q_B$ and $|Q_F - Q_B|$ in the $B$-tagged sample.

The analytic shapes of the $Q_b$ qnd $Q_{\bar{b}}$ distributions were taken from Monte Carlo, where a good description was found to be:

$$\begin{cases} Q_b = c_0\,[G(\mu,\sigma) + G(\alpha\mu,\alpha\sigma)] & \mu = -d\cdot A \\ & \quad with \\ Q_{\bar{b}} = c_0\,[G(\bar{\mu},\sigma) + G(\alpha\bar{\mu},\alpha\sigma)] & \bar{\mu} = d\cdot(1-A) \end{cases} \tag{5}$$

where the function $G$ represents a gaussian shape and $\alpha$ is a constant whose best value was determined to be $\alpha = 1.538 \pm 0.22$. In this way the $Q_b$ and $Q_{\bar{b}}$ distributions could be described in terms of only the three parameters $(d, \sigma, A)$ and a normalization $c_0$. The parameter $A$ simply accounts for the slight asymmetry between the positively and negatively charged tracks due to the interactions of particles with the detector material.

The $Q_F + Q_B$ and $|Q_F - Q_B|$ [1] distributions were then built up in the $B$-tagged sample, and the non-$b$ background was subtracted by taking its shape from Monte Carlo while

[1] actually a symmetrized version of $|Q_F - Q_B|$ was used

its fraction was just $(1 - P_B)$. Such distributions are plot in figure 8 *a)* and *b)* together with the estimated background. The background subtracted distributions were the best estimate of the real $Q_b + Q_{\bar{b}}$ and $|Q_b - Q_{\bar{b}}|$ ones, and were then simultaneously fitted by extracting $Q_b$ and $Q_{\bar{b}}$ from their analytic expressions with variable parameters. The best fit parameter values fully determined the $Q_b$ and $Q_{\bar{b}}$ distributions. The fitted distributions are shown in fig.8 *c)* and *d)*.

For a correct fitting it was very important to take into account the hemisphere-hemisphere charge correlation, which could be expressed in terms of a single correlation factor:

$$\rho_Q^b = \frac{\langle Q_b Q_{\bar{b}} \rangle - \langle Q_b \rangle \langle Q_{\bar{b}} \rangle}{\sigma_b \sigma_{\bar{b}}} \tag{6}$$

where $\sigma_{b(\bar{b})}$ are the standard deviations of the $Q_{b(\bar{b})}$ distributions. Both $\sigma_{b(\bar{b})}$ and $\langle Q_{b(\bar{b})} \rangle$ could be easily expressed in terms of the $(d, \sigma, A)$ parameters, and their inclusion in the fit was straightforward. $\langle Q_b Q_{\bar{b}} \rangle$ was estimated using the $\langle Q_F Q_B \rangle$ of the $B$-tagged sample, to which the non-$b$ contribution was subtracted in the form $\sum_{f \neq b} P_f \langle Q_f Q_{\bar{f}} \rangle$. The $\langle Q_f Q_{\bar{f}} \rangle$ were taken from Monte Carlo, while the $P_f$ were in the proportion given by simulation, but normalized to the $(1 - P_B)$ value. Such procedure gives $\langle Q_b Q_{\bar{b}} \rangle = -0.00494 \pm 0.00011$ where the error accounts for data and Monte Carlo statistics.

The unfolded $Q_b$ and $Q_{\bar{b}}$ distributions are shown in fig.9 for the chosen $B$-tag cut of $-log_{10} F_H^+ > 2.0$. Stability of the $C_b$ measurement with the tag was checked, as shown in figure 10. It should also be noted that the mixing effect is naturally included in the $C_b$ measurement. The measured $C_b$ value was then (at the chosen tag cut):

$$C_b = 0.6870 \pm 0.0065(stat) \pm 0.0031(syst) \tag{7}$$

where the statistical error includes not only the fit error, but also the statistical uncertainty (both from data and Monte Carlo) on $\langle Q_b Q_{\bar{b}} \rangle$. The details of the error are given in table 8 .

The systematic uncertainty coming from the tag was very small as its effect was anticorrelated between the $Q_F \pm Q_B$ and the $\langle Q_F Q_B \rangle$ background subtraction. The $P_B$ value was varied inside its estimated systematics, while the effect of varying the relative proportions of non-$b$ purities was negligible. More sizeable was the effect of varying the Monte Carlo parameters which influenced the non-$b$ hemisphere charge shapes. Such parameters are listed in tables 14 and 16 along with the range of their variation, while a procedure for the tuning of some event fragmentation parameters is described in section 3.3.3 . The variation of the $Q_f + Q_{\bar{f}}$ and $|Q_f - Q_{\bar{f}}|$ distributions, as well as the $\langle Q_f Q_{\bar{f}} \rangle$ were studied at generator level, and weighting factors were determined to apply to the fully simulated data.

The analytic shape of $Q_{b(\bar{b})}$ used for the fit was changed by varying the constant $\alpha$ by three standard deviations. Moreover, as a consistency check, the fit was repeated using just a gaussian for the $Q_{b(\bar{b})}$ shapes, and the obtained result is $C_b = 0.685 \pm 0.008\,(stat)$.

### 3.2.3 Results

The total sample of hadronic events collected at the $Z$ peak during 1994 was subjected to the event selection, $B$-enrichment and hemisphere charge determination. The charge-signed $cos\Theta$ distribution for selected events was corrected for the angular acceptance of

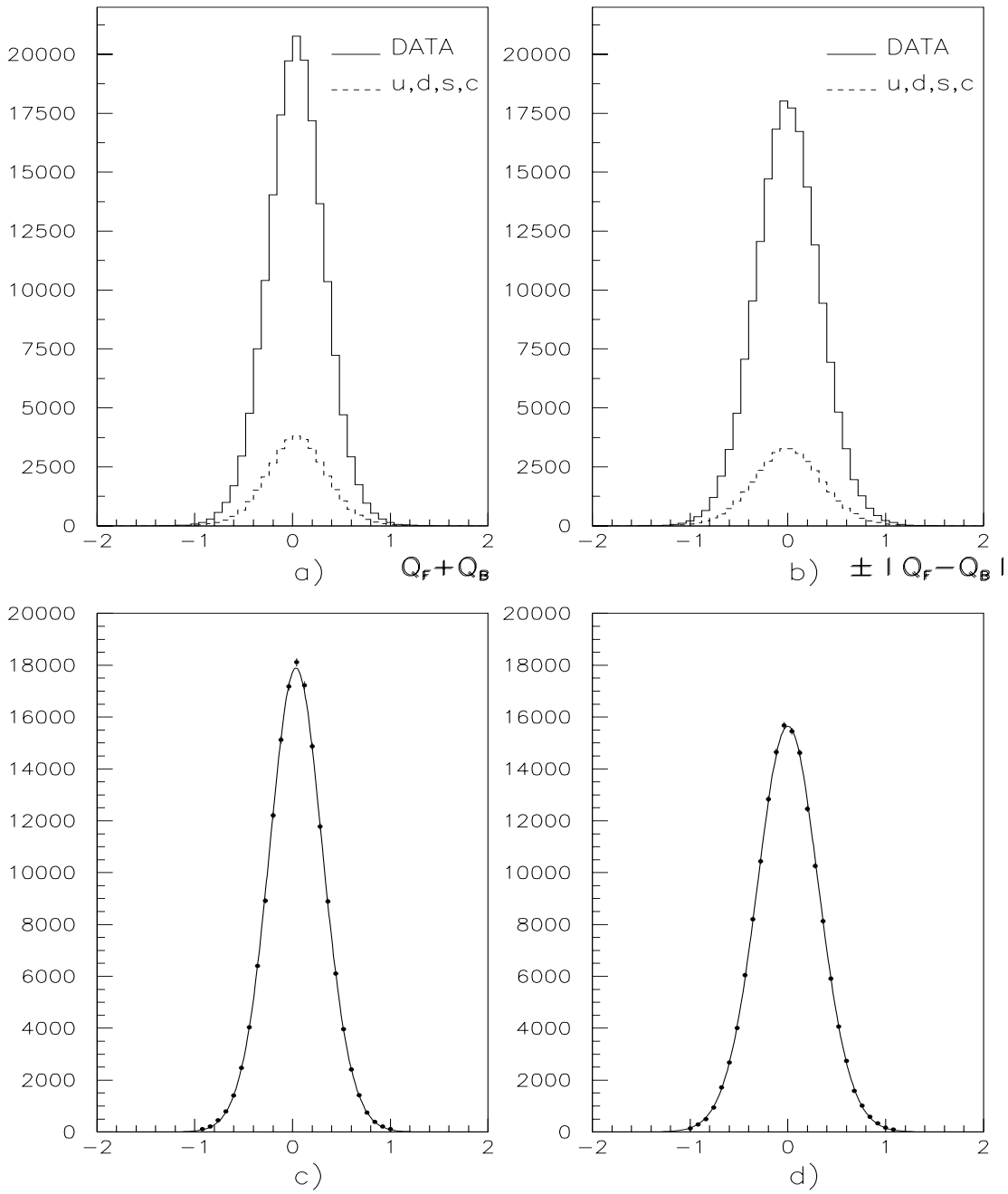


Figure 8: $Q_F + Q_B$ *a)* and a symmetrized version of $|Q_F - Q_B|$ *b)* in the $B$-tagged data sample ($b$ purity is 72.7% ), with the estimated non-$b$ background. The subtracted distributions are then shown in *c)* and *d)* where the fit result is superimposed.

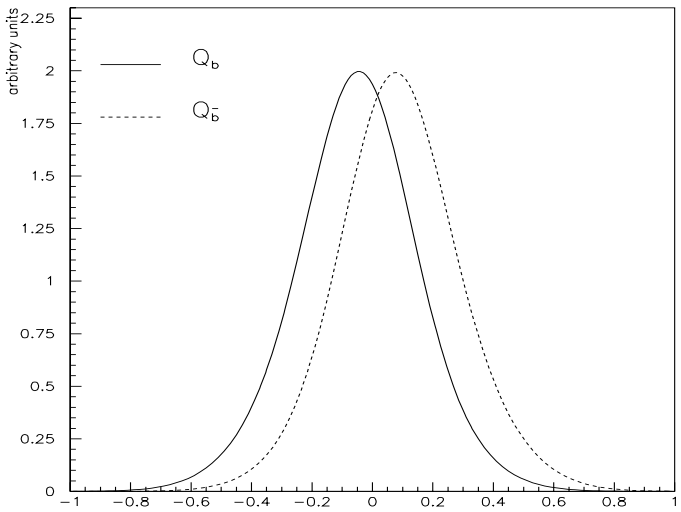


Figure 9: Unfolded $Q_b$ and $Q_{\bar{b}}$ distributions.

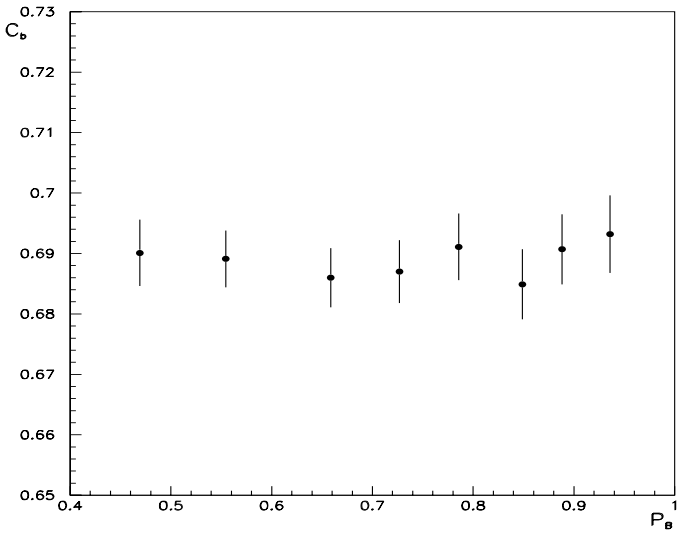


Figure 10: Fitted $C_b$ value for samples of increasing $b$-purity. All the points are statistically fully correlated.

| Error source | $\Delta C_b$ |
|---|---|
| Fit statistics | 0.0052 |
| $\langle Q_b Q_{\bar{b}} \rangle$ statistics | 0.0040 |
| tag systematics | 0.0008 |
| non-$b$ charge shapes | 0.0023 |
| $Q_{b(\bar{b})}$ analytic shapes | 0.0020 |

Table 8: Error contributions to $C_b$ measurement.

the microvertex detector and the overall acceptance of this analysis procedure by using the fraction of selected events as function of $|cos\theta_T|$. The experimental $cos\theta_T$ distribution was signed assuming that the lower (higher) hemisphere charge corresponded to the negatively (positively) charged fermion, namely:

$$cos\Theta \; = \; -sign(Q_F - Q_B) \cdot cos\theta_T$$

The distribution of $cos\Theta$ is shown in figure 11.

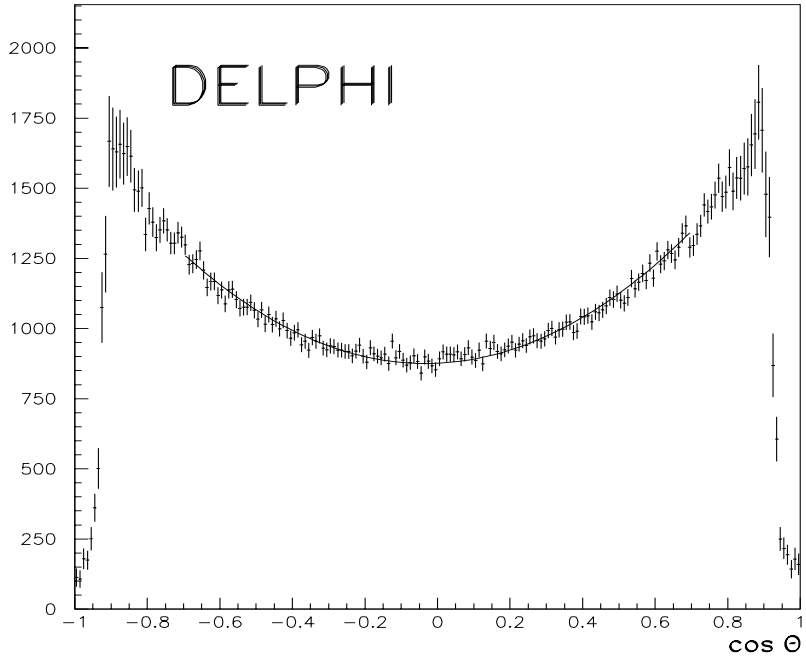


Figure 11: Fraction of selected events as function of the unsigned $cos\theta_T$

A $\chi^2$-fit was performed on this distribution over the angular region $|cos\Theta| \leq 0.70$, in the usual form

$$C \cdot \left(1 \, + \, cos\Theta^2 \, + \, \frac{8}{3} A_{FB}^{B-tag} cos\Theta\right).$$

The result was,

$$A_{FB}^{B-tag} = (2.49 \pm 0.27)\% \qquad \sqrt{s} = 91.205\,\mathrm{GeV}$$

The observed forward-backward asymmetry of the $B$-enriched sample, $A_{FB}^{B-tag}$, was a linear superposition of single $A_{FB}^{f\bar{f}}$ asymmetries weighted with the relative $B$-enrichment compositions $P_f$. *up*-quarks and *down*-quarks contributed with opposite sign to the observed asymmetry. Furthermore the probabilities $C_f$ reduced the original $A_{FB}^{f\bar{f}}$ by a factor $(2C_f - 1)$ :

$$A_{FB}^{B-tag} = \sum_f sign(-q_f) P_f (2\ C_f - 1) A_{FB}^{f\bar{f}} \tag{8}$$

The asymmetry for $b$-quark was then extracted assuming $A_{FB}^{c\bar{c}} = A_{FB}^{u\bar{u}}$ and $A_{FB}^{b\bar{b}} = A_{FB}^{d\bar{d}} = A_{FB}^{s\bar{s}}$, which in the Standard Model is violated by $b\bar{b}$ vertex corrections which are much smaller than the obtainable experimental uncertainties. It was then put $A_{FB}^{c\bar{c}} = \lambda A_{FB}^{b\bar{b}}$ and $\lambda$ was evaluated to be 0.645 using ZFITTER [18] at $\sqrt{s} = 91.205\,\mathrm{GeV}$ . By inverting the 8 the following result was then obtained:

$$A_{FB}^{b\bar{b}} = (0.0945 \pm 0.0102) \tag{9}$$

### 3.2.4 Consistency checks and systematic uncertainties

The possibility of any systematic $cos\Theta$ dependence was studied by repeating the fit in different angular regions. The results are reported in table 9. No significant variations were observed.

The analysis was repeated for different choices of the tagging probability cut ($-log_{10}F_H^+ > 1, 2.5$), for different momentum powers ($k = 0.3,\ 1.0$) in the jet charge algorithm, and for two different momentum ranges ($0.5\ \mathrm{GeV}/c < p < 50\ \mathrm{GeV}/c$ and $1\ \mathrm{GeV}/c < p < 50\ \mathrm{GeV}/c$ ) of charged particle tracks included in the hemisphere charge evaluation to check its consistency.

Several sources of systematic error were considered, they are summarized in table 11. In particular:

- Detector acceptance effect were considered by allowing the acceptance correction factors to vary within their errors. Possible variations of the acceptance correction with different flavours were also studied in Monte Carlo and found to be marginal.

- The possible dependence of $C_b$ on $cos\theta_T$, was studied allowing different values of $C_b$ for various regions of $cos\theta_T$ according to Monte Carlo.

- The statistical and systematic errors on $P_B$ were propagated on $A_{\mathrm{FB}}^{\mathrm{b\bar{b}}}$ (also through the $C_b$ measurement). A possible dependence of $P_B$ on $cos\theta_T$ was studied in Monte Carlo and found to have a negligible effect.

- The statistical uncertainties and the variation of the fit shape in the estimation of $C_b$ discussed in section 3.2.2 were propagated.

- The systematic uncertainties on $C_{f\neq b}$ due to the fragmentation parameters of the simulation were studied in the same way as done in section 3.2.2 for the $C_b$ measurement. A corelated variation of all the $C_f$ ($b$ included) were then applied to obtain the effect on $A_{\rm FB}^{\rm b\bar{b}}$ . The most important effects on $A_{\rm FB}^{\rm b\bar{b}}$ were coming from the popcorn parameter, $\Lambda_{QCD}$, $\gamma_s$ and the Peterson fragmentation parameter for charm events $\epsilon_c$.

Finally the systematic uncertainty related to the ratio $\lambda = \frac{A_{FB}^{c\bar{c}}}{A_{FB}^{b\bar{b}}}$ was negligible. The final result, at $\sqrt{s} = 91.205\,\mathrm{GeV}$ , was:

$$A_{FB}^{b\bar{b}} = 0.0945 \pm 0.0102(stat.) \pm 0.0057(syst.) \tag{10}$$

| Angular range | $A_{FB}^{B-tag}$ |
|---|---|
| $\lvert cos\Theta\rvert \leq 0.70$ | $0.0249 \pm 0.0027$ |
| $\lvert cos\Theta\rvert \leq 0.65$ | $0.0266 \pm 0.0029$ |
| $\lvert cos\Theta\rvert \leq 0.60$ | $0.0251 \pm 0.0032$ |
| $\lvert cos\Theta\rvert \leq 0.50$ | $0.0265 \pm 0.0041$ |
| $\lvert cos\Theta\rvert \leq 0.40$ | $0.0281 \pm 0.0055$ |
| $0.40 \leq \lvert cos\Theta\rvert \leq 0.55$ | $0.0227 \pm 0.0048$ |
| $0.55 \leq \lvert cos\Theta\rvert \leq 0.70$ | $0.0248 \pm 0.0041$ |

Table 9: Dependence of the asymmetry on different $cos\Theta$ intervals

| Consistency check | $A_{\rm FB}^{\rm b\bar{b}}$ |
|---|---|
| B enrichment with $-log_{10}F_H^+ > 1.0$ | $0.0921 \pm 0.0097$ |
| B enrichment with $-log_{10}F_H^+ > 2.5$ | $0.106 \pm 0.012$ |
| $Q_{Hemisphere}$ with k=0.3 | $0.102 \pm 0.010$ |
| $Q_{Hemisphere}$ with k=1.0 | $0.096 \pm 0.010$ |
| $Q_{Hemisphere}$ with k=0.5, $p > 0.5\mathrm{GeV}/c$ | $0.099 \pm 0.010$ |
| $Q_{Hemisphere}$ with k=0.5, $p > 1.0\mathrm{GeV}/c$ | $0.104 \pm 0.011$ |

Table 10: Consistency checks on $A_{\rm FB}^{\rm b\bar{b}}$ , only the statistical uncertainty is reported. The systematic uncertainties can be also very different between the various measurements.

| Source of uncertainty | $\Delta A_{\rm FB}^{\rm b\bar{b}}$ |
|---|---|
| Angular acceptance correction | 0.0011 |
| $C_b$ dependence on $cos\theta_T$ | 0.0016 |
| Statistical uncertainty on $P_B$ | 0.0004 |
| Systematic uncertainty on $P_B$ | 0.0033 |
| Statistical error from $C_b$ fit | 0.0027 |
| Stat. error from $\langle Q_b Q_{\bar{b}} \rangle$ measure | 0.0021 |
| $C_b$ fit shapes | 0.0010 |
| Fragmentation ($\epsilon_c = 0.064 \pm 0.015$) | 0.0012 |
| $\gamma_s$ $(0.26 - 0.32)$ | 0.0009 |
| Variation of $\Lambda_{QCD}$ $(250 - 400$ MeV) | 0.0006 |
| Variation of the "popcorn" parameter$(0.0 - 0.9)$ | 0.0015 |
| Other fragmentation effects | 0.0008 |

Table 11: Summary of systematic uncertainties on $A_{\rm FB}^{\rm b\bar{b}}$

### 3.2.5 Combination with previous years

The result obtained with the data collected during 1994 is compatible with those of the previous years of data taking [2, 10] with a different technique for the determination of the charge finding efficiency. The combination of all data taken at $\sqrt{s} \simeq M_Z$ from 1992 to 1994 had to take carefully into account the correlated systematics, yielding

$$A_{FB}^{b\bar{b}} = 0.1017 \pm 0.0080(stat.) \pm 0.0059(syst.) \tag{11}$$

at an average centre of mass energy of $\sqrt{s} = 91.230\,\mathrm{GeV}$ . Only a small part of the systematic error (about 0.001) is due to the mixing correction which had to be applied in the 1992 and 1993 data analysis.

## 3.3 The charge flow method

The forward-backward asymmetry for $b$-quarks ($A_{\rm FB}^{\rm b\bar{b}}$ ) can be measured using the observables charge flow and charge sum of the events which are defined as follows:

$$Q_{FB} = Q_F - Q_B \tag{12}$$
$$Q_{TOT} = Q_F + Q_B \tag{13}$$

Where the $Q_{F(B)}$ is defined as in formula 4. Except for detector influences $< Q_{TOT} >$ is expected to vanish, while $< Q_{FB} >$ is related to the various quark asymmetries:

$$< Q_{FB} >= \sum_{f=d,u,s,c,b} P_f \eta_f \delta_f A_{FB}^{f\bar{f}}. \tag{14}$$

$P_f$ is the relative fraction of a quark flavour $f$ in the hadronic event sample, $\delta_f$ is the so called charge separation that is related to the average charge flow which can be observed in the hadronic final state of quarks of type $f$.

$$< \delta_f >=< Q_{FB}(cos(\theta(f)) > 0) >= - < Q_{FB}(cos(\theta(f)) < 0) > \tag{15}$$

It depends on the charge of primary quarks and relies on details of the fragmentation and decays of unstable particles. $\eta_f$ is a correction factor depending on the details of the apparatus:

$$\eta_f = \frac{8}{3} \frac{\int_0^{cos(\theta_{max}^{thrust})} \varepsilon_f(y) y dy}{\int_0^{cos(\theta_{max}^{thrust})} \varepsilon_f(y)(1+y^2) dy} \tag{16}$$

$\varepsilon_f$ is the probability to observe an event of type $f$ at a given polar angle here defined as $cos(\theta^{thrust})$. The charge separation can be measured from the widths of the charge flow and charge sum distributions. Assuming that the observed hemisphere charge $Q_F$ for a single event can be written as sum of three independent terms:

$$Q_F = \frac{\delta_f}{2} + \frac{E_f}{2} + S_f \tag{17}$$

where $E_f$ is a non vanishing (positive) bias due to interaction of the produced hadrons in the detector material and $S_f$ is a specific (statistical) offset for a single event which cancels out for high statistics ($< S_f >=0$ ). That leads to the following formula for the average charge separation:

$$\bar{\delta}^2 = \sigma^2(Q_{FB}) - \sigma^2(Q_{TOT}) \tag{18}$$

which enters into the measurement of a combination of various charge separations on data.

$$\sum_{f=d,u,s,c,b} P_f \delta_f^2 = \bar{\delta}^2 + < Q_{FB} >^2 - < Q_{TOT} >^2 + 4 < S_f S_{\bar{f}} > \tag{19}$$

The non vanishing bias terms $E_f$ do not contribute to 19 as they do not influence the widths of the distributions. The term $< S_f S_{\bar{f}} >$ accounts for the correlation in the events which has to be present to fulfill quantum number conservation. It was taken from the simulation and is numerically small.

$$< S_f S_{\bar{f}} > = < Q_F * Q_B > + \frac{1}{4} \sum_{f=d,u,s,c,b} P_f \delta_f^2 \tag{20}$$

The three main observables $< Q_{TOT} >$,$< Q_{FB} >$ and $< Q_F * Q_B >$ which enter in formula 19 are plotted in figure 12 and base on the 94 data.

The formulae given up to this point allow each kind of quark mixture. $b$-quarks, because of their event topology, can be tagged with high efficiency and purity so it is possible to determine $\delta_b$ and $A_{\mathrm{FB}}^{\mathrm{b\bar{b}}}$ directly from data.

### 3.3.1 Measurement of the $b$-charge separation

Evaluating the $b$-charge separation while using formula 19 two different approaches can be achieved to control the influence of the light flavour background.

In the first approach formula 19 has been applied using selected events lying in an interval between two different event probabilities $F_E^+$ as defined in the first section. As the content of all intervals is uncorrelated the square of the $b$-charge separation could be obtained by fitting and extrapolating to 100% $b$-purity. The corresponding purities are measured partly from the data using the following formula which is valid for both methods:

$$b - purity(cut) = \frac{\mathcal{F}(cut) - R_c \times \epsilon_c(cut) - (1 - R_c - R_b) \times \epsilon_{uds}(cut)}{\mathcal{F}(cut)} \tag{21}$$

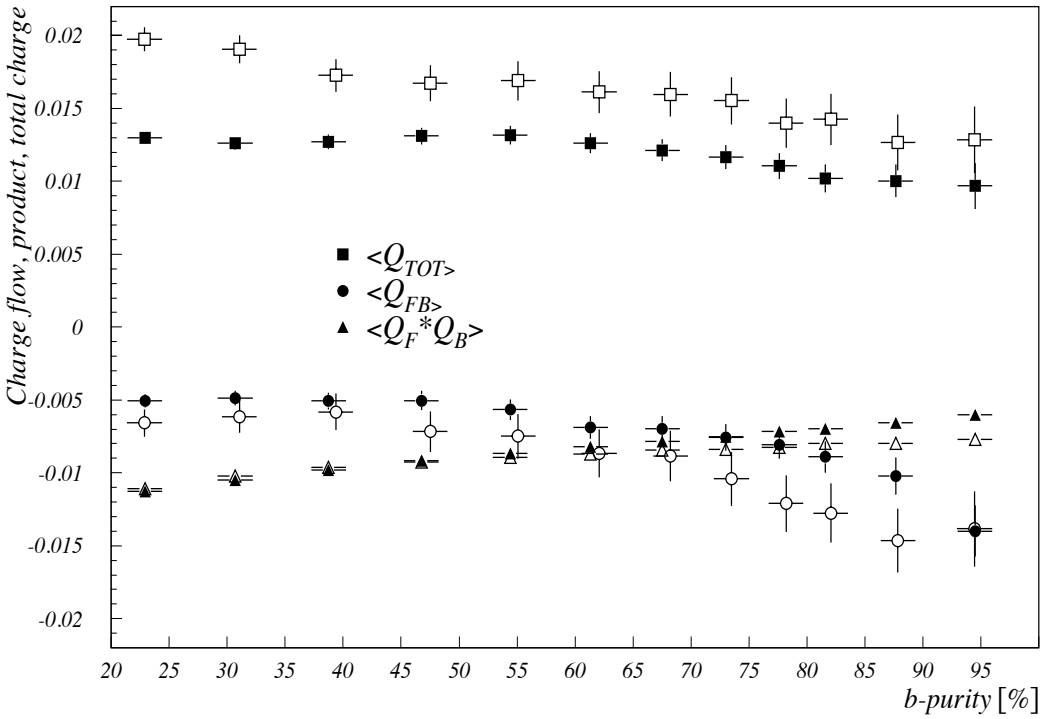


Figure 12: Measurement of the three Observables $Q_{FB}, Q_{TOT}$ and $Q_F * Q_B$ for the 94 data together with the simulation in empty symbols

Where $\mathcal{F}$ is the number of events fulfilling a given cut and normalized to all events passing the selection criteria. The selection efficiencies for the light and charm sector $\epsilon_{uds}$ and $\epsilon_c$ are obtained from the simulation. $R_c$ (0.171) is assumed to be the standard model value whereas $R_b$ (0.221) is taken from the DELPHI measurement given in [16].

In figure 13 $\bar{\delta}^2$ is shown as function of the $b$-purity separately for different years of data taking. It decreases slightly with higher $b$-fraction as expected, because the average charge separation for all quark types is bigger than for $b$-quarks alone due to the initial small $b$-quark charge. The method was checked by using the same technique on fully simulated data and the charge separation was reproduced within one standard deviation. Possible polar and azimuth angle dependencies of $\bar{\delta}^2$ were checked and found to be negligible. For the extrapolation a first order polynomial is used. The fits lead to consistent charge separations for the four data sets, see table 12.

For the second method different cut values in the event probability $F_E^+$ were used to enrich the $b$-quark events. Again the corresponding flavour fractions were taken from the simulation. In this case high $b$-purities are achieved by dropping more and more events due to increasing cut values in the probability. For the determination of the charge separation formula 19 has been rewritten:

$$|\delta_b| = \sqrt{\frac{1}{P_b}\left(\bar{\delta}^2 + < Q_{FB} >^2 - < Q_{TOT} >^2 + 4 < S_f S_{\bar{f}} > - \sum_{f=d,u,s,c} P_f \delta_f^2\right)} \qquad (22)$$

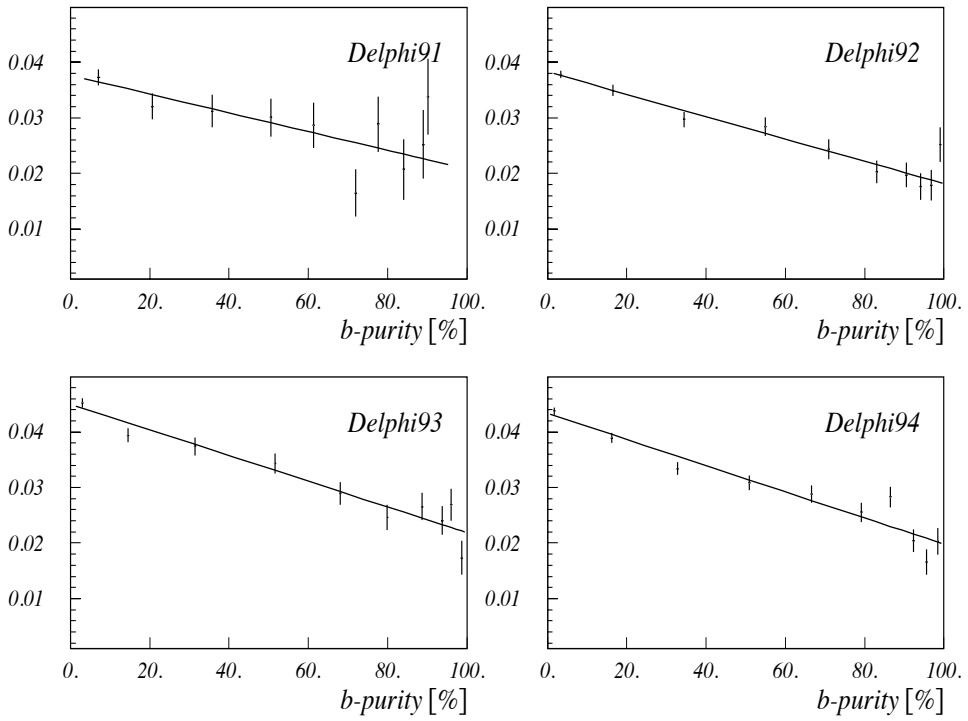


Figure 13: $\bar{\delta}^2 + < Q_{FB} >^2 - < Q_{TOT} >^2 + 4 < S_f S_{\bar{f}} >$ as function of the $b$-purity for DELPHI data 91-94

| year | $b$-charge separation $\delta_b$ | Monte Carlo input $\delta_b$ | Monte Carlo fitted $\delta_b$ |
|---|---|---|---|
| 1991 | 0.1539±0.0055±0.0055±0.0008 | 0.156±0.002 | 0.146±0.013 |
| 1992 | 0.1321±0.0041±0.0043±0.0010 | 0.156±0.002 | 0.164±0.009 |
| 1993 | 0.1480±0.0040±0.0041±0.0008 | 0.156±0.002 | 0.159±0.008 |
| 1994 | 0.1433±0.0033±0.0035±0.0015 | 0.162±0.002 | 0.164±0.010 |

Table 12: Result of fitted and extrapolated charge separation, the uncertainty is divided in three parts due to statistics, correlation and tagging separately. In addition the same procedure was applied on the Monte Carlo where the input values were reproduced.

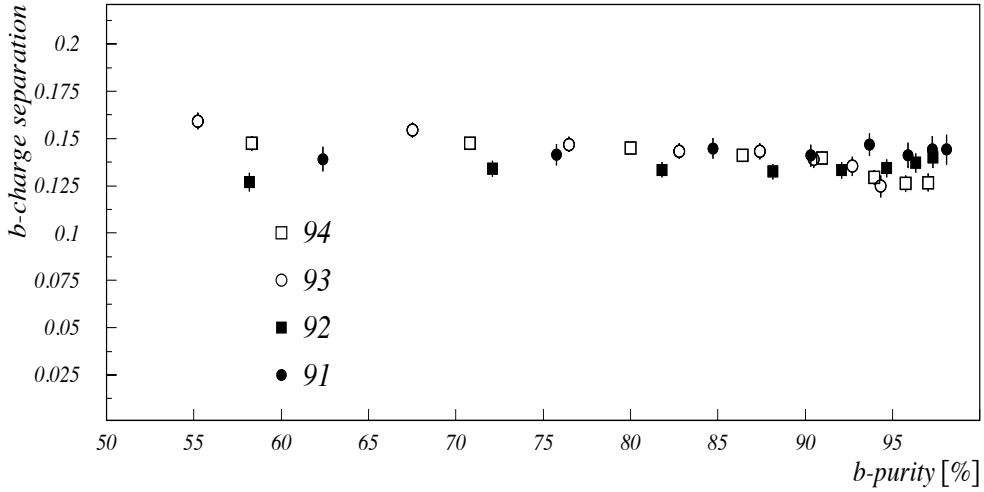


Figure 14: Charge separation for DELPHI data according to the method of background subtraction

As a crosscheck the charge separation was evaluated by using the method described in section 3.2.2 , where the $b$ and $\overline{b}$ hemisphere charge distributions are unfolded from data. For 94 data, with a $b$ tagging cut of $-log_{10}F_H^+ > 2.0$, the value $\delta_b = 0.1445 \pm 0.0040(stat.)$ was obtained, which shows that both approaches are in good agreement.

The light flavour charge separations are determined from the standard DELPHI simulation and in addition from a random walk in the parameter space of the JETSET 7.3 Monte Carlo. Details of this procedure are described in the section of systematic studies. The results of this method are given in figure 14 for a $b$-fraction above 50% and $|\delta_b|$ turns out to be stable against the variation of the $b$-purity, respectively against different cuts in the event probability.

### 3.3.2 Measurement of the $b$-Asymmetry

The weak mixing angle $\sin^2\theta_{eff}$ and the corresponding $b$-asymmetry $A_{\rm FB}^{\rm b\overline{b}}$ are obtained from the individual measurements of $\delta_b$ and $< Q_{FB} >$ using equation 14. For this mea-

surement as described above different cut values in the event probability are used to go from low to high $b$-purities. This procedure guaranties the maximal statistics but without fitting possibility due to the high correlation between adjacent bins.

Explicitly $\sin^2\theta_{eff}$ is fitted to equation 14 following the standard model description as given by the program ZFITTER [18] for the dependence between the mixing angle, the asymmetries and the partial hadronic widths. For this fit the following $\chi^2$ function was used:

$$\chi^2 = \frac{\left(Q_{FB}^{measured} - \sum\limits_{f=d,u,s,c,b} P_f \eta_f \delta_f A_{FB}^{f\bar{f}}\right)^2}{\left(\Delta Q_{FB}^{measured}\right)^2 + \Delta\left(\sum\limits_{f=d,u,s,c,b} P_f \eta_f \delta_f A_{FB}^{f\bar{f}}\right)^2} \tag{23}$$

For this fit a special version of ZFITTER was used which does not apply QCD final state corrections, because that part is included in the observables already. As the $b$-charge separation is measured from the data no mixing correction has to be applied. The results for the individual data sets are in good agreement and stable against $b$-purity variations. The results are obtained using a lifetime cut of $-log_{10}(F_E^+) = 2.5$ at a purity around 80%. The final result of the two approaches with the full systematic uncertainty at an average

| Year | $\delta_b$ by extrapolation | $\delta_b$ by background subtraction |
|---|---|---|
| 91 | 0.0882±0.0234 | 0.0966±0.0258 |
| 92 | 0.1340±0.0168 | 0.1335±0.0168 |
| 93 | 0.0988±0.0157 | 0.1001±0.0159 |
| 94 | 0.0858±0.0096 | 0.0873±0.0098 |

Table 13: Results of the two methods for the asymmetry together with statistical uncertainty.

centre of mass energy of 91.230 GeV is

$$A_{FB}^{b\bar{b}}(\delta_b(\text{by extrapolation})) = 0.0970 \pm 0.0070 \pm 0.0037 \tag{24}$$

$$A_{FB}^{b\bar{b}}(\delta_b(\text{by background sub.})) = 0.0990 \pm 0.0072 \pm 0.0038 \tag{25}$$

The results show a very good agreement between the two approaches for the measurement of the charge separation.

### 3.3.3 Systematic studies

**Systematic uncertainties of the $b$-purity evaluation**

The $b$-purity is evaluated using the tagging efficiencies for light and charm quarks from the simulation. Concerning the study of their systematics we followed the strategy applied in the measurement of $R_b$ [19].

The uncertainties of the light quark efficiency for each considered source is plotted versus the cut value as shown in figure 15. This numbers rely on the 94 simulation and the chosen working point is marked by a vertical line in the right plot. To estimate the error arising from the detector resolution an anti $b$-tag was applied ($-\log_{10}(F_E^+) \leq 0.5$). Assuming

that the difference of events fulfilling equal cuts in $-\log_{10}(F_E^-)$ gives a systematic error related to the detector resolution a corresponding $b$-purity error can be evaluated using formula 21. The production of long lived particles influences also the light quark tagging efficiency. Therefore the production rate in light quark events was changed by $\pm 10\%$ in the simulation. This range is motivated from the observed differences of these rates between data and simulation and recommended in [20]. The uncertainty of the fraction of events with gluon splitting ($g \to c\bar{c}$, $g \to b\bar{b}$) is taken into account by varying that kind of events by $\pm 50\%$, respectively.

$\epsilon_c$ is related to all properties of charm production and decays. A detailed study is described in [19] where the double tagging method depending on the hemisphere probability was used. It is assumed that the ratios between the different contributions are not dependent on changing from the hemisphere to the event probability. As a result of the $R_b$ measurement the biggest contribution to their systematic error turns out to be the $D^+$ fraction whereas the $D^0$ part has nearly no influence. As a conclusion the $(D^0 + D^+)$ fraction in $c\bar{c}$ events was varied in the simulation by $\pm 17\%$ the corresponding error on $\epsilon_c$ is shown in figure 16 as a function of $-\log_{10}(F_E^+)$ analogous to the figure 15. The individual scaling factors for the other systematic sources were evaluated and taken also into account.

As a further uncertainty the value of $R_b$ ($R_c$) was lowered by 2% (5%) which results in a -0.00012 (+0.00012) change of $A_{\mathrm{FB}}^{\mathrm{b\bar{b}}}$ .

**Systematic uncertainties of the charge separation**

The uncertainties of the light quark charge separations due to the fragmentation were estimated using the following procedure:
A analytic representation similar to a quadratic taylor expansion has been calculated for each bin of each Monte Carlo distribution used. The coefficients of this expression are determined using a linear fit to many event samples generated with JETSET 7.3 with different model parameter settings [21]. The expected Monte Carlo response for each

| JETSET 7.3 parameter and variation range | | | |
|---|---|---|---|
| Parameter | default | lower bound | upper bound |
| Lund a | 0.300 | 0.100 | 0.500 |
| Lund b | 0.750 | 0.500 | 1.000 |
| $\sigma_q$ | 0.350 | 0.250 | 0.450 |
| $\Lambda_{QCD}$ | 0.325 | 0.250 | 0.400 |
| $Q_0$ | 1.75 | 1.00 | 2.50 |

Table 14: Variation range together with default value used for the determination of the uncertainty caused by the fragmentation

distribution is then available as continuous analytic function of the model parameters. Those parameter settings which turn out to give a resonable $\chi^2$ when compared to data were further used afterwards to evaluate the charge separation. As the inclusive and event shape distributions which are primarily relevant to the determination of the general

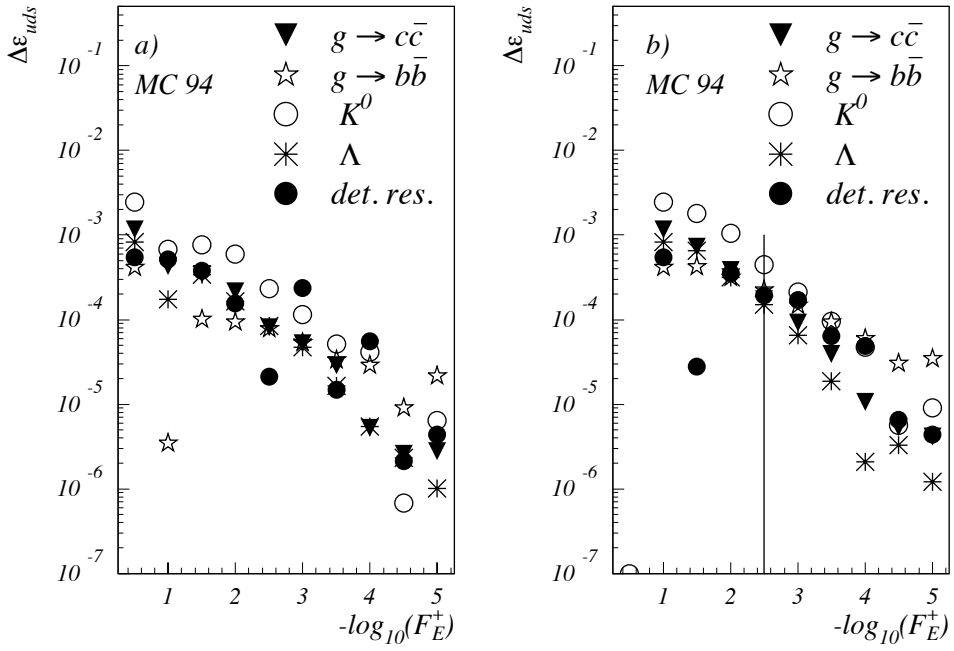


Figure 15: systematic errors on $\epsilon_{uds}$ versus $-\log_{10}(F_E^+)$ for Monte Carlo 94
a) extrapolation method, b) background subtraction method

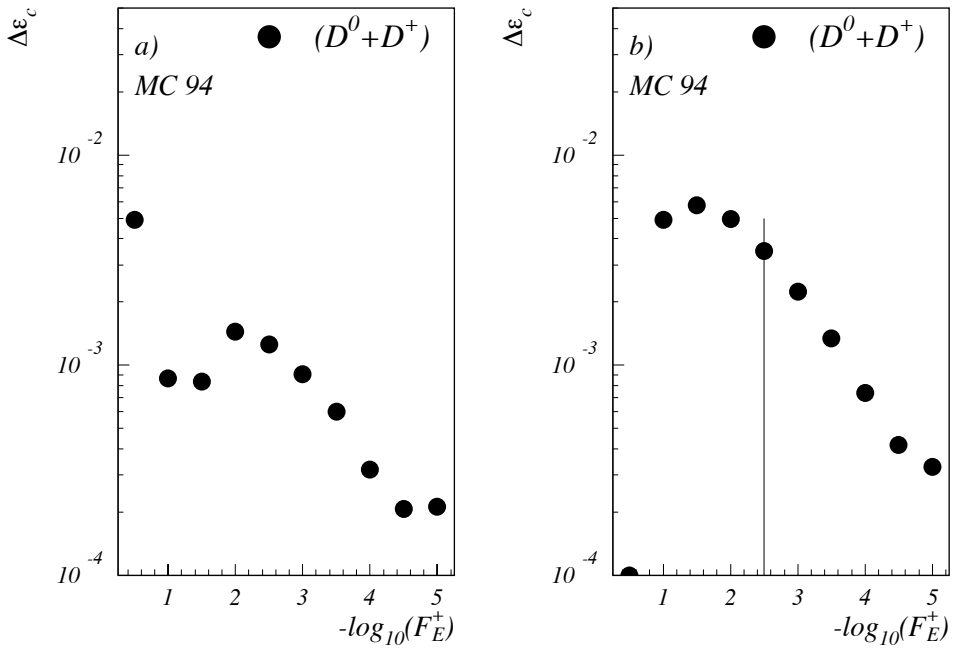


Figure 16: systematic error of $(D^0+D^+)$ fraction in charm events on $\epsilon_c$ versus $-\log_{10}(F_E^+)$ for Monte Carlo 94
a) extrapolation method, b) background subtraction method

| tuning distributions | |
|---|---|
| 1. | $N_{char}, X_p, Y_t, Pt^{in}_{thr}, Pt^{out}_{thr}, T, M, m, D_2^{durh.}$ |
| 2. | $N_{char}, X_p, Y_s, Pt^{in}_{sph}, Pt^{out}_{sph}, S, A, P, D_2^{jade}$ |
| 3. | $N_{char}, X_p, Y_t, Pt^{in}_{thr}, Pt^{out}_{thr}, T, M, m, D_{234}^{durh.}$ |
| 4. | $N_{char}, X_p, Y_s, Pt^{in}_{sph}, Pt^{out}_{sph}, S, A, P, D_{234}^{jade}$ |
| 5. | $X_p, Y_t, Pt^{in}_{thr}, Pt^{out}_{thr}, T, M, m, D_2^{durh.}$ |
| 6. | $X_p, Y_s, Pt^{in}_{sph}, Pt^{out}_{sph}, S, A, P, D_2^{jade}$ |
| 7. | $X_p, Y_t, Pt^{in}_{thr}, Pt^{out}_{thr}, T, M, m, D_{234}^{durh.}$ |
| 8. | $X_p, Y_s, Pt^{in}_{sph}, Pt^{out}_{sph}, S, A, P, D_{234}^{jade}$ |

Table 15: Distributions used for the uncertainty due to the fragmentation and for the first tuning of the Monte Carlo [21]

fragmentation parameters are precisely known these parameters have been adjusted to determine optimal charge separations. Uncertainties in particle production related parameters are only used to determine the systematic error of the charge separation. The investigation has been split in 2 parts, one related to general fragmentation parameters, see table 14 and one related to particle production, see table 16. The distributions used for calculating the $\chi^2$ are given in table 15 for the first and in table 17 for the second part of this study.

| JETSET 7.3 parameter and variation range | | | | |
|---|---|---|---|---|
| Variable | Parameter | default | lower bound | upper bound |
| $\gamma$ s | Parj(2) | 0.29 | 0.26 | 0.32 |
| P(qq/q) | Parj(1) | 0.10 | 0.08 | 0.12 |
| P(us/ud) | Parj(3) | 0.55 | 0.40 | 0.70 |
| P(1/3) Spin1 diquark | Parj(4) | 0.075 | 0.040 | 0.110 |
| Popcorn | Parj(5) | 1.100 | 0.200 | 2.000 |
| extra baryon supr. at string end | Parj(19) | 0.50 | 0.30 | 0.70 |
| $P(^1S_0)ud$ | – | 0.300 | 0.100 | 0.500 |
| $P(^3S_1)ud$ | – | 0.300 | 0.100 | 0.500 |
| $P(^1S_0)s$ | – | 0.300 | 0.100 | 0.500 |
| $P(^3S_1)s$ | – | 0.300 | 0.100 | 0.500 |

Table 16: Variation range together with default value used for the determination of the uncertainty caused by the particle parameters in the JETSET 7.3 Monte Carlo

As the value of the popcorn probability is badly known a variation between 30% and 70% of this probability has been considered and leading to an extra uncertainty. The central value of the charge separations used refers to set 3 of the tuning distributions where a large number of distributions is used and in addition the mean charged multiplicity is

| | |
|---|---|
| $\rho^{\circ}$ | DELPHI[22] |
| $\omega$ | L3[23] |
| $f_0$, $f_2$ | DELPHI[22] |
| $K^0$ | ALEPH[25], OPAL[26] |
| $K^{\pm}$ | ALEPH[24], DELPHI[28], OPAL[27] |
| $K^{*0}$ | OPAL[29] |
| $K^{*\pm}$ | ALEPH[30], DELPHI[22], OPAL[29] |
| $\Phi$ | DELPHI[28], OPAL[27] |
| $p$ | ALEPH[24],DELPHI[28] |
| $p$ | OPAL[27] |

Table 17: Overview of the identified particle data used for the JETSET fits.

| Systematic uncertainty of charge separations | | | | | | | | | | |
|---|---|---|---|---|---|---|---|---|---|---|
| flavour | central value | $\pm$ | fragmentation | $\pm$ | tuning sets | $\pm$ | particle parameters | $\pm$ | popcorn parameter | |
| $d$ | $-0.1696$ | $\pm$ | 0.0032 | $\pm$ | 0.0005 | $\pm$ | 0.0043 | $\pm$ | 0.0041 | |
| $u$ | 0.2830 | $\pm$ | 0.0044 | $\pm$ | 0.0054 | $\pm$ | 0.0052 | $\pm$ | 0.0124 | |
| $s$ | $-0.2101$ | $\pm$ | 0.0032 | $\pm$ | 0.0020 | $\pm$ | 0.0049 | $\pm$ | 0.0078 | |
| $c$ | 0.1602 | $\pm$ | 0.0015 | $\pm$ | 0.0030 | $\pm$ | 0.0041 | $\pm$ | 0.0058 | |

Table 18: Light flavour charge separations and their systematic uncertainties due to fragmentation and particle parameters used by the JETSET 7.3 (DELPHI version) program

fixed similar as in [21]. For the systematic error due to fragmentation we consider four contributions. The first systematic error determined is the RMS of the charge separation distribution cutting at twice the minimal $\chi^2$. The second refers to the variation of the central value due to the usage of the different input distributions. The third refers to the variation of the particle parameters and the fourth due to the variation of the popcorn probability. The charge separations on detector level are calculated by folding the MC generator result with the acceptance matrices obtained from a detailed simulation of the DELPHI detector. The full systematic uncertainty of the light flavour charge separation is given in table 18.

**Systematic uncertainties due to detector effects**

Uncertainties due to not perfect modeling of the DELPHI detector or interactions of particles inside the detector material were studied by varying the cut applied on their central value. The smearing due to fragmentation and experimental resolution leads to a shift of events at small angles to larger angles. This effect has been estimated from the simulation and is considered as systematic error. As the product $< Q_F * Q_B >$ in the simulation reproduces the data value only up to 15% this relative error has been assumed for the correlating term. The systematic uncertainty of the angular correction factor is

assumed to be twice the statistical error. A summary of the systematic uncertainties is given in table 19.

| Contribution | $A_{\rm FB}^{\rm b\bar{b}}$ with $\delta_b$ extra. | $A_{\rm FB}^{\rm b\bar{b}}$ with $\delta_b$ backgr. sub. |
|---|---|---|
| Event and track selection | 0.00220 | 0.00220 |
| Angular correction $d$ | 0.00014 | 0.00014 |
| Angular correction $u$ | 0.00015 | 0.00015 |
| Angular correction $s$ | 0.00013 | 0.00013 |
| Angular correction $c$ | 0.00025 | 0.00025 |
| Angular correction $b$ | 0.00070 | 0.00070 |
| Charge separation $\delta_d$ | 0.00015 | 0.00010 |
| Charge separation $\delta_u$ | 0.00017 | 0.00052 |
| Charge separation $\delta_s$ | 0.00023 | 0.00020 |
| Charge separation $\delta_c$ | 0.00043 | 0.00108 |
| Extrapolation uncertainty | 0.00090 | 0.00000 |
| Correlation | 0.00270 | 0.00270 |
| Impact resolution | 0.00015 | 0.00015 |
| Gluon splitting $g \longrightarrow c\bar{c}$ | 0.00008 | 0.00008 |
| Gluon splitting $g \longrightarrow b\bar{b}$ | 0.00012 | 0.00012 |
| $K^0$ variation | 0.00015 | 0.00015 |
| $\Lambda$ variation | 0.00007 | 0.00007 |
| $(D^0, D^+)$ fraction in $c\bar{c}$ | 0.00010 | 0.00010 |
| $D_s$ fraction in $c\bar{c}$ events | 0.00004 | 0.00004 |
| $D^0$ lifetime | 0.00003 | 0.00003 |
| $D^+$ lifetime | 0.00005 | 0.00005 |
| $D_s$ lifetime | 0.00005 | 0.00005 |
| $D$ decay multiplicity | 0.00003 | 0.00003 |
| $BR(D \longrightarrow K^0 X)$ | 0.00003 | 0.00003 |
| $R_b$ - 2% | 0.00012 | 0.00012 |
| $R_c$ - 5% | 0.00012 | 0.00012 |
| Usage of thrust axis | 0.00002 | 0.00002 |
| Resolution of thrust axis | 0.00020 | 0.00020 |

Table 19: Systematic uncertainties and their influence of the asymmetry

### 3.3.4 Final result with the charge flow approach

Two measurements of $A_{\rm FB}^{\rm b\bar{b}}$ have been obtained with the charge flow method, by adopting two different techniques for the $\delta_b$ evaluation. The two results are in very good agreement and their errors are almost equal. Although the extrapolation technique lead to slightly lower errors, the influence of the tag systematics on the extrapolation itself needs a deeper investigation, and the correlation between the different sources of uncertainty have to be better understood. For this reason it was found better to choose the second result given in 25 as the final one for this approach.

### 3.4 Final $A_{FB}^{b\bar{b}}$ result with a lifetime tag technique

Two measurements of $A_{FB}^{b\bar{b}}$ at the $Z$ resonance peak were performed with different approaches. The two results given in (11) and (25) are very well compatible with each other. Both the statistical and the systematic error are highly correlated between the two approaches, so that it was not useful to average the obtained results. The final $A_{FB}^{b\bar{b}}$ measurement with a lifetime tag technique was then chosen to be the one obtained with the charge flow approach, which gave the lowest error:

$$A_{FB}^{b\bar{b}} = 0.0990 \pm 0.0072(stat.) \pm 0.0038(syst.). \quad (26)$$

Such measurement includes all data collected by DELPHI from 1991 to 1994, at an average centre of mass energy of 91.230 GeV .

## 4 Asymmetry measurement using reconstructed D mesons

In this analysis, the forward-backward asymmetries for the processes $e^+e^- \to c\bar{c}$ and $e^+e^- \to b\bar{b}$ at the $Z$ resonance are measured using reconstructed $D$ mesons [2]. The analysis is based on about 3,037,000 events taken by the DELPHI experiment in the years from 1991 to 1994. The results presented update the analysis previously published in [31].

A $D$ meson carries a charm quark and therefore provides a clean signature of a $c$ event or a decay of a heavy $B$ meson in a $b$ event. The charge of the $D^{*+}$ is directly correlated to the charge of the primary quark.

A $D^{*+}$ is identified through its decay into $D^\circ\pi^+$, while the $D^\circ$ is reconstructed in the decay modes $K^-\pi^+$, $K^-\pi^+(\pi^\circ)$, $K^-\mu^+\nu$, $K^-e^+\nu$ and $K^-\pi^+\pi^-\pi^+$. In addition the $D^+ \to K^-\pi^+\pi^+$ decay mode and two $D^\circ$ decay modes into $K^-\pi^+$ and $K^-\pi^+(\pi^\circ)$ are used to enrich the sample. The energy of the $D$ and a topological lifetime tag for $b$ events [11] are used to separate $c$ and $b$ events. Particle identification, provided by the DELPHI Ring Imaging Cherenkov Counters (RICH) and the Time Projection Chamber (TPC), is used to reduce the combinatorial background.

After a brief explanation of the $D$ reconstruction technique and the particle identification methods, the measurements of the forward-backward asymmetries are described. The results obtained for three different centre of mass energies are compared to the Standard Model prediction.

### 4.1 Hadronic event selection

First the primary vertex is fitted from the measured tracks using a beam spot constraint. The beam spot position and its error are determined for each LEP fill. For each event the primary vertex is fitted by constraining all charged tracks to the beam spot position. This process is iterated by rejecting the tracks with the largest contribution to the overall $\chi^2$ from the primary vertex fit until $\chi^2/NDF$ is lower than 1.5.

[2] Throughout the paper charge-conjugated states are implicitly included.

The momentum resolution for tracks at small polar angles, determined using only the Forward Chambers FCA and FCB, is improved by a constrained fit to the primary vertex.

Particles satisfying the following selection criteria are used in the analysis:

- track length $> 30$ cm ,
- $20° \leq \theta_{track} \leq 160°$ ,
- momentum $p$ between 0.4 and 50.0 GeV/$c$ ,
- relative error on $p < 100\%$ ,
- impact parameters $|\Delta xy| \leq 4.0$ cm and $|\Delta z| \leq 10.0$ cm .

Here the impact parameters $\Delta xy$ and $\Delta z$ are the distances of closest approach to the primary vertex. No impact parameter cuts are applied to tracks measured by FCA and FCB only.

Events are accepted if:

- the total energy of charged particles $E_{ch} > 12\% \cdot \sqrt{s}$, where $\sqrt{s}$ is the centre of mass energy ,
- the charged particle multiplicity $n_{ch} \geq 5$ .

These selection criteria ensure a good tracking quality and agreement of DELPHI data and simulation. A sample of about 3,037,000 hadronic events at a centre of mass energy between 89 and 93 GeV has been selected from the data taken by DELPHI from 1991 till 1994, corresponding to a selection efficiency of 96%. A sample of 6,532,000 JETSET 7.3 Parton Shower [4] $Z \to q\bar{q}$ events with DELPHI modifications of $b$ and $c$ decays and a full detector simulation [6] is used in this analysis.

## 4.2 Reconstruction of $D$ Mesons Decays

Reconstructed $D$ mesons are used as a signature for $c\bar{c}$ and $b\bar{b}$ events and are identified through their decay products. The $D$ mesons are reconstructed in eight different decay modes :

- $D^{*+} \to (K^-\pi^+)\pi^+$
- $D^{*+} \to (K^-\pi^+(\pi^\circ))\pi^+$ with and without $\pi^\circ$ reconstruction
- $D^{*+} \to (K^-\pi^+\pi^-\pi^+)\pi^+$
- $D^{*+} \to (K^-e^+\nu)\pi^+$
- $D^{*+} \to (K^-\mu^+\nu)\pi^+$
- $D^+ \to K^-\pi^+\pi^+$
- $D^\circ \to K^-\pi^+$
- $D^\circ \to K^-\pi^+(\pi^\circ)$

In the following a brief description of the selection criteria for the $D$ candidates is given, a detailed description of the reconstruction method can be found in [31]. For all decay modes the selection of candidates is performed in a similar way. A number of charged particles with momentum p $>$ 1 GeV/$c$ corresponding to the multiplicity of the specific $D^{\circ/+}$ decay mode are combined, requiring the total charge to be zero in case of the $D^{\circ}$ and one in case of $D^{+}$ decays. The invariant mass $m_D$ of the $D^{\circ/+}$ candidate is calculated, assuming one of the particles to be a kaon and the others pions. In addition the kaon momentum has to exceed 2 GeV/$c$. For the semileptonic decay modes $D^{\circ} \to K^{-}e^{+}\nu$ and $D^{\circ} \to K^{-}\mu^{+}\nu$ the lepton is required to be identified, using standard DELPHI identification criteria [1]. For the reconstruction of $\pi^{\circ} \to \gamma\gamma$ decays, either $\pi^{\circ}$ with two photons merged in the HPC or two photons measured in the HPC or reconstructed from conversions are used [1, 32].

| decay mode | $\Delta L$ for $D$ [cm] | vertex probability | $D^{\circ/+}$ mass interval [GeV/$c^2$] | max.$\Delta m$ [GeV/$c^2$] | min $X_E$ |
|---|---|---|---|---|---|
| $D^{*+} \to (K^{-}\pi^{+})\pi^{+}$ | -0.05 to 2.0 | $10^{-5}$ | 1.79 to 1.94 | 0.1600 | 0.2 |
| $D^{*+} \to (K^{-}\pi^{+}(\pi^{\circ}))\pi^{+}$ | 0.0 to 2.0 | $10^{-5}$ | 1.35 to 1.75 | 0.1750 | 0.2 |
| $D^{*+} \to (K^{-}\pi^{+}\pi^{-}\pi^{+})\pi^{+}$ | 0.0 to 2.0 | $2 \cdot 10^{-2}$ | 1.83 to 1.90 | 0.1600 | 0.3 |
| $D^{*+} \to (K^{-}\pi^{+}\gamma\gamma)\pi^{+}$ | 0.0 to 2.0 | $10^{-4}$ | 1.77 to 1.94 | 0.1600 | 0.3 |
| $D^{*+} \to (K^{-}e^{+}\nu)\pi^{+}$ | 0.0 to 2.0 | $10^{-5}$ | 0.75 to 1.75 | 0.2500 | 0.2 |
| $D^{*+} \to (K^{-}\mu^{+}\nu)\pi^{+}$ | 0.0 to 2.0 | $10^{-5}$ | 0.75 to 1.75 | 0.2500 | 0.2 |
| $D^{\circ} \to K^{-}\pi^{+}$ | 0.05 to 2.0 | $\chi^2 < 25$ | 1.75 to 2.20 | - | 0.3 |
| $D^{\circ} \to K^{-}\pi^{+}(\pi^{\circ})$ | 0.05 to 2.0 | $\chi^2 < 25$ | 1.50 to 1.75 | - | 0.3 |
| $D^{+} \to K^{-}\pi^{+}\pi^{+}$ | 0.15 to 2.0 | $10^{-2}$ | 1.70 to 2.05 | - | 0.3 |

Table 20: Cuts for the $D$ selection.

A $D^{*+}$ candidate is obtained by associating a low momentum pion to the reconstructed $D^{\circ}$ meson. The charge of the pion is required to be opposite to that of the kaon from the $D^{\circ}$ decay.

For all decay modes a secondary vertex fit for the $D^{\circ/+}$ is performed and the $D^{\circ/+}$ flight distance and improved track parameters are obtained. A secondary vertex fit using the track information is performed if at least two tracks have at least one hit in the VD. Otherwise, an additional constraint is used to improve the vertex resolution, and thus the $D^{\circ/+}$ mass signal, by requiring the vertex to be in the direction of flight of the $D^{\circ/+}$ candidate as determined from the momentum vector starting at the primary vertex. This approximation is also applicable for $D^{\circ/+}$ mesons from $B$ decays, due to the low impact parameter resolution for tracks without VD information. No significant bias on the reconstructed decay length is introduced by this method. Afterwards the slow pion from the $D^{*+}$ decay is constrained to the $D^{\circ}$ vertex, which is a good approximation for the $D^{*+}$ decay vertex because of the small transverse momentum of the slow pion with respect to the direction of flight of the $D^{\circ}$.

The distance between the primary and the $D^{\circ/+}$ vertex is calculated in the $xy$ plane and projected onto the $D^{\circ/+}$ direction of flight to obtain the decay length $\Delta L$. A vertex combination is accepted if $\Delta L$ is within the range specified in table 20 for the different

decay modes. A further reduction of background is achieved by rejecting track combinations with large impact parameters $\Delta xy$ with respect to the fitted $D^{\circ/+}$ vertex. Therefore a vertex probability is obtained from the impact parameters of the tracks using the measured resolution function from the lifetime tagging of $b$-events [11]. In case of the $D^\circ \to K^-\pi^+/K^-\pi^+(\pi^\circ)$ decay without $D^{*+}$ constraint a $\chi^2$ cut is used instead. A list of cuts can be found in table 20. After this the vertex information is used to improve the track parameters and thus the invariant mass resolution.

| decay mode | cut on helicity angle $\cos\theta_H$ |
|---|---|
| $D^{*+} \to (K^-\pi^+)\pi^+$ | $\lvert\cos\theta_H\rvert < 1/3 \cdot \ln(2 \cdot X_E - 0.1) + 1$ |
| $D^{*+} \to (K^-\pi^+(\pi^\circ))\pi^+$ | $\lvert\cos\theta_H\rvert < 1/3 \cdot \ln(2 \cdot X_E - 0.1) + 1$ |
| $D^{*+} \to (K^-\pi^+\gamma\gamma)\pi^+$ | $\lvert\cos\theta_H\rvert < 1/2 \cdot \ln(2 \cdot X_E - 0.1) + 1$ |
| $D^{*+} \to (K^-\pi^+\pi^-\pi^+)\pi^+$ | $\lvert\cos\theta_H\rvert < 1/2 \cdot \ln(2 \cdot X_E - 0.1) + 1$ |
| $D^{*+} \to (K^-e^+\nu)\pi^+$ | $\lvert\cos\theta_H\rvert < 1/3 \cdot \ln(2 \cdot X_E - 0.1) + 1$ |
| $D^{*+} \to (K^-\mu^+\nu)\pi^+$ | $\lvert\cos\theta_H\rvert < 1/3 \cdot \ln(2 \cdot X_E - 0.1) + 1$ |
| $D^\circ \to K^-\pi^+$ | $\lvert\cos\theta_H\rvert < 1/2 \cdot \ln(2 \cdot X_E - 0.2) + 1$ |
| $D^\circ \to K^-\pi^+(\pi^\circ)$ | $\lvert\cos\theta_H\rvert < 1/2 \cdot \ln(2 \cdot X_E - 0.2) + 1$ |
| $D^+ \to K^-\pi^+\pi^+$ | $\lvert\cos\theta_H\rvert < 1/2 \cdot \ln(2 \cdot X_E - 0.2) + 1$ |

Table 21: Helicity angle cuts.

Cuts on the helicity angle distribution (see table 21) are used to achieve a further significant reduction of the combinatorial background. The helicity angle $\cos\theta_H$ is defined as the angle of the sphericity axis in the $D^{\circ/+}$ rest frame with respect to the $D^\circ$ direction of flight. $D^{\circ/+}$ decays are isotropic in $\cos\theta_H$, whereas the background is extremely peaked at $\cos\theta_H = \pm 1$. Due to the energy spectrum of charged particles in hadronic $Z$ events the combinatorial background is concentrated at small scaled energies $X_E(D^{*+})$. Therefore $X_E$ dependent cuts on the helicity angle are used to allow for higher background contributions at small $D^{*+}$ energies. The $X_E$ of the $D$ combination is required to exceed the limits given in table 20.

The mass bands to select the different $D^{\circ/+}$ decay modes and the cuts on the mass difference are listed in table 20. The mass differences and $D^\circ$ and $D^+$ mass distributions are shown in figures 17 and 18, respectively. The histograms show the simulated distributions normalized to the data samples. The contributions of signal and background are adjusted to compensate for different $D$ rates in data and simulation.

For the $D^+ \to K^-\pi^+\pi^+$ mode a cut of $\Delta m > 200$ MeV is used to veto $D^{*+}$ decays. The wrong sign combination for $D^\circ \to K^-\pi^+$, where the assignment of the kaon mass is used for the pion is also shown in the figure.

### 4.2.1 Particle identification

A reduction of the combinatorial background has been obtained using the particle identification provided by the barrel RICH detector and the $dE/dx$ measurement of the TPC. Due to the large number of pions in the hadronic final state, combinations in which a

pion is assigned as a kaon candidate provide the main contribution to the background. To optimize the efficiency of the $D$ signal, a pion veto, rather than a kaon identification, has been introduced.

In this analysis only the RICH gas radiator information has been used, because the relevant momentum range for kaons from $D$ decays corresponds to the gas radiator. Due to the Cherenkov thresholds for the different particles, a positive identification is not possible over the whole momentum range. Above 3 GeV/$c$, pions radiate light in the gas radiator, while the threshold for kaons is 8 GeV/$c$. Separation between kaons and pions is possible up to 20 GeV/$c$.

The different thresholds are taken into account in the calculation of the probabilities $P^{RICH}_{e,\mu,\pi,K,p}$ from the measured single photon distributions [33]. For a pion veto it is sufficient to calculate only the probabilities for pions, kaons and protons, because in the relevant momentum range the Cherenkov angle for photons from light particles (pions, muons and electrons) is almost maximal and they can all be treated as pions. A momentum independent two class separation is obtained by normalizing the probabilities for kaon and proton to the sum for kaon, proton and pion:

$$tag|_{RICH} \;=\; \frac{P^{RICH}_K + P^{RICH}_P}{P^{RICH}_K + P^{RICH}_P + P^{RICH}_\pi} \;.$$

The pion veto identification for kaons and pions taken from the decay $D^{*+} \to (K^-\pi^+)\pi^+$ is shown in figure 19. Due to the good separation quality the cut on the $tag|_{RICH}$ distribution of the kaon candidates is fixed for the whole $D^{*+}$ energy range and for all analysed decay modes:

$$tag|_{RICH} \;>\; 0.20 \;.$$

At least 70 independent TPC measurements per track are required to obtain the $dE/dx$ information. A calibration is performed to obtain a standard Gaussian distribution around the correct particle expectation for the measured $dE/dx$, normalized to its error $\sigma$ [34]. The expectation values $dE/dx|_{K/\pi}$ for kaons and pions are distinguished for momenta $p$ greater than 1.5 GeV/$c$. In this region an average separation of 1.4 standard deviations between kaons and pions is provided by the $dE/dx$ measurement. No $dE/dx$ information is used for particles below 1.5 GeV/$c$. The probability density to measure a $dE/dx$ value for a pion or a kaon is given by a Gaussian distribution around the pion or kaon expectation value:

$$P^{TPC}_{K/\pi} \;=\; e^{-\frac{1}{2}\left(\frac{\frac{dE}{dx} - \frac{dE}{dx}^{expected}\Big|_{K/\pi}}{\sigma_{dE/dx}}\right)^2} \;.$$

Here $\sigma_{dE/dx}$ is the expected error for kaons or pions, respectively. In general, light particles $(\pi, e, \mu)$ have a higher pion probability $P^{TPC}_\pi$ than kaon probability $P^{TPC}_K$, while heavy particles $(K, p)$ have a higher kaon than pion probability. For this reason, the two class separation needed for a veto is obtained by renormalizing the kaon probability density:

$$tag|_{TPC} \;=\; \frac{P^{TPC}_K}{P^{TPC}_K + P^{TPC}_\pi} \;.$$

The $K/\pi$ separation is also shown in figure 19 for a pion and an enriched kaon sample from the decay $D^{*+} \to (K^-\pi^+)\pi^+$, respectively. For all analysed decay modes, the cut

used for the kaon candidates as a veto against pions is:

$$tag|_{TPC} > 0.30 .$$

In order to reduce the background for the decay modes without $D^{*+}$ constraint, only candidates with RICH or $dE/dx$ information are considered in the sample.

## 4.3 Measurement of $A_{\rm FB}^{\rm c\bar{c}}$ and $A_{\rm FB}^{\rm b\bar{b}}$

For a measurement of $A_{\rm FB}^{\rm c\bar{c}}$ and $A_{\rm FB}^{\rm b\bar{b}}$ from the $\cos\theta$ distribution of $D$ mesons, it is necessary to separate $D$ from $c\bar{c}$ and $b\bar{b}$ events and the combinatorial background. Since the $c$ and $b$ asymmetries are expected to be of comparable size and to have the same relative sign, the statistical precision of the measurement is limited by the negative correlation between both asymmetries. In this analysis, a good separation with a relatively small correlation, is obtained by using the scaled energy distribution $X_E$ of the $D$ candidates and the topological lifetime tag probability (*bprob*) for $b$-events, based on the DELPHI Vertex Detector [11].

The hadronization of primary $c$ quarks leads to high energy $D$ mesons, whereas $b$ quarks fragment into $B$ hadrons which then decay into $D$ mesons with a softer energy spectrum. On the other hand, $b$ events can be identified due to the long lifetime of $B$ hadrons, compared to the short lifetime of $D$ mesons. Combinatorial background is concentrated at low $X_E$ and is expected to have a flat distribution of the lifetime $b$ tag probability.

The shape of the combinatorial background is tested using the sidebands in the mass (or the mass difference) distribution. Due to the different relative acceptance of $D^{*+}$ mesons and background at small and large polar angles, the fit method has to account for the $|\cos\theta|$ dependence of the different classes.

For the asymmetry measurement, partially reconstructed $D^{*+}$ mesons ($\pi_{sl} + X$) and reflections from other decay modes (see figures 17 and 18) have to be considered as signal to avoid charge correlations in the background. The contributions from reflections, where some particles from the $D$ decay are assigned to wrong mass or are missing, and true $D$ decays are treated as one class, because of the similar shape of the signals and the charge correlation with the primary quark. This leads to a significant increase of the sample for the $K^-\pi^+(\pi^\circ)$ decay mode, where about 46% of the signal originates from reflections. The rate of partially reconstructed $D^{*+}$ mesons, where a slow pion from a $D^{*+}$ decay is combined with a fake $D^\circ$ candidate which includes some particles not from the $D^\circ$ decay, depends on the branching ratio $D^{*+} \to D^\circ\pi^+$, the $D^{*+}$ production rate and the efficiency in the relevant mass difference interval. The contribution of partially reconstructed $D^{*+}$ decays to the signal is taken from the simulation and contributes to the systematic error. In case of the $D^\circ \to K^-\pi^+/K^-\pi^+(\pi^\circ)$ decay modes without $D^{*+}$ constraint the candidates with wrong mass assignments flip the sign of the estimated primary quark direction. This is taken into account in the fit.

To avoid double counting of events, only one $D$ candidate per event is retained. For $D^{*+}$ decay modes where the $D^\circ$ is completely reconstructed the candidate with a $D^\circ$ mass closest to the nominal value is used. In case of an incomplete reconstruction and for the $D^\circ$ without $D^{*+}$ constraint and the $D^+$ decay mode the candidate with the largest $\Delta$L is used. Due to this method no artificial peak is introduced in the mass difference distribution, as shown in figures 17 and 18. Events entering the signal region for the

$K^-\pi^+$ decay mode are removed from the $K^-\pi^+\pi^-\pi^+$ distribution and events from both decay modes are then removed from the $K^-\mu^+\nu$ or $K^-e^+\nu$ distribution and so forth. The number of reconstructed $D$ decays given in table 22 is obtained from the fit to the mass spectra. A total sample of 33600 reconstructed $D$ decays is used for the asymmetry measurement. The $D$ mass bands to select $D$ meson candidates are listed in table 20.

| decay mode | signal events | signal region $\Delta$m [GeV/$c^2$] | signal region m$_D$ [GeV/$c^2$] | $R_{S/B}$ |
|---|---|---|---|---|
| $D^{*+} \to (K^-\pi^+)\pi^+$ | 3870 | 0.143-0.148 | - | 0.75 $\pm$ 0.03 |
| $D^{*+} \to (K^-\pi^+(\pi^\circ))\pi^+$ | 7849 | $< 0.155$ | - | 1.16 $\pm$ 0.03 |
| $D^{*+} \to (K^-\pi^+\gamma\gamma)\pi^+$ | 2481 | 0.143-0.149 | - | 0.94 $\pm$ 0.05 |
| $D^{*+} \to (K^-\pi^+\pi^-\pi^+)\pi^+$ | 1878 | 0.143-0.149 | - | 0.96 $\pm$ 0.05 |
| $D^{*+} \to (K^-e^+\nu)\pi^+$ | 1430 | $< 0.180$ | - | 1.17 $\pm$ 0.06 |
| $D^{*+} \to (K^-\mu^+\nu)\pi^+$ | 2446 | $< 0.180$ | - | 1.12 $\pm$ 0.05 |
| $D^\circ \to K^-\pi^+$ | 4884 | - | 1.80-1.93 | 1.06 $\pm$ 0.04 |
| $D^\circ \to K^-\pi^+(\pi^\circ)$ | 6377 | - | 1.50-1.75 | 1.61 $\pm$ 0.06 |
| $D^+ \to K^-\pi^+\pi^+$ | 2360 | - | 1.83-1.91 | 1.07 $\pm$ 0.06 |

Table 22: $D$ mesons sample used for the measurement, cuts to select signal region and the relative normalization $R_{S/B}$ of signal to background.

### 4.3.1 The minimum $\chi^2$ fit

The determination of the asymmetries is achieved by a minimum $\chi^2$ fit to the $D$ samples using the scaled energy ($X_E$), the $b$ tag probability (*bprob*) and the polar angle ($\cos\theta$). Figures 20-26 compare the measured distributions for the different decay modes with the predictions of the simulation, split into charm, bottom and background events. The $D^{*+} \to (K^-e^+\nu)\pi^+$ and $D^{*+} \to (K^-\mu^+\nu)\pi^+$ samples have been added to obtain larger event samples. Also $D^{*+} \to (K^-\pi^+\pi^-\pi^+)\pi^+$ and $D^{*+} \to (K^-\pi^+\gamma\gamma)\pi^+$ decays are added for the $D^{*+} \to (K^-n\pi)\pi^+$ mode. The simulated prediction is normalized to the data to reproduce the signal to background ratio. Therefore a factor $R_{S/B}$ (see table 20) is introduced for each decay mode, which compensates for different $D^{*+}$ rates in data and simulation. After this correction a good agreement is found in all distributions. The shape of the background distribution, as obtained from the sidebands, is well reproduced by the Monte Carlo.

The lifetime $b$ tagging probability *bprob* [11] calculated from the impact parameters of all charged tracks enters into the fit using the transformation:

$$tr(bprob) = \frac{4}{4 - \ln(bprob)}.$$

Bins in the three dimensional $X_E$, $tr(bprob)$ and $\cos\theta$ space have been chosen such that each bin contains about 55 events. In each bin $i$ the differential asymmetry:

$$A_{FB}^{obs,i} = \frac{N_i^+ - N_i^-}{N_i^+ + N_i^-}$$

is calculated from the events $N_i^+$ and $N_i^-$ with $Q \cdot \cos\theta$ greater or less than zero, respectively. The observed asymmetry receives contributions from $c$, $b$ and combinatorial background. The fractions $f_{j,i}$ of $D^*$ signal and reflection from $c$ and $b$ events as well as the fractions of partially reconstructed $D$ mesons and combinatorial background are taken from the simulation. Furthermore the combinatorial background is divided into $c$, $b$ and $uds$ contributions to account for small charge correlation in the background especially for the semileptonic decay mode of the $D^\circ$

The $\chi^2$ to be minimized is given by:

$$\chi^2 = \sum_{i=1}^{N_{bins}} \frac{\left\{ A_{FB}^{obs,i} - \sum_{j=1}^{7} f_{j,i} C_{j,i} A_{FB}^{j}(\cos\theta) \right\}^2}{\sigma_i^2}$$

where $\sigma_i$ allows for the statistical error of both, data and simulation. $A_{FB}^{j}(\cos\theta)$ is the differential asymmetry:

$$A_{FB}^{j}(\cos\theta) = \frac{8}{3} A_{FB}^{j} \frac{\cos\theta}{1+\cos^2\theta},$$

of $b$, $c$ or $uds$ events. $C_{j,i}$ is the charge correlation of the class $j$. For charm signal and partially reconstructed $D$ mesons $C_{j,i} = 1$ is used. For $b$ events the mixing effect as a function of the $b$ tagging probability has to be taken into account leading to smaller values of $C_{j,i}$ and thus to a smaller observed $b$ asymmetry. The combinatorial background from $c$ and $b$ events is expected to have only very small charge correlation $C_{j,i}$ to the primary quark at large energies $X_E$. Therefore the $X_E$ and *bprob* dependence is considered in the fit. The asymmetry of the combinatorial background and $D$ mesons from gluon splitting in $uds$ events is expected to be very small. The predictions from the simulations for each bin are subtracted in the fit. The agreement of data and simulation was tested in the sidebands of the different samples where no deviations have been found.

### 4.3.2 The fit results

The comparison of data and simulation in the $X_E$, *bprob* and $\cos\theta$ distributions for the different samples is given in figure 20–26. The results of the 2 parameter fits of the $c$ and $b$ asymmetries is given in table 23. The $D^+ \to K^-\pi^+\pi^+$ decay mode is not used for the 2 parameter fit because of the marginal lifetime separation for $b$ and $c$ events as can be seen in figure 26. This sample is only used in the fit where the $b$ asymmetry is fixed to the LEP average.

Combining the results of the different samples leads to:

$$A_{\mathrm{FB}}^{\mathrm{c\bar{c}}} = 0.0752 \pm 0.0122\,(\mathrm{stat}) \quad \text{and} \quad A_{\mathrm{FB}}^{\mathrm{b\bar{b}}} = 0.0713 \pm 0.0250\,(\mathrm{stat}) \ ,$$

with a correlation coefficient of $-0.44$. The average centre of mass energy is $\sqrt{s} = 91.23$ GeV . In figure 27 the fit results for the forward-backward asymmetries of the different samples are compared to the average. The forward-backward asymmetry averaged over all samples as a function of $\cos\theta$ is shown in figure 28.

In order to reduce the error on the charm asymmetry, a one parameter fit of the constrained charm asymmetry $A_{FB}^{c,const}$ is performed. From the LEP average [35] $A_{\mathrm{FB}}^{\mathrm{b\bar{b}}} = 0.0915 \pm 0.0037$ and $A_{\mathrm{FB}}^{\mathrm{c\bar{c}}} = 0.0675 \pm 0.0091$ using prompt leptons and lifetime

| decay mode | $A_{\rm FB}^{\rm c\bar{c}}$ | $A_{\rm FB}^{\rm b\bar{b}}$ | correlation | $\chi^2/N.D.F.$ |
|---|---|---|---|---|
| $D^{*+} \to (K^-\pi^+)\pi^+$ | $0.1009 \pm 0.0309$ | $0.0671 \pm 0.0571$ | $-0.37$ | 1.20 |
| $D^{*+} \to (K^- n\pi)\pi^+$ | $0.0679 \pm 0.0280$ | $0.0930 \pm 0.0620$ | $-0.40$ | 0.91 |
| $D^{*+} \to (K^- l^+\nu)\pi^+$ | $0.0701 \pm 0.0313$ | $0.1280 \pm 0.0721$ | $-0.47$ | 1.16 |
| $D^{*+} \to (K^-\pi^+(\pi^\circ))\pi^+$ | $0.0834 \pm 0.0246$ | $0.0588 \pm 0.0478$ | $-0.44$ | 1.04 |
| $D^\circ \to K^-\pi^+$ | $0.0352 \pm 0.0367$ | $0.0424 \pm 0.0685$ | $-0.49$ | 0.94 |
| $D^\circ \to K^-\pi^+(\pi^\circ)$ | $0.0787 \pm 0.0321$ | $0.0652 \pm 0.0735$ | $-0.54$ | 1.20 |
| Average | $0.0752 \pm 0.0122$ | $0.0713 \pm 0.0250$ | $-0.44$ | |

Table 23: Fit results of the two parameter fit to the individual decay modes. The average centre of mass energy is 91.23 GeV.

| decay mode | $A_{FB}^{c,const}$ | $\chi^2/N.D.F.$ |
|---|---|---|
| $D^{*+} \to (K^-\pi^+)\pi^+$ | $0.0953 \pm 0.0288$ | 1.18 |
| $D^{*+} \to (K^- n\pi)\pi^+$ | $0.0682 \pm 0.0251$ | 0.91 |
| $D^{*+} \to (K^- l^+\nu)\pi^+$ | $0.0778 \pm 0.0282$ | 1.15 |
| $D^{*+} \to (K^-\pi^+(\pi^\circ))\pi^+$ | $0.0755 \pm 0.0215$ | 1.04 |
| $D^\circ \to K^-\pi^+$ | $0.0231 \pm 0.0318$ | 0.94 |
| $D^\circ \to K^-\pi^+(\pi^\circ)$ | $0.0725 \pm 0.0265$ | 1.20 |
| $D^+ \to K^-\pi^+\pi^+$ | $0.1098 \pm 0.0403$ | 1.05 |
| Average | $0.0734 \pm 0.0104$ | |

Table 24: Fit results of the one parameter fit to the individual decay modes.

tag, one obtains $A_{FB}^{b,const} = 0.0882 + 0.049 \cdot A_{FB}^{c,const}$ for the constrained bottom asymmetry, taking into account for this measurement a correlation of $+0.12$ between the charm and bottom asymmetry. A list of the results of one parameter fits to the individual samples is given in table 24 and also shown in figure 27.

Combining these measurements yields :

$$A_{FB}^{c,const} = 0.0734 \pm 0.0104\,(\text{stat}) \ .$$

## 4.4 Systematic errors

Differences between the signal and background efficiency as a function of $\cos\theta$ are considered in the calculation of the probabilities from the simulation. Since the asymmetry enters in the $\chi^2$ as a function of $\cos\theta$, the sensitivity to efficiency variations is small.

For all decay modes the relative normalization $R_{S/B}$ is obtained from a fit of the simulated $D$ signal and background to the data. A variation of $\pm 10\%$ is included in the systematic error, not only to account for the error of the fitted $R_{S/B}$, but also for uncertainties in the agreement of the shape of the mass difference signals in data and simulation.

The simulation is adjusted in order to reproduce the production rates and the average energy of $D$ mesons in charm and bottom events as measured by the LEP experiments

[36, 37, 38]. The systematic errors are derived taking differences between the energy spectrum in data and simulation into account. A variation of $\pm 10\%$ of the ratio of charm to bottom events is considered as the systematic error. The error due to the uncertainty of the average $D^{*+}$ energy is considered by varying the average energy fraction carried by $b$ hadrons between 0.675 and 0.715 and the average $D$ energy in $c$ events between 0.485 and 0.515.

In the simulation a $B$ lifetime $\tau_B = 1.6$ ps is used, which is in good agreement with the world average [39]. A variation between 1.45 and 1.75 ps is considered in the determination of the systematic error on the lifetime tag of $b$ events.

The systematic error due to the contribution of partially reconstructed $D$ decays is estimated by a 30% variation of the prediction of the simulation. This includes uncertainties on the efficiency to reconstruct such $\pi_{sl} + X$ combinations as well as on the total rate of $D^{*+} \to D^{\circ}\pi^{+}$ decays in hadronic $Z$ events.

The rate and charge correlation for the combinatorial background from $b$ and $c$ events is taken from the simulation. A variation of 50% has been considered in the systematic error on the asymmetry.

The asymmetry of the *uds* quark background is taken from the simulation and subtracted in the fit. The agreement between data and simulation is tested using the side bands, where good agreement is found. A 100% variation enters into the systematic error.

The $B^0 - \overline{B^0}$ mixing correction as a function of the $b$ tagging variable is taken from the simulation. Therefore the oscillation frequency $\Delta m$ was adjusted to the present world average $\Delta m = 0.500 \pm 0.033\ ps^{-1}$ [40] and the average lifetime of $B$ hadrons was set to 1.6 $ps$.

The observed oscillation in $D^{*+}$ events depends in principle on the $B \to D$ decay properties and tensor meson rates in $b$ events. Changing the tensor mesons rates and branching ratios leads to variations of 20% in the observed mixing rates inside the JETSET model, which is therefore included in the systematic error.

The systematic error due to the fit method is estimated by varying the binning of the $\chi^2$-fit to test the stability w.r.t. a change of the average number of events from 55 down to 40 and up to 85. Furthermore the results of the $\chi^2$ fit are compared to the results obtained assuming a Poissonian distribution and neglecting in both cases the error on the simulation. The observed 0.25% difference is included in the systematic error.

The error of the asymmetry due to the determination of the primary quark direction by the $D^{*+}$ direction is derived from the predictions of the JETSET model.

The error of the constrained fit of the charm asymmetry, using the LEP average on $A_{\mathrm{FB}}^{\mathrm{b\bar{b}}}$ , is obtained from the errors quoted in [35].

The contributions to the systematic errors for the combined fit of the charm and bottom asymmetries and for the constrained fit are listed in table 25. The relative sign of the systematic error indicates the direction in which the results change for a particular error source. The estimated correlation coefficient between the systematic errors of $A_{\mathrm{FB}}^{\mathrm{c\bar{c}}}$ and $A_{\mathrm{FB}}^{\mathrm{b\bar{b}}}$ in the combined fit is $-0.37$.

## 4.5 The energy dependence of the $c$ and $b$ asymmetry

Based on 165000 events taken at an average centre of mass energy $\sqrt{s} = 92.94$ GeV and 119000 events taken at $\sqrt{s} = 89.54$ GeV during 1991 and 1993 the energy dependence of the $b$ and $c$ asymmetry has been studied.

| systematic error source | mean | variation | $\delta A_{\rm FB}^{\rm c\bar{c}}$ | $\delta A_{\rm FB}^{\rm b\bar{b}}$ | $\delta A_{FB}^{c,const}$ |
|---|---|---|---|---|---|
| $(\gamma_b \cdot P_{b\to D^*})/(\gamma_c \cdot P_{c\to D^*})$ | 1.15 | $\pm 0.10$ | $\pm 0.0016$ | $\mp 0.0014$ | $\pm 0.0008$ |
| $\langle X_E \rangle_c$ | 0.502 | $\pm 0.15$ | $\mp 0.0005$ | $\pm 0.0012$ | $\pm 0.0004$ |
| $\langle X_E \rangle_b$ | 0.695 | $\pm 0.20$ | $\pm 0.0004$ | $\pm 0.0007$ | $\pm 0.0003$ |
| $\tau_b$ $[ps]$ | 1.6 | $\pm 0.15$ | $\pm 0.0008$ | $\mp 0.0008$ | $\pm 0.0008$ |
| normalization $\frac{signal}{background}$ | — | $\pm 10\%$ | $\mp 0.0024$ | $\mp 0.0030$ | $\mp 0.0036$ |
| $\pi_{slow}$,wrong sign | — | $\pm 30\%$ | $\mp 0.0022$ | $\pm 0.0025$ | $\mp 0.0012$ |
| $A_{FB}^{uds}(background)$ | — | $\pm 100\%$ | $\pm 0.0014$ | $\mp 0.0024$ | $\pm 0.0010$ |
| $A_{FB}^{b,c}(background)$ | — | $\pm 50\%$ | $\mp 0.0018$ | $\mp 0.0055$ | $\mp 0.0034$ |
| $B^\circ - \overline{B^\circ}$ mixing | — | $\pm 20\%$ | $\mp 0.0008$ | $\pm 0.0075$ | $\pm 0.0016$ |
| fit method | — | — | $\pm 0.0034$ | $\mp 0.0084$ | $\mp 0.0030$ |
| $D^*$ instead of quark direction | — | — | $\pm 0.0010$ | $\pm 0.0010$ | $\pm 0.0010$ |
| $\Delta A_{\rm FB}^{\rm b\bar{b}}$ LEP | 0.0915 | $\pm 0.0037$ | — | — | $\mp 0.0010$ |
| total | — | — | $\pm 0.0057$ | $\mp 0.0136$ | $\pm 0.0065$ |

Table 25: Contributions to the systematic errors on the measured asymmetries. The estimated correlation coefficient between the systematic errors of $A_{\rm FB}^{\rm c\bar{c}}$ and $A_{\rm FB}^{\rm b\bar{b}}$ in the combined fit is $-0.37$.

For these samples the fit method has to take into account the small statistics. Therefore a binned maximum likelihood fit was used to extract the asymmetries:

$$\mathcal{L} = -\sum_{i=1}^{N_{bins}} \left\{ \ln \frac{{\lambda_i^+}^{N_i^+}}{e^{\lambda_i^+} \cdot N_i^+!} + \ln \frac{{\lambda_i^-}^{N_i^-}}{e^{\lambda_i^-} \cdot N_i^-!} \right\}$$

where $N_i^+$ and $N_i^-$ are the measured positive and negative events in each bin. $\lambda_i^+$ and $\lambda_i^-$ are the expected number of positive and negative events calculated from simulation:

$$\lambda_i^\pm = \frac{N_i^{tot}}{2} \sum_j f_{j,i} C_{j,i} (1 \pm A_{FB}^j(\cos\theta)).$$

Here $f_{j,i}$, $C_{j,i}$ and $A_{FB}^j(\cos\theta)$ are defined like in section 4.2. The total number $N_i^{tot}$ of events per bin is an external parameter. The sum of the positive and negative likelihood

| decay mode | $A_{\rm FB}^{\rm c\bar{c}}$ | $A_{\rm FB}^{\rm b\bar{b}}$ | correlation |
|---|---|---|---|
| $D^{*+} \to (K^-\pi^+)\pi^+$ | $0.1273 \pm 0.1455$ | $-0.0788 \pm 0.2420$ | $-0.36$ |
| $D^{*+} \to (K^- n\pi)\pi^+$ | $-0.0285 \pm 0.1102$ | $-0.1669 \pm 0.2361$ | $-0.34$ |
| $D^{*+} \to (K^- l^+ \nu)\pi^+$ | $0.0400 \pm 0.1471$ | $0.3239 \pm 0.3430$ | $-0.40$ |
| $D^{*+} \to (K^-\pi^+(\pi^\circ))\pi^+$ | $0.0083 \pm 0.0927$ | $-0.0084 \pm 0.1831$ | $-0.39$ |
| $D^\circ \to K^-\pi^+$ | $0.0449 \pm 0.1787$ | $0.0122 \pm 0.3644$ | $-0.42$ |
| $D^\circ \to K^-\pi^+(\pi^\circ)$ | $-0.1774 \pm 0.1452$ | $0.3292 \pm 0.3090$ | $-0.47$ |
| Average | $0.0020 \pm 0.0518$ | $0.0194 \pm 0.1045$ | $-0.39$ |

Table 26: Fit results of the two parameter fit to the individual decay modes at an average centre of mass energy of 89.54 GeV.

| decay mode | $A_{\rm FB}^{\rm c\bar{c}}$ | | | $A_{\rm FB}^{\rm b\bar{b}}$ | | | correlation |
|---|---|---|---|---|---|---|---|
| $D^{*+} \to (K^-\pi^+)\pi^+$ | 0.0307 | $\pm$ | 0.1243 | 0.0252 | $\pm$ | 0.2398 | $-0.35$ |
| $D^{*+} \to (K^-n\pi)\pi^+$ | 0.1284 | $\pm$ | 0.1235 | $-0.0246$ | $\pm$ | 0.2701 | $-0.36$ |
| $D^{*+} \to (K^-l^+\nu)\pi^+$ | 0.0677 | $\pm$ | 0.1209 | 0.3316 | $\pm$ | 0.2696 | $-0.44$ |
| $D^{*+} \to (K^-\pi^+(\pi^\circ))\pi^+$ | 0.2181 | $\pm$ | 0.0960 | $-0.1312$ | $\pm$ | 0.1770 | $-0.40$ |
| $D^\circ \to K^-\pi^+$ | $-0.0519$ | $\pm$ | 0.1287 | 0.3272 | $\pm$ | 0.2864 | $-0.42$ |
| $D^\circ \to K^-\pi^+(\pi^\circ)$ | 0.0160 | $\pm$ | 0.0924 | 0.0662 | $\pm$ | 0.2163 | $-0.44$ |
| Average | 0.0797 | $\pm$ | 0.0453 | 0.0563 | $\pm$ | 0.0951 | $-0.40$ |

Table 27: Fit results of the two parameter fit to the individual decay modes at an average centre of mass energy of 92.94 GeV .

per bin gives a minimal contribution to the overall result if

$$N_i^{tot} = N_i^+ + N_i^-.$$

The results of the fit of the $c$ and $b$ asymmetry at average energy of $\sqrt{s} = 89.54$ GeV and $\sqrt{s} = 92.94$ GeV are listed in table 26 and 27, respectively. A comparison is also shown in figure 29. Combining the results leads to

$$A_{\rm FB}^{\rm c\bar{c}} = 0.0020 \pm 0.0518\,(\text{stat}) \pm 0.0069\,(\text{sys})$$

$$A_{\rm FB}^{\rm b\bar{b}} = 0.0194 \pm 0.1045\,(\text{stat}) \pm 0.0162\,(\text{sys})$$

at $\sqrt{s} = 89.54$ GeV , and

$$A_{\rm FB}^{\rm c\bar{c}} = 0.0797 \pm 0.0453\,(\text{stat}) \pm 0.0069\,(\text{sys})$$

$$A_{\rm FB}^{\rm b\bar{b}} = 0.0563 \pm 0.0951\,(\text{stat}) \pm 0.0162\,(\text{sys})$$

at $\sqrt{s} = 92.94$ GeV . The statistical correlation is estimated to $-0.39$ and $-0.40$, respectively. The binned Likelihood fit does not allow for the statistical error of the simulation. Using the $\chi^2$ fit the contribution of the simulation to the overall error was estimated to be $\pm 0.0038$ for $A_{\rm FB}^{\rm c\bar{c}}$ and $\pm 0.0088$ for $A_{\rm FB}^{\rm b\bar{b}}$ and is included in the systematic errors.

## 4.6 Summary of $A_{\rm FB}^{\rm c\bar{c}}$ and $A_{\rm FB}^{\rm b\bar{b}}$ results using reconstructed $D$ mesons

The forward-backward asymmetries for charm and bottom quarks at the $Z$ pole are measured simultaneously from a fit to the polar angle, scaled energy and lifetime tag distributions of 33,600 $D$ mesons, which yields for the $c$ asymmetry :

$$A_{\rm FB}^{\rm c\bar{c}} = 0.0020 \pm 0.0518\,(\text{stat}) \pm 0.0069\,(\text{sys}) \quad \text{at} \quad \sqrt{s} = 89.54 \text{ GeV}$$

$$A_{\rm FB}^{\rm c\bar{c}} = 0.0752 \pm 0.0122\,(\text{stat}) \pm 0.0057\,(\text{sys}) \quad \text{at} \quad \sqrt{s} = 91.23 \text{ GeV}$$

$$A_{\rm FB}^{\rm c\bar{c}} = 0.0797 \pm 0.0453\,(\text{stat}) \pm 0.0069\,(\text{sys}) \quad \text{at} \quad \sqrt{s} = 92.94 \text{ GeV}$$

and for the $b$ asymmetry:

$$A_{\rm FB}^{\rm b\bar{b}} = 0.0194 \pm 0.1045\,(\text{stat}) \pm 0.0162\,(\text{sys}) \quad \text{at} \quad \sqrt{s} = 89.54 \text{ GeV}$$

$$A_{\rm FB}^{\rm b\bar{b}} = 0.0713 \pm 0.0250\,(\text{stat}) \pm 0.0136\,(\text{sys}) \quad \text{at} \quad \sqrt{s} = 91.23 \text{ GeV}$$

$$A_{\rm FB}^{\rm b\bar{b}} = 0.0563 \pm 0.0951\,(\text{stat}) \pm 0.0162\,(\text{sys}) \quad \text{at} \quad \sqrt{s} = 92.94 \text{ GeV}$$

The total correlation coefficient between $A_{\rm FB}^{\rm c\bar{c}}$ and $A_{\rm FB}^{\rm b\bar{b}}$ at $\sqrt{s} = 91.23$ GeV is $-0.34$. Constraining the $b$ asymmetry to the present LEP average [35], the charm asymmetry at $\sqrt{s} = 91.23$ GeV is determined to be:

$$A_{FB}^{\rm c,const} = 0.0734 \pm 0.0104\,(\text{stat}) \pm 0.0065\,(\text{sys})\ .$$

# 5 conclusion

| Method | Asymmetry | Energy in GeV | Value | Errors Sta. | Sys. |
|---|---|---|---|---|---|
| Leptons | $A_{\rm FB}^{\rm b\bar{b}}$ | 89.43 | 0.062 | $\pm$ 0.038 | $\pm$ 0.002 |
| | | 91.23 | 0.1049 | $\pm$ 0.0076 | $\pm$ 0.0038 |
| | | 93.02 | 0.147 | $\pm$ 0.035 | $\pm$ 0.007 |
| | $A_{\rm FB}^{\rm c\bar{c}}$ | 91.23 | 0.084 | $\pm$ 0.014 | $\pm$ 0.013 |
| Ch-flow | $A_{\rm FB}^{\rm b\bar{b}}$ | 91.23 | 0.0990 | $\pm$ 0.0072 | $\pm$ 0.0038 |
| $D^*/D$ | $A_{\rm FB}^{\rm c\bar{c}}$ | 89.54 | 0.002 | $\pm$ 0.052 | $\pm$ 0.007 |
| | | 91.23 | 0.075 | $\pm$ 0.012 | $\pm$ 0.006 |
| | | 92.94 | 0.080 | $\pm$ 0.045 | $\pm$ 0.007 |
| | $A_{\rm FB}^{\rm b\bar{b}}$ | 89.54 | 0.019 | $\pm$ 0.105 | $\pm$ 0.016 |
| | | 91.23 | 0.071 | $\pm$ 0.025 | $\pm$ 0.014 |
| | | 92.94 | 0.056 | $\pm$ 0.095 | $\pm$ 0.016 |
| Combined results | $A_{\rm FB}^{\rm b\bar{b}}$ | 89.55 | 0.062 | $\pm$ | 0.036 |
| | | 91.26 | 0.1006 | $\pm$ | 0.0062 |
| | | 92.94 | 0.139 | $\pm$ | 0.035 |
| | $A_{\rm FB}^{\rm c\bar{c}}$ | 89.55 | -.004 | $\pm$ | 0.049 |
| | | 91.26 | 0.0747 | $\pm$ | 0.0103 |
| | | 92.94 | 0.066 | $\pm$ | 0.043 |

Table 28: *Summary of the different heavy quarks asymmetries presented in this note. This results have been obtained with the DELPHI data samples collected between 1991 and 1994.*

Using three independent approaches, the forward-backward asymmetries of the heavy quarks $b$ and $c$ have been measured at 3 energies near the $Z$ pole. A summary of the results presented in this note can be found table 28. The combined results, taking into account the statistical and systematical correlations between the different measurements, are included in table 28. To obtain this combined asymmetries a fit to the DELPHI heavy flavour data has been performed. This fit include all the quoted asymmetry from this note , $R_b$ [3] from ref. [19] and $b \to l$ , $b \to c \to l$ , $\chi$ from [42]. A comparison between the measured asymmetries and the Standard Model prediction at different energies for $m_{top}$ = 174 GeV/$c^2$ , $m_{Higgs}$= 300 GeV/$c^2$ and $\alpha_2$=0.123 is given figure 30.

Following ref.[9] the usual corrections have been applied to the combined results and give the bare asymmetries :

$$A_{\rm FB}^{\circ,b} = 0.1066 \pm 0.0064 \to \sin^2\theta_{eff}^{lep} = 0.2309 \pm 0.0011$$

$$A_{\rm FB}^{\circ,c} = 0.0814 \pm 0.0104 \to \sin^2\theta_{eff}^{lep} = 0.2297 \pm 0.0024$$

with a negligible correlation between $A_{\rm FB}^{\circ,b}$ and $A_{\rm FB}^{\circ,c}$ ( = 0.003 ).

[3] the value of $R_c$ has been left to its Standard Model value of .171

Good agreement with recent results from other experiments using the same methods [37, 38, 41] is found.
The 2 values obtained for $\sin^2\theta^{lep}_{eff}$ are compatible and can be combined :

$$\sin^2\theta^{lep}_{eff} = 0.2306 \pm 0.0010$$

This result is in good agreement with the effective electroweak mixing angle derived from several measurements at LEP and SLC [9].

## Acknowledgements

We are greatly indebted to our technical collaborators and to the funding agencies for their support in building and operating the DELPHI detector, and to the members of the CERN-SL Division for the excellent performance of the LEP collider.

# References


[1] DELPHI collaboration, P..Abreu et al. *Performance of the DELPHI Detector* DELPHI 95-112 PHYS 547
EPS-HEP 95 Ref eps0764.

[2] DELPHI collaboration, P.Abreu et al. Z.Phys **C 65** (1995) 569.

[3] DELPHI collaboration, P.Abreu et al.
*Measurement of the Forward-Backward asymmetry of* $e^+e^- \to Z \to b\bar{b}$ *using prompt leptons*
DELPHI 94-107 PHYS 424
EPS-HEP 94 Ref gls0230

[4] T.Sjöstrand, Comp. Phys. Comm. **39** (1986) 347;
T.Sjöstrand and M.Bengtsson, Comp. Phys. Comm. **43** (1987) 367;
T.Sjöstrand: JETSET 7.3 manual, preprint CERN-TH6488/92 (1992).

[5] C.Peterson et al.,Phys. Rev. **D27** (1983) 105.

[6] DELSIM Reference Manual, DELPHI 87-98 PROG 100, Geneva, 1989.

[7] JADE Collaboration, Z. Phys. **C33** (1986) 23; JADE Collaboration, Phys. Let. **B213** (1988) 235.

[8] DELPHI collaboration, P.Abreu et al. Zeit. für Phys. **C56** (1992) 47.

[9] LEP Electroweak Working group *A combination of preliminary LEP electroweak results for the 1995 winter conferences* , DELPHI 95-37 PHYS 482 .

[10] T.Baroncelli et al., *New measurement of the forward-backward Asymmetry in* $Z \to b\bar{b}$ *events using a lifetime tag and the jet charge algorithm*, DELPHI note 95-27 PHYS 478

[11] ALEPH Collaboration, D.Buskulic et al., Phys.Lett. **B313** (1993) 535.

[12] G.V.Borisov, Lifetime tag of events $Z^0 \to b\bar{b}$ with the DELPHI detector. AABTAG program. , DELPHI note 94-125

[13] DELPHI collaboration, P.Abreu et al., CERN-PPE/94-131

[14] N. Bingefors et al. CERN–PPE/92-173, submitted to Nucl. Instr. and Meth.

[15] The Delphi Silicon Strip Microvertex Detector with Double Sided Readout, DELPHI 94-87 PHYS 404, submitted to the Glasgow conference

[16] DELPHI Collaboration, CERN-PPE/95-08

[17] J.Berge et al., Nucl.Phys. **B184** (1981) 13-30
JADE collaboration, *A measurement of the charge asymmetry of hadronic events in electron positron annihilation*, DESY 88-154.

[18] D.Bardin et al. Z.Phys **C44** (1989) 493; Nucl. Phys. **B351** (1991) 1; Phys. Lett. **B229** (1989) 405; Phys Lett **B255** (1991) 290
D.Bardin et al. ZFITTER, an Analytical Program for Fermion Pair Production in $e^+e^-$ Annihilation, CERN-TH 6443/92 , May 1992.

[19] DELPHI Collaboration, P.Abreu et al. *Measurement of the partial decay width* $R_b = \Gamma_{b\overline{b}}/\Gamma_{had}$ *with the DELPHI detector at LEP*
DELPHI 95-89 PHYS 524 , EPS-HEP 95 Ref. eps0570

[20] The LEP Electroweak Working Group, ALEPH Note 94-30, DELPHI 94-23 Phys 357, L3 Note 1577, OPAL Technical Note TN213, 28 February, 1994;
The LEP Electroweak Working Group, ALEPH Note 94-90, DELPHI 94-23 Phys 357/add, L3 Note 1613, OPAL Technical Note TN237, 10 June, 1994.

[21] K. Hamacher , M. Weierstall Tuning and Test of Fragmentation Models Based on Identified Particles and Precision Event Shape Data DELPHI 95-80 PHYS 515, BUGH Wuppertal WUB 95-07

[22] DELPHI Coll., P. Abreu et al., Z. Phys. C65 (1995) 587

[23] L3 Coll., Y. Pei, talk given at the CERN PPE Seminar

[24] ALEPH Coll., D. Busculic et al., CERN-PPE/94-201, submitted to Z. Phys. C.

[25] ALEPH Collaboration, Production of $K^\circ$ and $\Lambda$ in Hadronic Z Decays, CERN - PPE / 94-74, submitted to Z. Phys. C.

[26] OPAL Coll., R. Akers et al., CERN-PPE 95-24 (1995), submitted to Z. Phys. C.

[27] OPAL Coll., R. Akers et al., Z. Phys. C.63 (1994) 181

[28] DELPHI Coll., P. Abreu et al., Nucl. Phys. B444 (1995) 3

[29] OPAL Coll., Inclusive strange vector and tensor meson production in hadronic Z0 decays, preliminary results presented at ICHEP94 Glasgow.

[30] ALEPH Coll., preliminary results presented at ICHEP94 Glasgow, GLS0548. Holger Hepp (ALEPH Coll.), Inklusive Produktion von geladenen $K^*$-Mesonen in hadronischen Z-Zerfällen, Diplomarbeit, HD-IHEP 93-04.

[31] DELPHI Collaboration, P.Abreu et al., Z. Phys. **C66** (1995) 341

[32] M.Feindt, O.Podobrin, M.Wielers, *Measurement of Inclusive* $\pi^\circ$ *Production in* $Z^\circ$ *decays*, DELPHI Note 94-81 PHYS 398, Geneva 1994

[33] W.Adam et al., *The Ring Imaging Cherenkov Detectors of DELPHI*, DELPHI Note 95-9 RICH 65, Geneva 1995

[34] J.Dahm, M.Elsing, M.Reale, *Calibration of the DELPHI dE/dx for 1991 F and 1992 D data*, DELPHI Note 95-48 TRACK 81, Geneva 1995

[35] The LEP Collaborations ALEPH, DELPHI, L3 and OPAL and the LEP Electroweak Working Group, *Combined Preliminary Data on Z Parameters from LEP Experiments and Constraints on the Standard Model*, CERN-PPE/94-187, Geneva 1994.

[36] DELPHI Collaboration, P.Abreu et al., Z. Phys. **C59** (1993) 533

[37] ALEPH Collaboration, D Buskulic et al., Z. Phys. **C62** (1994) 1

[38] OPAL Collaboration, R.Akers et al., Z. Phys. **C60** (1993) 601

[39] P. Roudeau, *Heavy Flavours - strong interactions*, talk given at the 27th International Conference on High Energy Physics, Glasgow, 1994

[40] R. Forty, *CP violation and $B\bar{B}$ mixing*, talk given at the 27th International Conference on High Energy Physics, Glasgow, 1994

[41] ALEPH Collaboration, D.Buskulic et al., Z. Phys. **C62** (1994) 179
ALEPH Collaboration, D.Buskulic et al., Phys. Lett. **B335** (1994) 99
L3 Collaboration, O.Adriani et al., Phys. Lett. **B335** (1994) 542
OPAL Collaboration, R.Akers at al., Z. Phys. **C60** (1993) 199

[42] DELPHI Collaboration, P.Abreu et al. , Z.phys **C66** (1995) 323

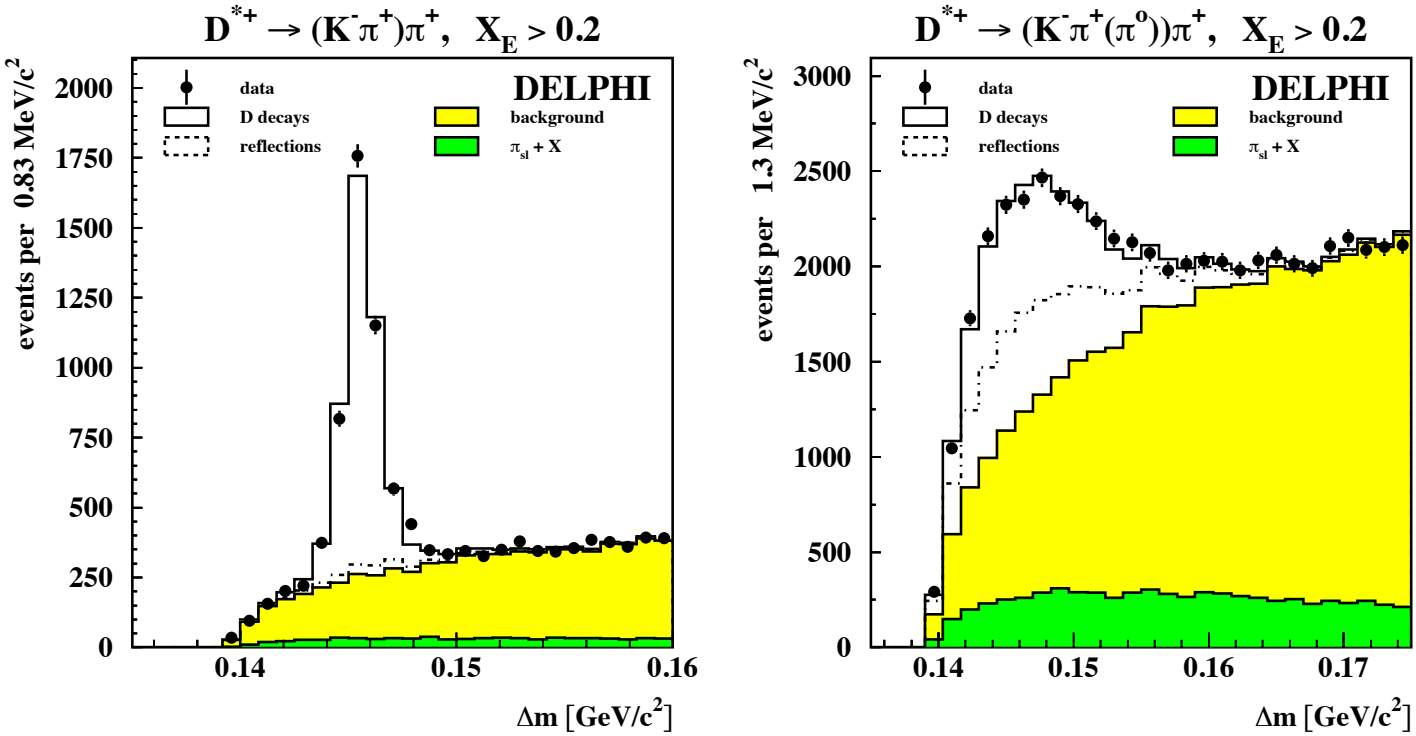


Figure 17: The mass difference distributions $\Delta m$ for the different decay modes. $\Delta m$ is defined as the difference between the mass of the $D^{*+}$ and the $D^{\circ}$ candidate. The data are compared to the simulation. Contributions from reflections, partially reconstructed $D^{*+}$ decays ($\pi_{sl} + X$) and combinatorial background are also shown. See section 4.3 for the discussion of these contributions

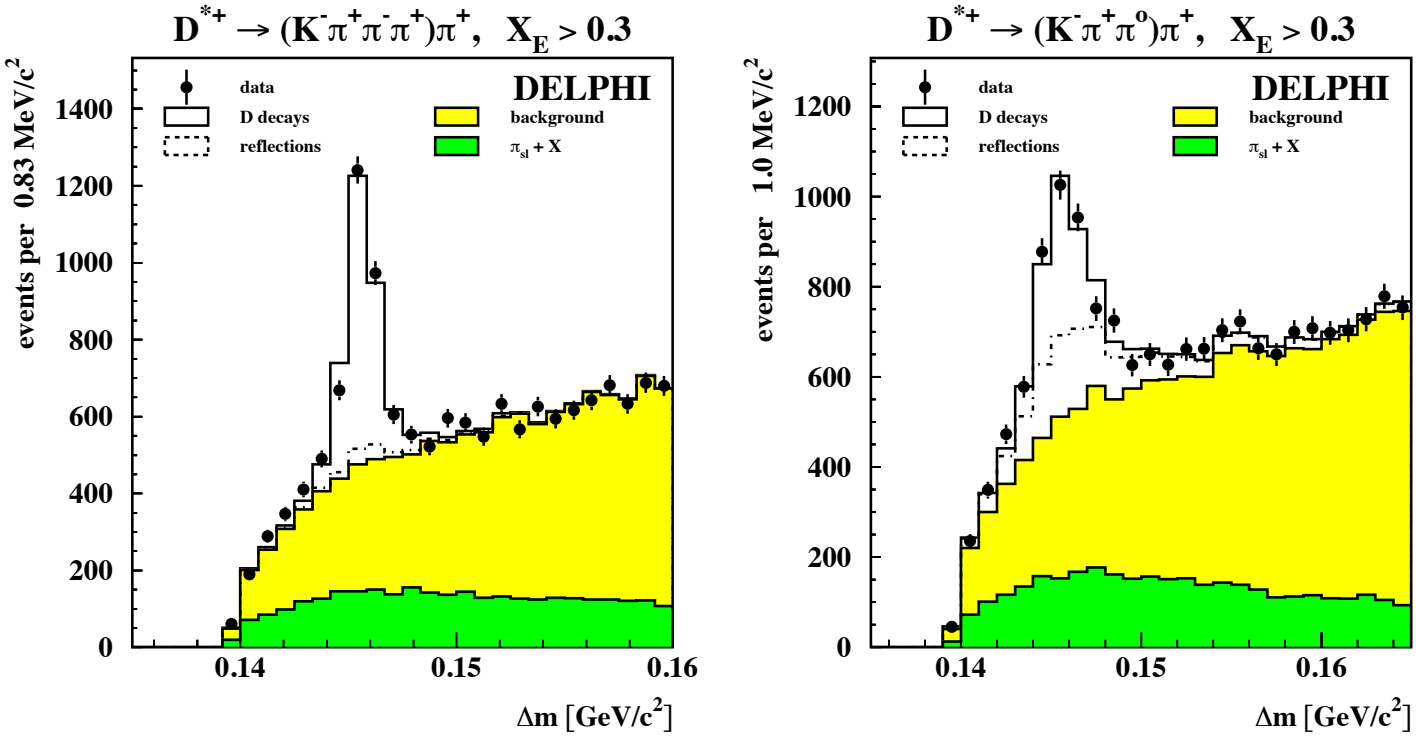

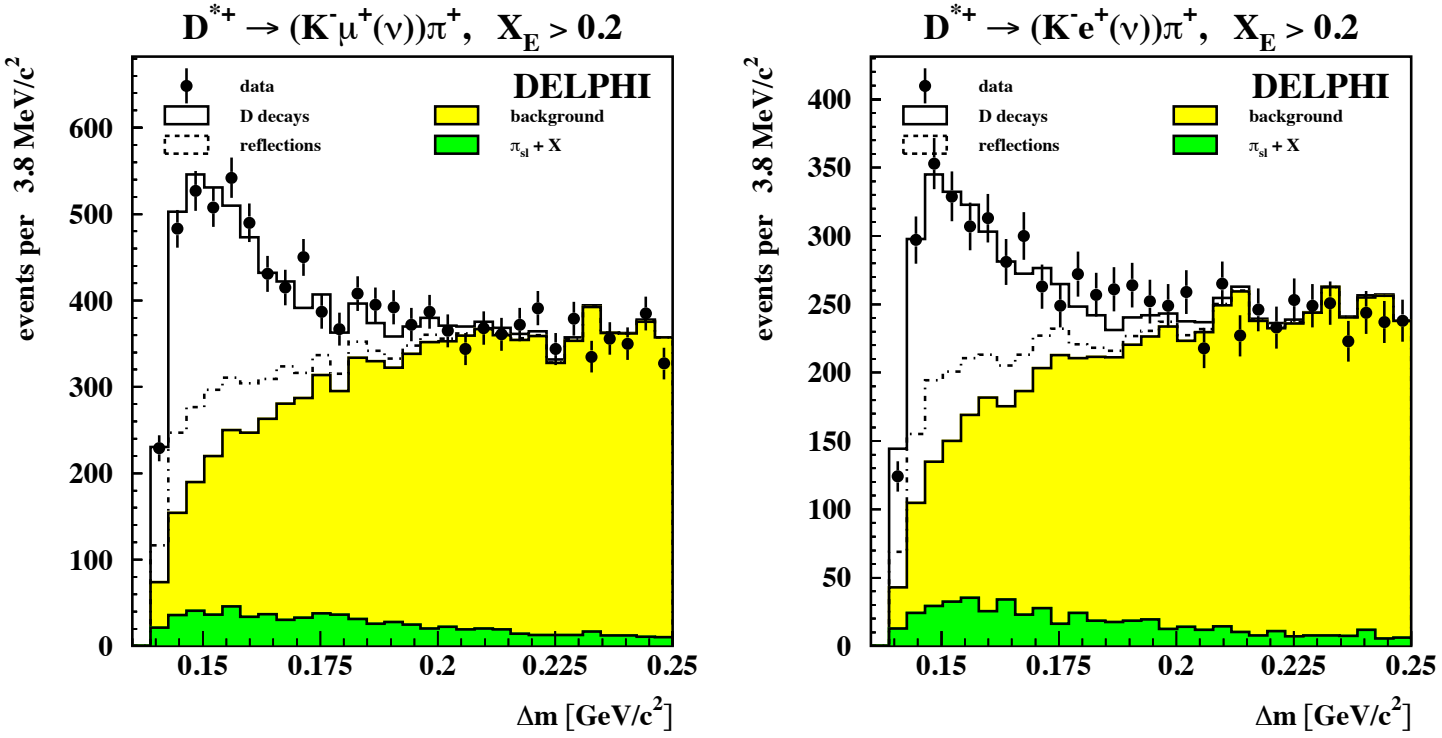


Figure 18: The mass difference distributions $\Delta$m for the semileptonic decay modes are shown above. $\Delta$m is defined as the difference between the mass of the $D^{*+}$ and the $D^\circ$ candidate. The data are compared to the simulation. Contributions from reflections, partially reconstructed $D^{*+}$ decays and combinatorial background are also shown. The picture below shows the $D^\circ$ and $D^+$ mass distributions. For the $D^\circ$ the background composition of candidates with wrong mass assignment is also shown.

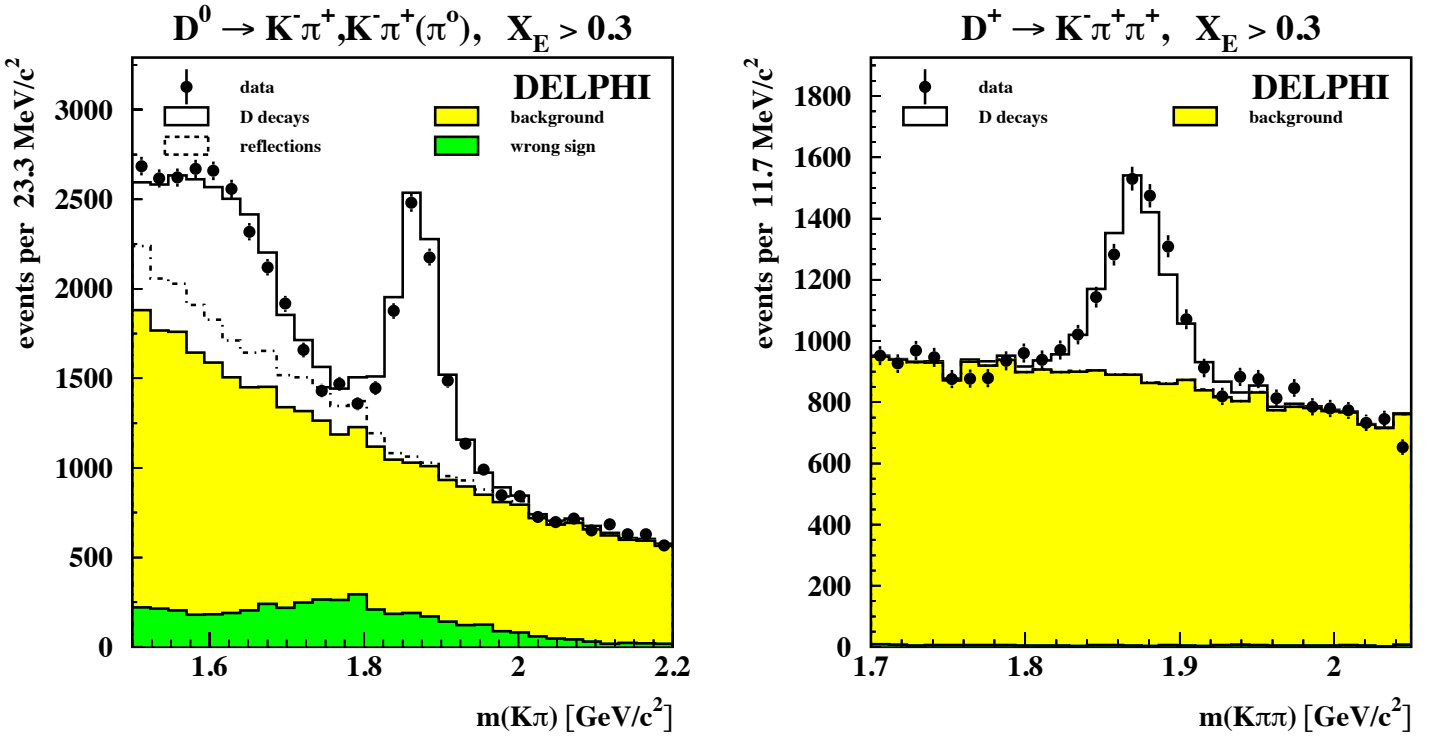

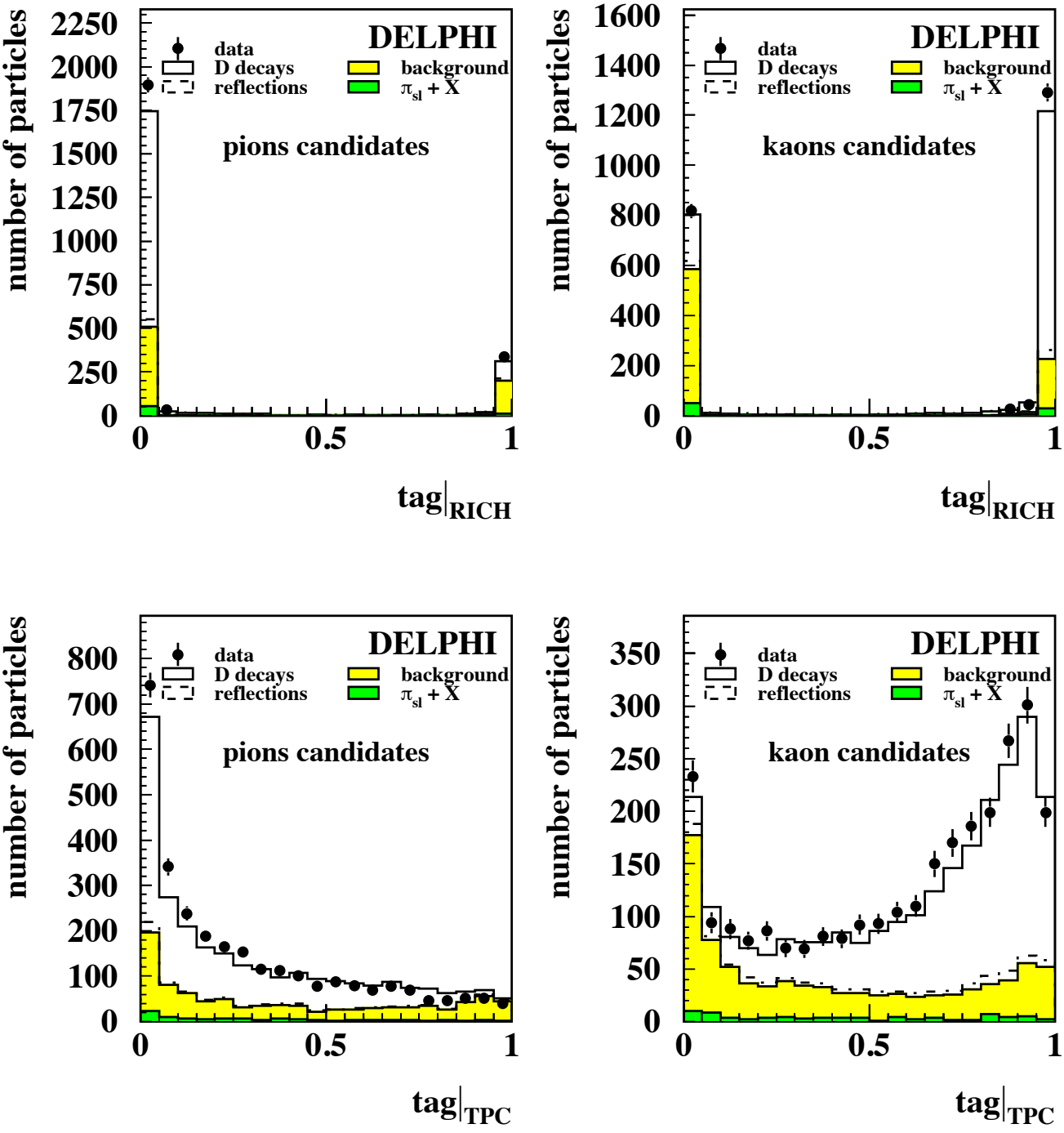


Figure 19: Distributions of the probabilities for $K^{\pm}$ and $\pi^{\pm}$ candidates from $D^{\circ} \to K^{-}\pi^{+}$ in $D^{*+} \to D^{\circ}\pi$ decays. The upper plots show the distributions as obtained from the RICH, below the corresponding distributions from the $dE/dx$ measurement of the TPC. The dots represent the data points and the solid lines refer to the different sample components. See section 3 for the definition of $tag_{|RICH}$ and $tag_{|TPC}$.

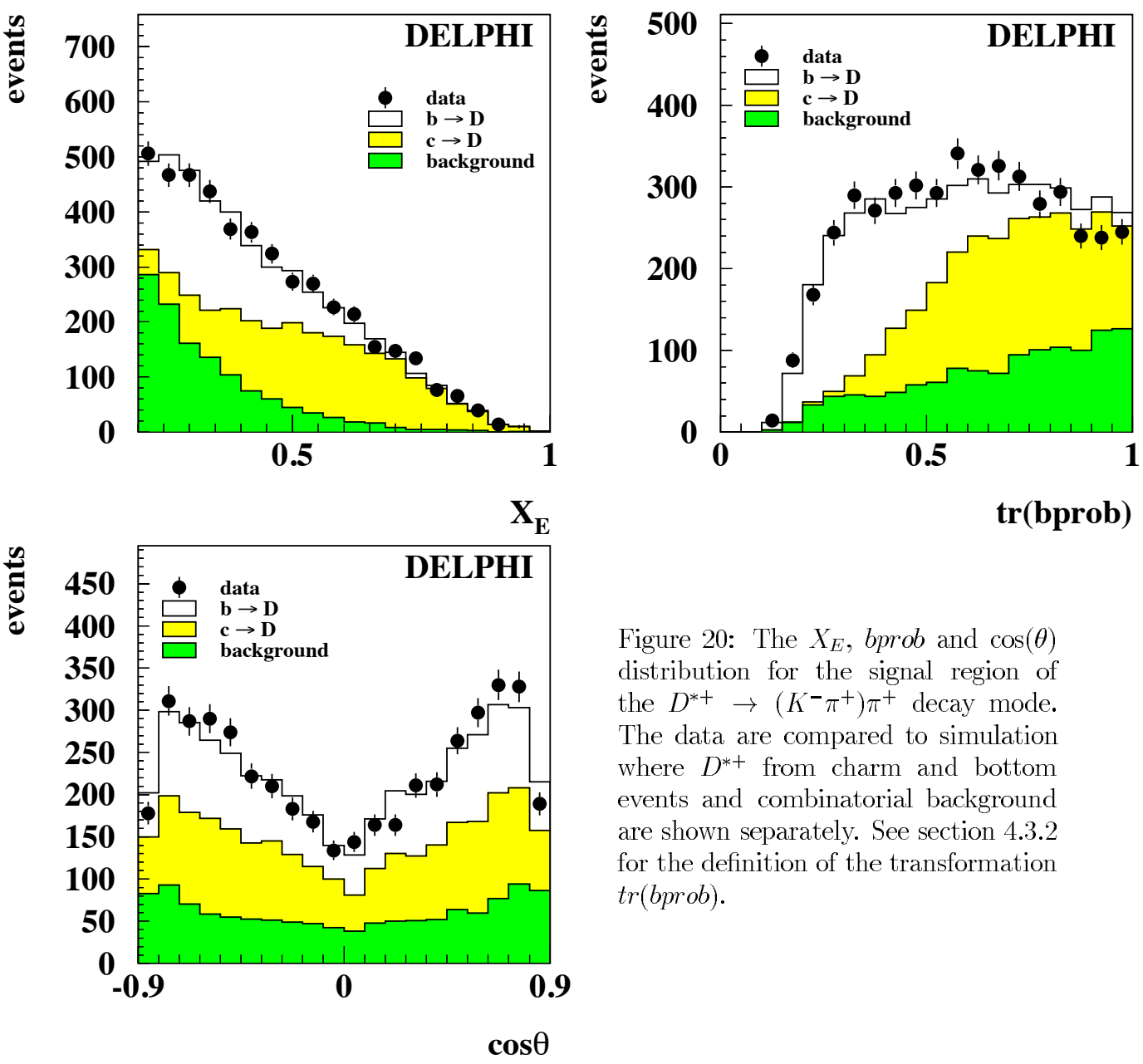


Figure 20: The $X_E$, *bprob* and $\cos(\theta)$ distribution for the signal region of the $D^{*+} \rightarrow (K^-\pi^+)\pi^+$ decay mode. The data are compared to simulation where $D^{*+}$ from charm and bottom events and combinatorial background are shown separately. See section 4.3.2 for the definition of the transformation $tr(bprob)$.

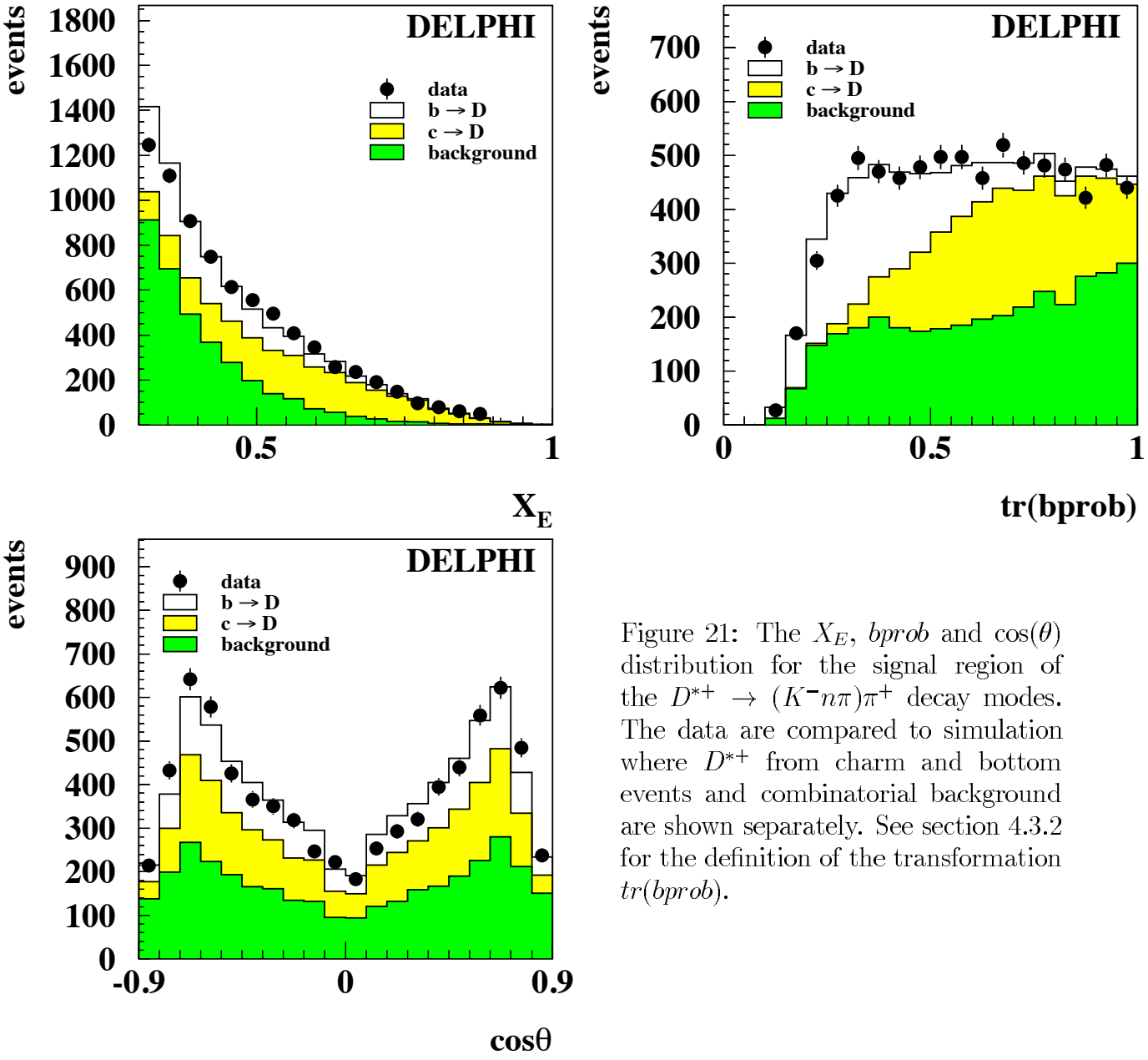


Figure 21: The $X_E$, *bprob* and $\cos(\theta)$ distribution for the signal region of the $D^{*+} \rightarrow (K^-n\pi)\pi^+$ decay modes. The data are compared to simulation where $D^{*+}$ from charm and bottom events and combinatorial background are shown separately. See section 4.3.2 for the definition of the transformation $tr(bprob)$.

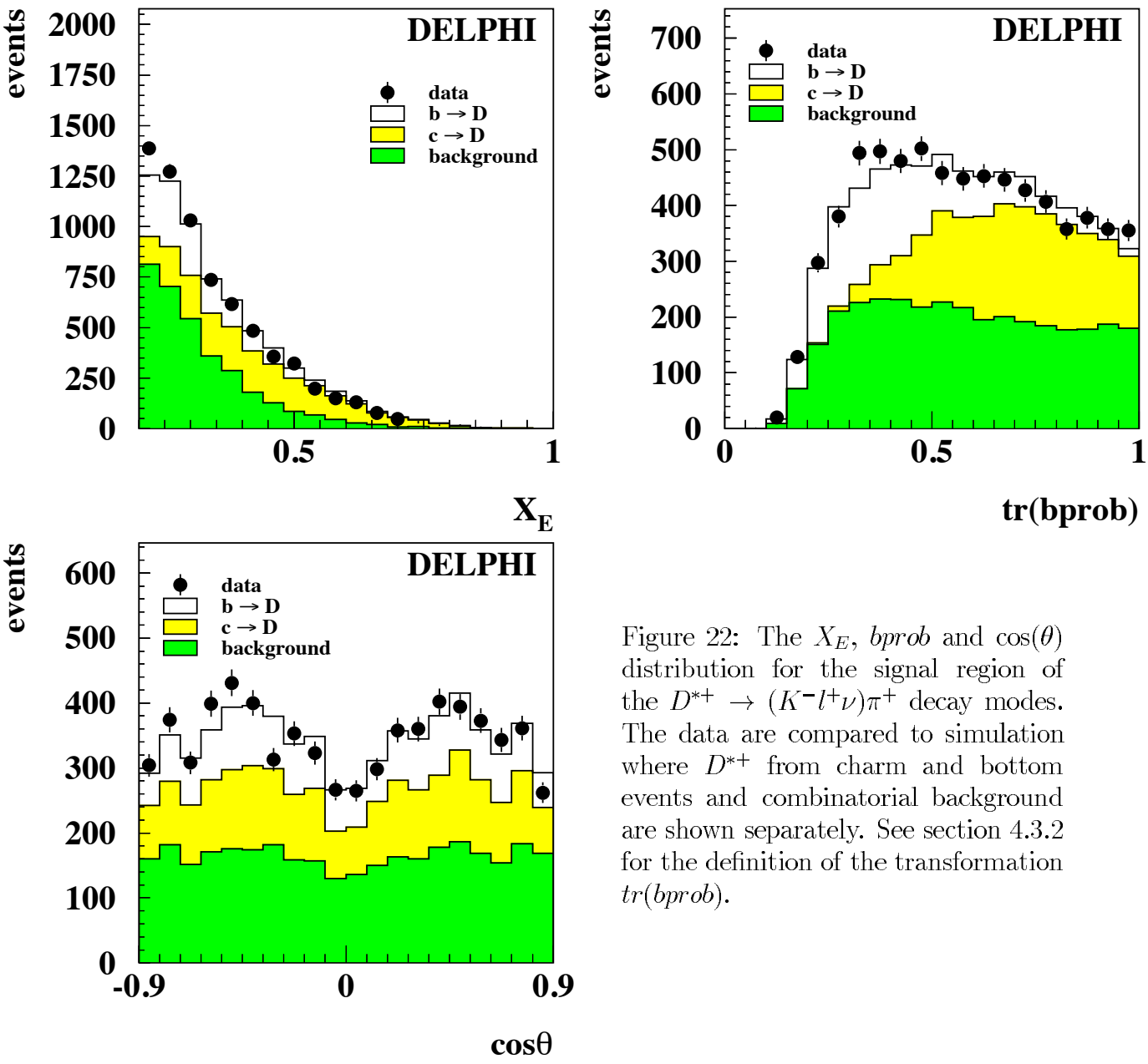


Figure 22: The $X_E$, *bprob* and $\cos(\theta)$ distribution for the signal region of the $D^{*+} \rightarrow (K^- l^+ \nu)\pi^+$ decay modes. The data are compared to simulation where $D^{*+}$ from charm and bottom events and combinatorial background are shown separately. See section 4.3.2 for the definition of the transformation $tr(bprob)$.

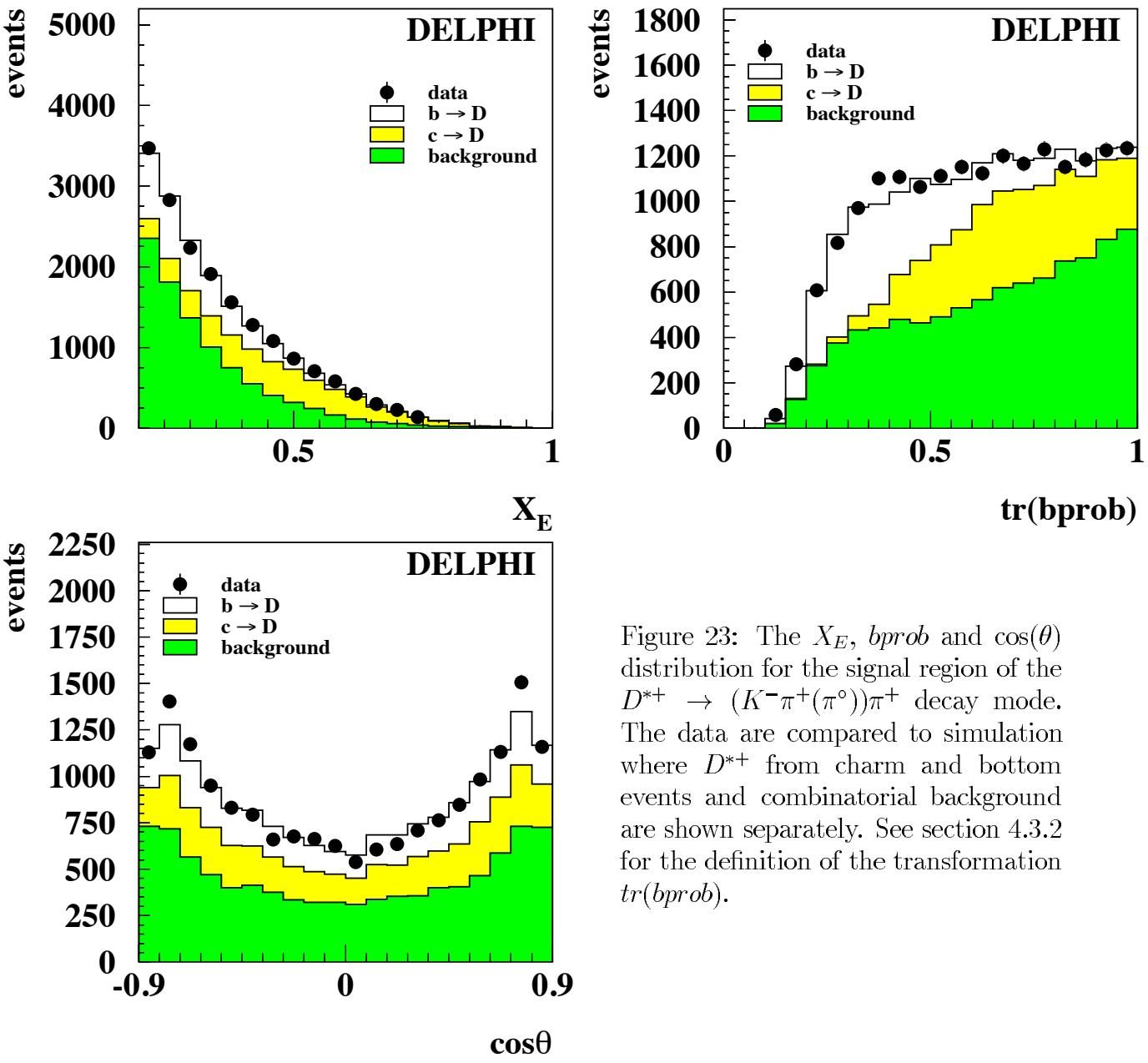


Figure 23: The $X_E$, *bprob* and $\cos(\theta)$ distribution for the signal region of the $D^{*+} \rightarrow (K^-\pi^+(\pi^\circ))\pi^+$ decay mode. The data are compared to simulation where $D^{*+}$ from charm and bottom events and combinatorial background are shown separately. See section 4.3.2 for the definition of the transformation $tr(bprob)$.

# $D^0 \rightarrow K^-\pi^+$

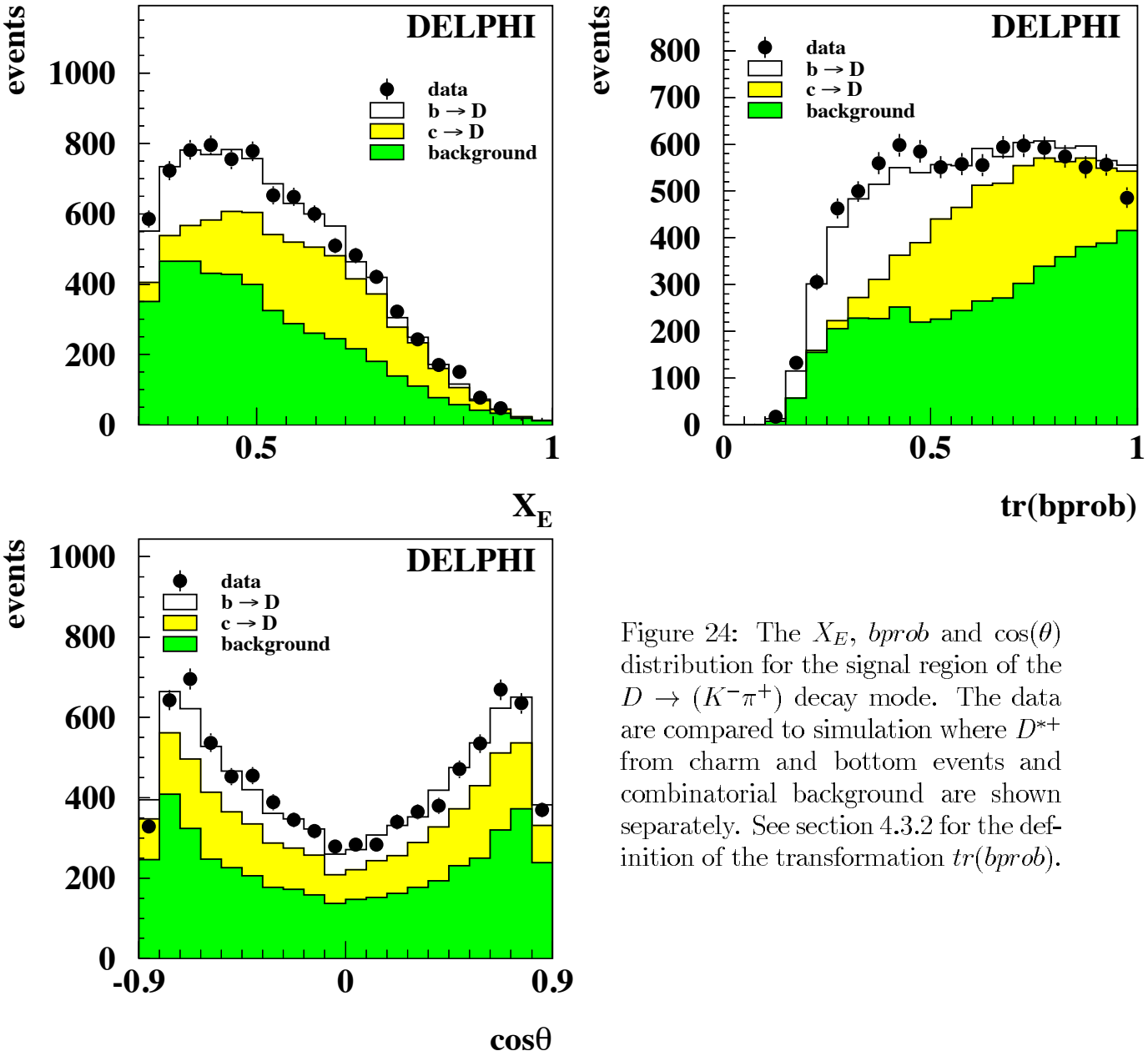


Figure 24: The $X_E$, *bprob* and $\cos(\theta)$ distribution for the signal region of the $D \rightarrow (K^-\pi^+)$ decay mode. The data are compared to simulation where $D^{*+}$ from charm and bottom events and combinatorial background are shown separately. See section 4.3.2 for the definition of the transformation $tr(bprob)$.

# $D^0 \to K^-\pi^+(\pi^o)$

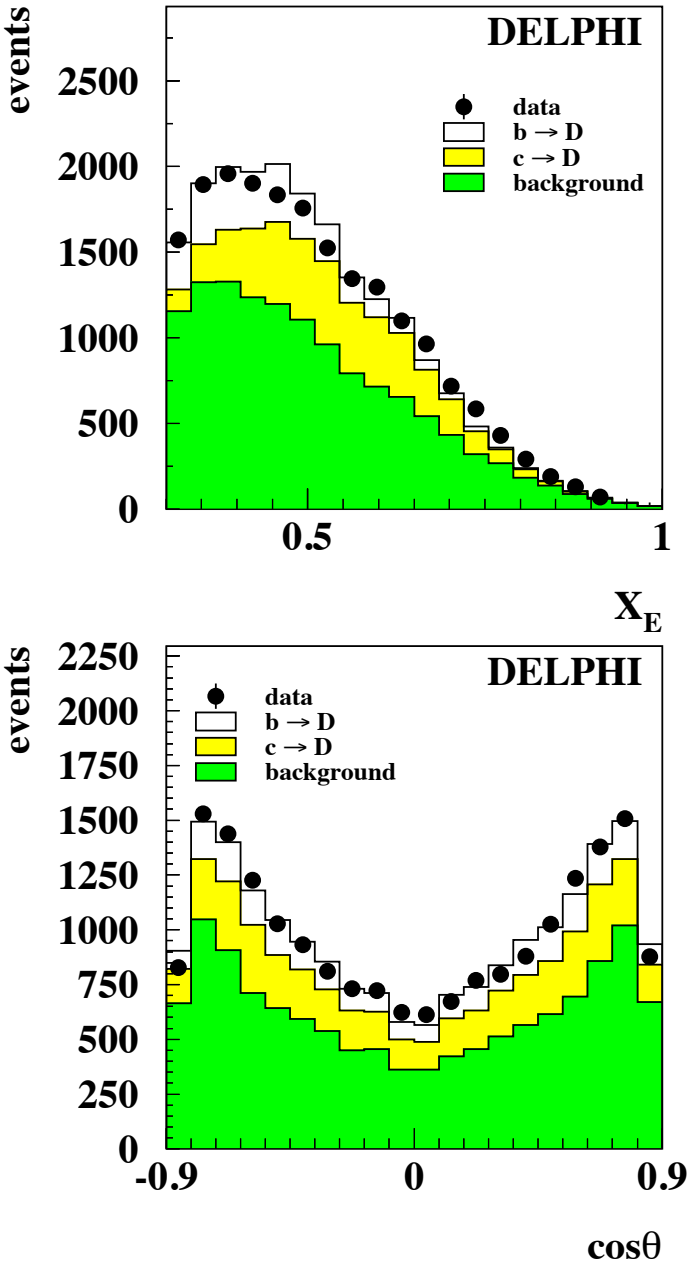


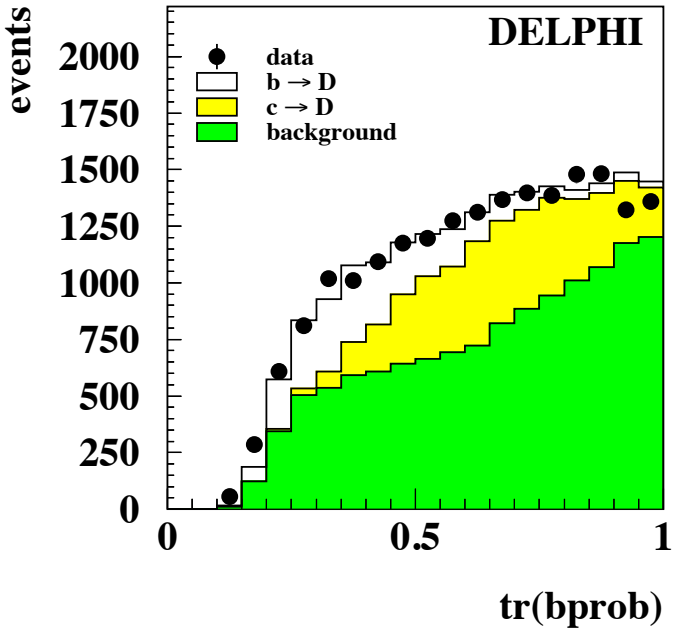





Figure 25: The $X_E$, *bprob* and $\cos(\theta)$ distribution for the signal region of the $D^{*+} \to (K^-\pi^+(\pi^\circ))$ decay mode. The data are compared to simulation where $D^{*+}$ from charm and bottom events and combinatorial background are shown separately. See section 4.3.2 for the definition of the transformation $tr(bprob)$.

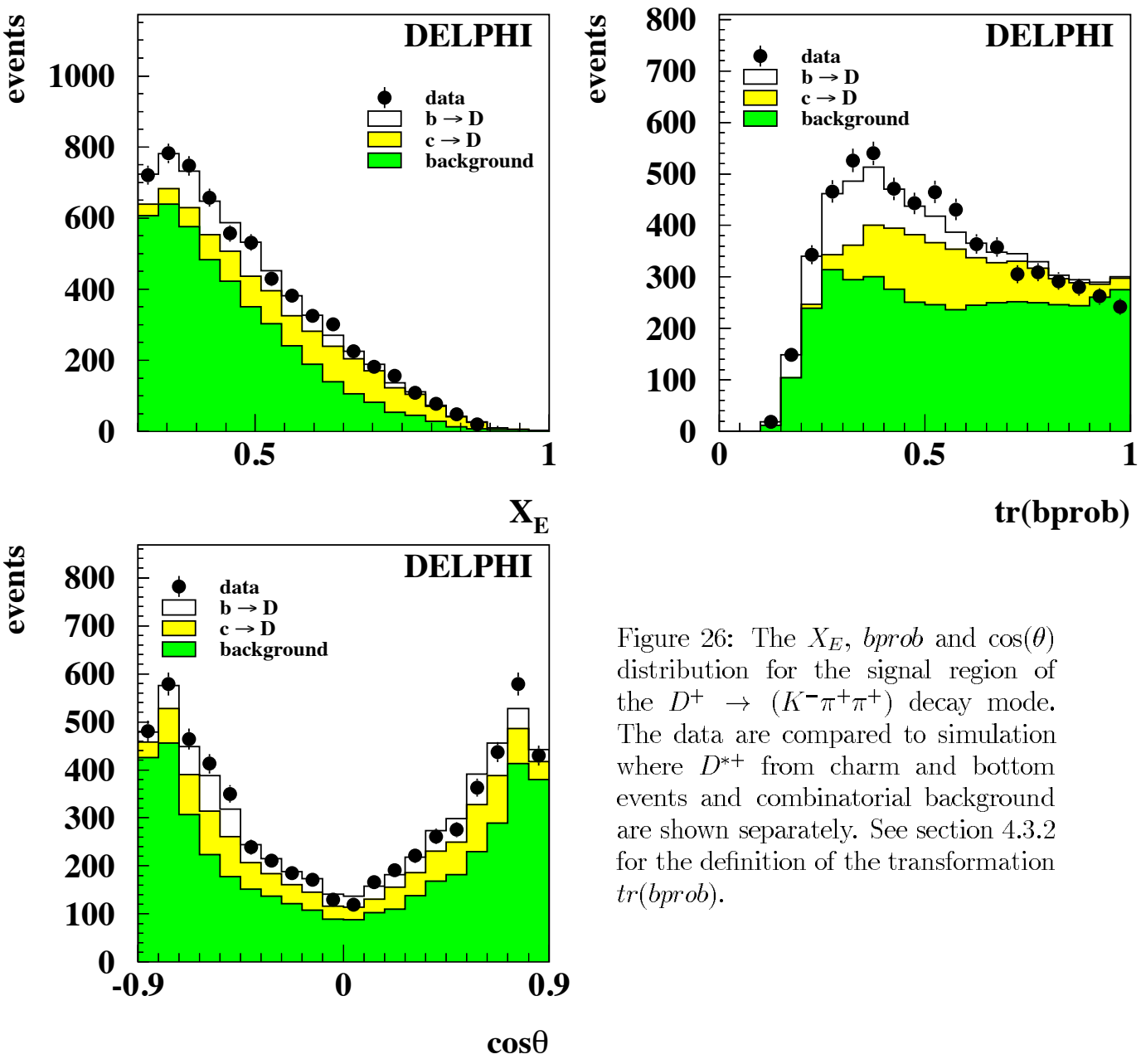


Figure 26: The $X_E$, *bprob* and $\cos(\theta)$ distribution for the signal region of the $D^+ \to (K^-\pi^+\pi^+)$ decay mode. The data are compared to simulation where $D^{*+}$ from charm and bottom events and combinatorial background are shown separately. See section 4.3.2 for the definition of the transformation $tr(bprob)$.

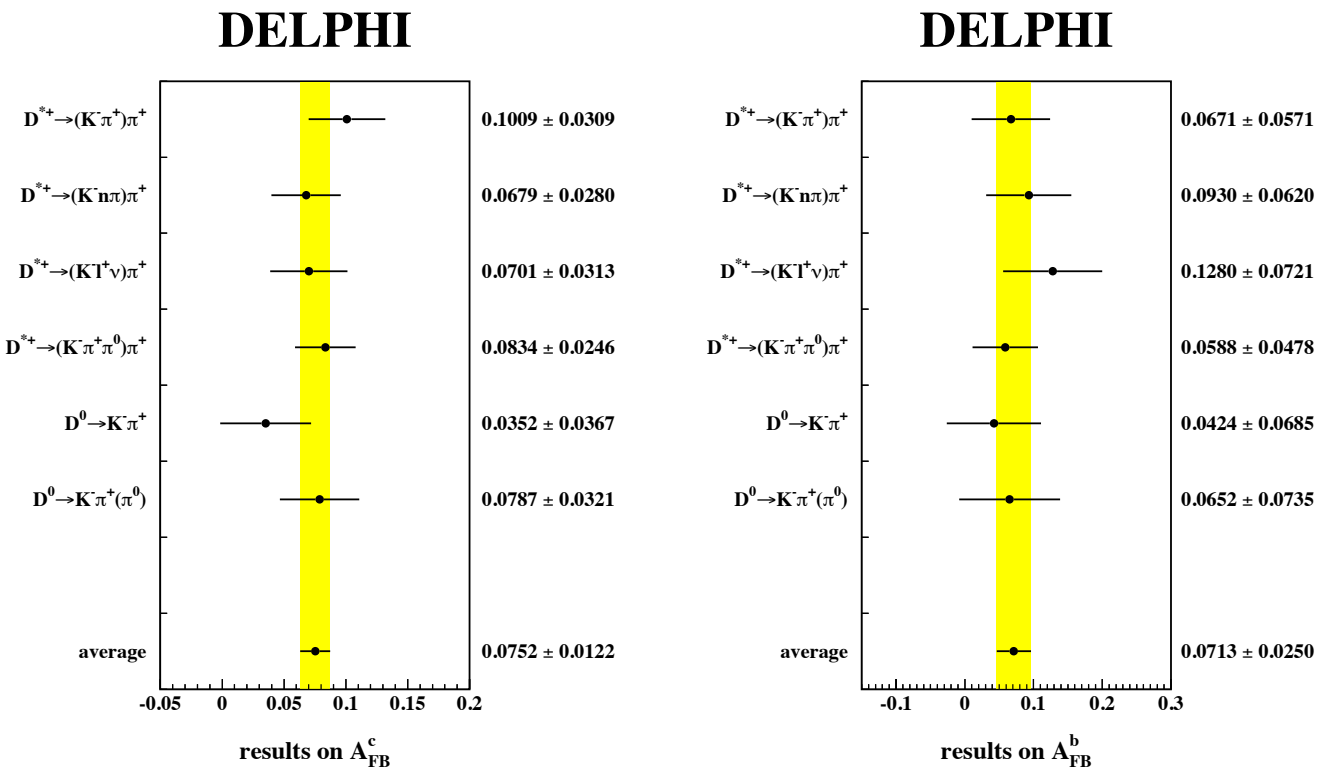


Figure 27: The results of the two parameter fit of the $c$ and $b$ asymmetry at an average centre of mass energy of 91.23 GeV for the different $D$ samples are shown in the two pictures above. The grey band represents the average over all these measurements. Only statistical errors are shown. The comparison of the results for $A^c_{FB}$ measurements from different samples constraining the $b$ asymmetry to the mean LEP average is shown below.

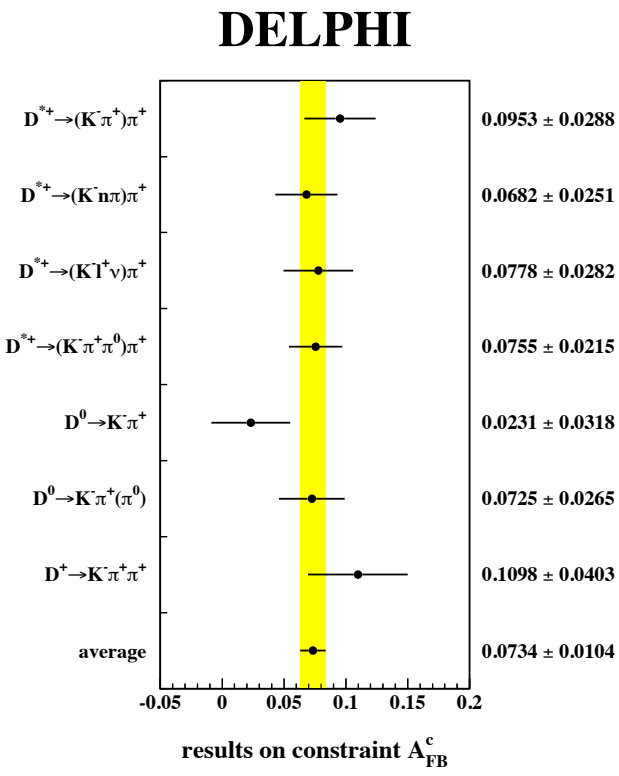

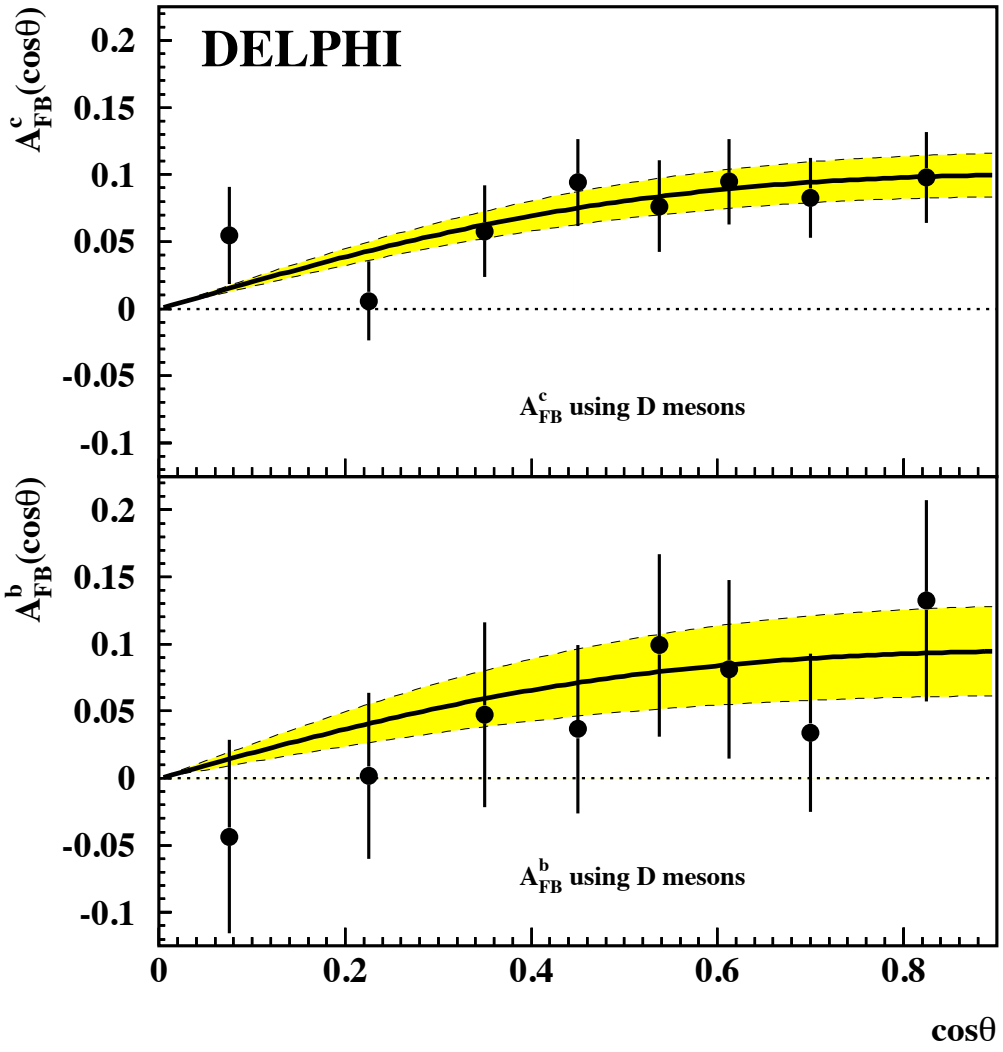


Figure 28: The $c$ and $b$ forward-backward asymmetries at an average centre of mass energy of 91.23 GeV as a function of $\cos\theta$. Only statistical errors are show, the correlation between the $c$ and $b$ asymmetry is $-0.44$. The bands represent the fit results.

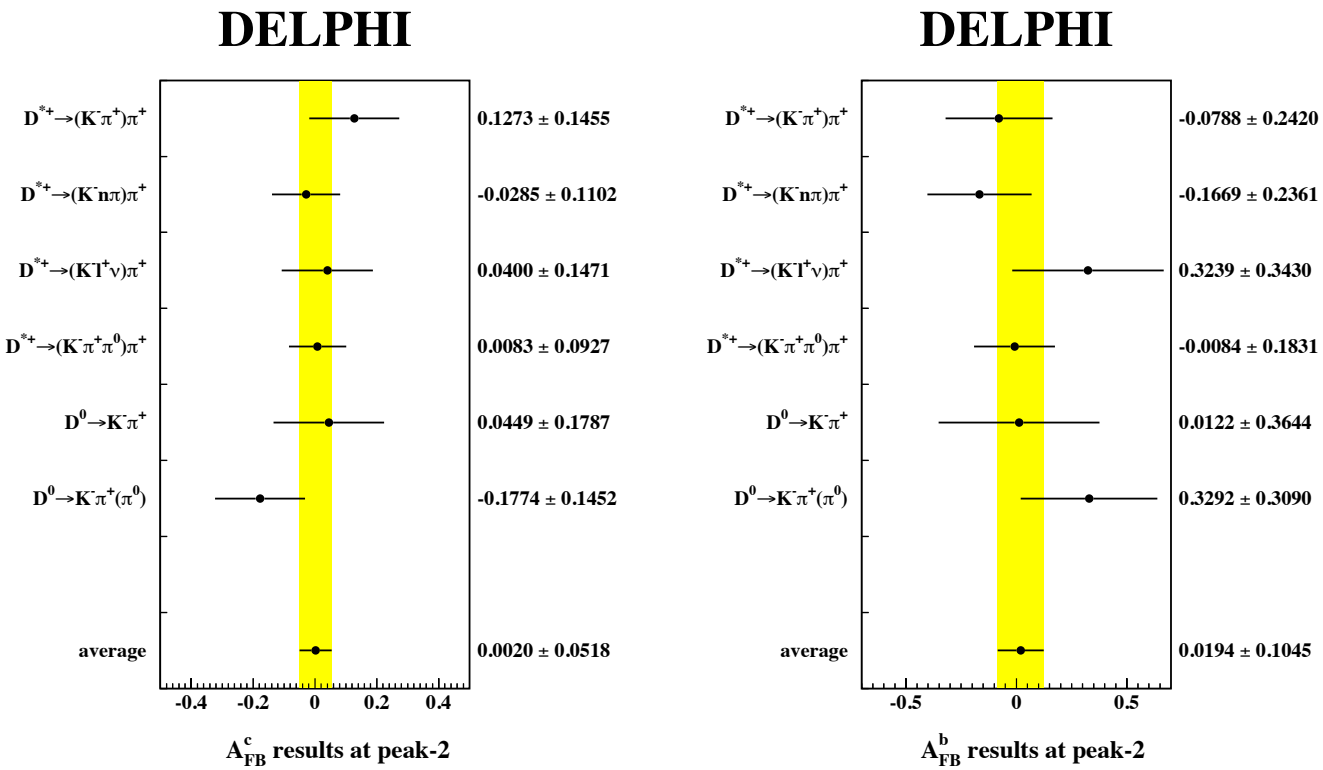


Figure 29: The results of the two parameter fit of the $c$ and $b$ asymmetry at an average centre of mass energy of 89.54 GeV for the different $D$ samples are shown in the two pictures above. The grey band represents the average over all these measurements. Only statistical errors are shown. Below the corresponding results for a centre of mass energy of 92.94 GeV are shown.

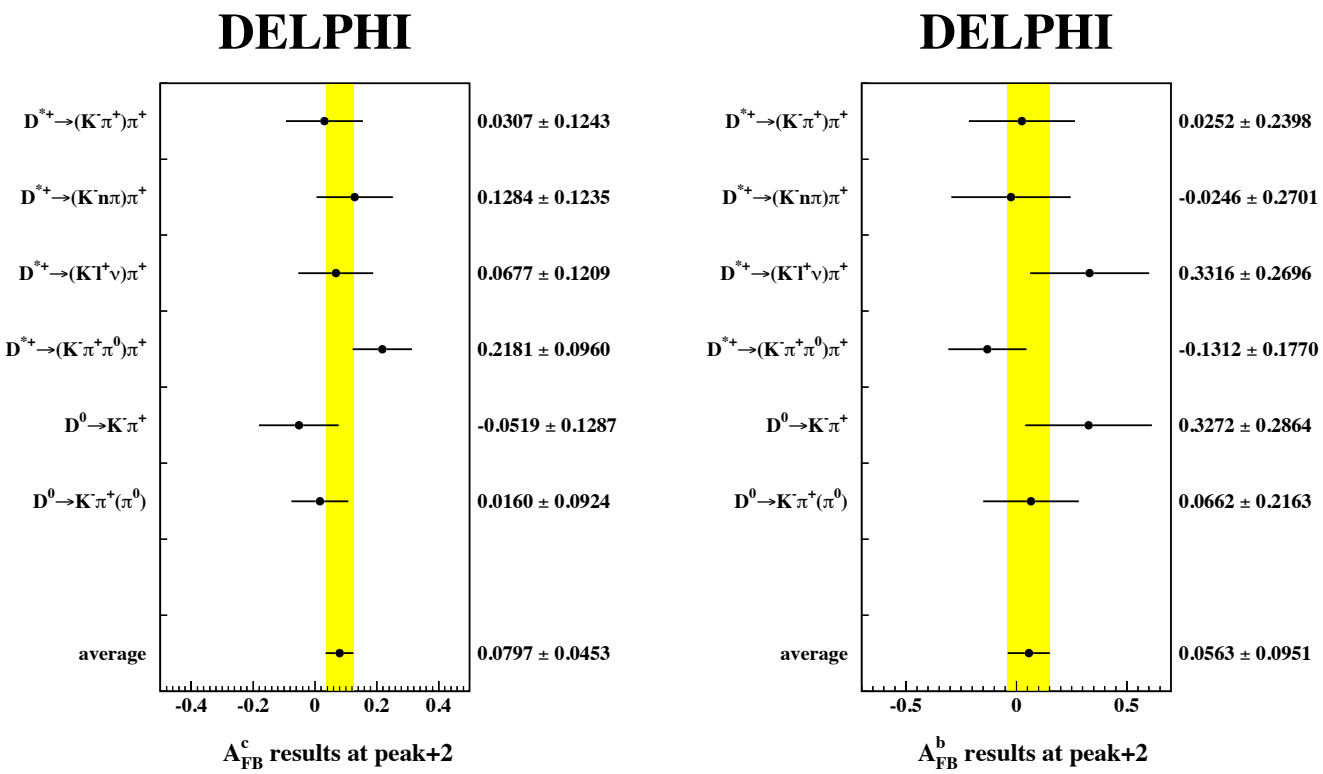

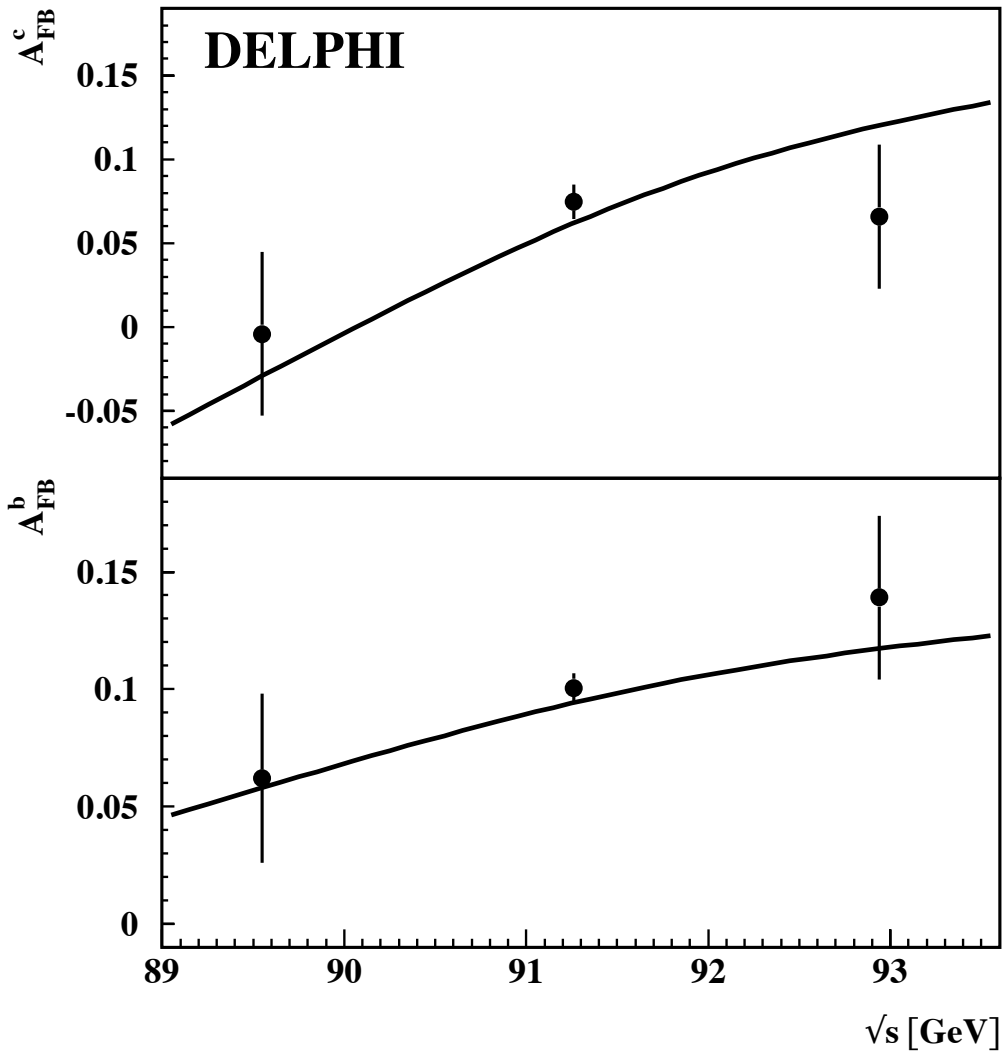


Figure 30: The energy dependence of the forward-backward asymmetry of charm and bottom quarks near the $Z$ pole as measured by DELPHI with the 1991 to 1994 data sample. Statistical and systematic erros are added in quadrature. The standard model parameterization for $m_{top} = 174$ GeV/$c^2$ , $m_{Higgs} = 300$ GeV/$c^2$ and $\alpha_s = 0.123$ is given by the superimposed line.